Max Planck Graduate Center
mit der Johannes Gutenberg-Universität Mainz

Applications of Para-Hydrogen Induced Polarization

Dissertation
zur Erlangung des Grades

„Doktor rerum naturalium“
(Dr. rer. nat.)

der Fachbereiche:
08 - Physik, Mathematik und Informatik
09 - Chemie, Pharmazie und Geowissenschaften,
10 - Biologie,
Universitätsmedizin

der Johannes Gutenberg-Universität
in Mainz

Barbara Helena Ripka
(geb. Piechalska)

geb. in Warschau/Polen
Mainz, den 22.10.2018

Diese Dissertationsarbeit wurde angefertigt am Max-Planck-Institut für Polymerforschung in Mainz, im Rahmen der Graduiertenschule Max Planck Graduate Center mit der Johannes Gutenberg-Universität Mainz.

Erstgutachterin: Prof. Dr. Katharina Landfester

Zweitgutachter: Univ.-Prof. Dr. Dmitry Budker

Betreuerin: Dr. Kerstin Münnemann

Datum der Prüfung:

I hereby declare that I wrote the dissertation submitted without any unauthorized external assistance and used only sources acknowledged in the work. All textual passages which are appropriated verbatim or paraphrased from published and unpublished texts as well as all information obtained from oral sources are duly indicated and listed in accordance with bibliographical rules. In carrying out this research, I complied with the rules of standard scientific practice as formulated in the statutes of Johannes Gutenberg-University Mainz to insure standard scientific practice.

Barbara Ripka

Abstract

This work deals with applications of Parahydrogen Induced Polarization (PHIP) to achieve signal enhancement in solution-state Nuclear Magnetic Resonance (NMR) spectroscopy. Parahydrogen is the nuclear spin singlet state isomer of molecular hydrogen. PHIP is a chemical method to create nuclear spin hyperpolarization by transferring the nuclear spin order of enriched parahydrogen into a molecule. This can be achieved by a spin-order conserving pairwise hydrogenation of an unsaturated covalent bond with enriched parahydrogen (hydrogenative PHIP), or the spin-order is transferred though nuclear spin couplings within a short-lived complex to which both parahydrogen and the substrate molecule to be polarized are temporarily bound (non-hydrogenative PHIP, Signal Amplification By Reversible Exchange (SABRE)). PHIP is able to create nuclear spin polarization of the order $\mathcal{O} \sim 10^{-1} - 1$. Therefore, in comparison with NMR spectroscopy on thermal polarization ($\mathcal{O} \sim 10^{-5}$) PHIP holds a signal enhancement potential of 4-5 orders of magnitude. However, every kind of nuclear spin hyperpolarization in solution decays within seconds to minutes due to spin-lattice-relaxation, which poses a big problem for technical or medical applications. In three projects it was attempted to overcome this time limitation either by continuous re-polarization or by making use of a molecular long-lived nuclear spin singlet state. The long-lived molecular singlet-state was created on fumaric acid disodium salt dissolved in water, which is biocompatible and therefore of interest for future applications as hyperpolarized MRI (Magnetic Resonance Imaging) contrast agent. Hyperpolarization stored in fumarate's long-lived singlet state can be converted into strong detectable nuclear spin magnetization by metabolism. Continuous re-polarization using SABRE was applied as source of magnetization for long-time measurements with zero- to ultralow-field (ZULF) NMR spectroscopy.

Zusammenfassung

Diese Promotionsarbeit befasst sich mit Anwendungen von Parawasserstoff Induzierter Hyperpolarisation (PHIP) zur Signalverstärkung der Kernspinresonanz Spektroskopie (NMR-Spektroskopie) in Lösung. Parawasserstoff ist molekularer Wasserstoff im Kernspin Singulett-Zustand. PHIP ist eine chemische Methode zur Herstellung von Kernspin-Hyperpolarisation durch Übertragung der Spinordnung von angereichertem Parawasserstoff auf Kernspins in einem Molekül. Dies kann durch eine die Spinordnung erhaltende paarweise Hydrierung einer ungesättigten kovalenten Bindung mit angereichertem Parawasserstoff geschehen (hydrogenative PHIP), oder durch Übertragung der Spinordnung über Kernspin-Kopplungen innerhalb eines kurzlebigen Komplexes, an den sowohl Parawasserstoff als auch das zu polarisierende Substratmolekül vorübergehend gebunden werden (non-hydrogenative PHIP, Signal Amplification By Reversible Exchange (SABRE)). Da mittels PHIP Kernspinpolarisationen der Ordnung $\mathcal{O} \sim 10^{-1} - 1$ erreicht werden können, birgt die Methode im Vergleich zur NMR Spektroskopie mit thermischer Polarisation ($\mathcal{O} \sim 10^{-5}$) ein Signalverstärkungspotenzial von 4-5 Größenordnungen. Die Problemstellung dieser Arbeit liegt darin, dass jede Art von Kernspin-Hyperpolarisation in Lösung innerhalb von Sekunden bis Minuten mittels Spin-Gitter-Relaxation zerfällt, was für technische und medizinische Anwendungen ein großes Problem darstsellt. In drei Unterprojekten wurde daran gearbeitet diese zeitliche Limitierung entweder durch kontinuierliche re-polarisation oder durch Ausnutzung eines langlebigen Kernspin-Singulettzustandes im Molekül zu umgehen. Der Kernspin-Singulettzustand wurde auf Fumarsäure Dinatriumsalz gelöst in Wasser hergestellt, welches biokompatibel und damit interessant für eine zukünftige Anwendung als hyperpolarisiertes MRT (Magnetresonanztomographie) Kontrastmittel ist. Hierbei kann die im Singulett-Zustand gespeicherte Hyperpolarisation durch Verstoffwechselung in detektierbare starke Kernspin-Magnetisierung konvertiert werden. Kontinuierliche re-polarisation mittels SABRE wurde als Magnetisierungsquelle für Langzeitmessungen mit Null- bis Ultraniedrigfeld (ZULF) NMR Spektroskopie angewendet.

Contents

Chapter 1.

Introduction

This chapter provides a motivation for the research performed in this work by sketching its historical and scientific context.

Nuclear Magnetic Resonance (NMR) spectroscopy was developed 1946 by Felix Bloch and Edward Mills Purcell and since then became an important spectroscopy method in analytical chemistry which lead to a Nobel Prize for the developers in 1952.
Based on the principle of NMR spectroscopy Paul C. Lauterbur and Sir Peter Mansfield developed Magnetic Resonance Imaging (MRI) which became one of the most important diagnostic imaging techniques. Paul C. Lauterbur and Sir Peter Mansfield were honored with the Nobel Prize for mecidine in 2003.
Today, both methods have become indispensable and are still subject of current research. One of their major limitations, which is attempted to be overcome is their intrinsically low sensitivity. Due to the low gyromagnetic ratio of nuclear spins, only a small fraction of all spins contribute to the observable NMR signal (e. g. around 10^{-5} proton spins at 7 T and room temperature). The applicability of NMR in medicine is therefore mainly based on the huge amount of abundant nuclear spins. However, the observation of a small amount of molecules would be beneficial for e. g. cancer diagnostic.
An approach to realize this are hyperpolarization techniques, which artificially create a strong alignment of nuclear magnetic moments and hold a signal enhancement potential of up to 5 orders of magnitude. Several hyperpolarization techniques have been developed so far and comprise Dynamic Nuclear Polarization (DNP) [1], Parahydrogen Induced Polarization (PHIP) [2] and hyperpolarization by laser

optical pumping of noble gases [3, 4]. The chemically inert noble gases serve as NMR probes and were mostly applied for the investigation of void spaces (e.g. the lung [5]), whereas via DNP and PHIP a large number of different molecules in the gas (PHIP), liquid (DNP, PHIP) and solid (DNP) phase can be hyperpolarized.
A drawback of all hyperpolarization techniques is that the signal enhancement they create is relatively short-lived. Every nuclear spin configuration that differs from the equilibrium state, relaxes back to it eventually. Relaxation effects therefore impose a time limit for applications of hyperpolarized substances of seconds (protons in solution state), minutes (heteronuclei in solution state) or maximum hours (hyperpolarized noble gases) for technical or medical application.
This work is focused on research to overcome the time limitation of Parahydrogen Induced Polarization. There are two general approaches to overcome the time limitation of hyperpolarization, one is to prolong the lifetime of the polarization itself, the other is to provide freshly hyperpolarized material continuously.
The main project of this work makes use of the fact that strongly coupled nuclear spins can form hyperpolarized singlet-states, whose total nuclear spin is zero. Several relaxation mechanisms depend on coupling to a non-zero nuclear spin, which significantly increases the lifetime of overpopulated singlet state spin configurations. Chapter 3 covers the successful overpopulation of a long-lived molecular singlet state in fumaric acid disodium salt dissolved in water. The singlet state lifetime was determined to exceed 6 minutes which leaves enough time for applications. Since fumaric acid is biocompatible it is of high interest for medical application as a hyperpolarized MRI contrast agent. Another very appealing fact is that the hyperpolarization stored in fumarate's singlet state can be released by metabolism.
Chapters 4 and 5 deal with applications of continuously providing freshly polarized molecules. A remarkable success was achieved in chapter 4 by keeping up continuous hyperpolarization for more than five hours. This can be an enabling technology for hyperpolarized long-term experiments.

Chapter 2.

Theory

This chapter explains the theory that is required to understand the content of this work. It does not explain the basic concepts of quantum mechanics, atomic physics and Nuclear Magnetic Resonance (NMR) spectroscopy, which are however required for understanding and can be acquired from literature [6, 7, 8, 9, 10, 11, 12, 13, 14].

2.1. Nuclear Spin Polarization and T_1 Relaxation

Each nucleus has a nuclear spin angular momentum, which is quantized in absolute value and orientation. The absolute value of the nuclear spin angular momentum is described by the quantum number I, shorter often called nuclear spin quantum number. I can take the value zero or multiples of $\frac{1}{2}$, thus $I = 0, \frac{1}{2}, 1, \frac{3}{2}, 2, \ \ldots\ $. The direction of the nuclear spin angular momentum is described by the corresponding magnetic quantum number m_I which describes the azimuthal component of $\vec{I}$ and thus its projection on the z-axis. m_I can take values between $-I$ and I in steps of one, hence $m_I = -I, -I+1, \ \ldots\ , I-1, I$.

The nuclear spin angular momentum gives rise to the nuclear magnetic moment,

$$\vec{\mu}_I = \gamma \vec{I}\,.$$

γ is the gyromagnetic[1] ratio, a characteristic constant of each isotope. A nonzero nuclear magnetic moment and nuclear spin is a necessary condition for nuclear

[1] More precisely, γ is called magnetogyric ratio. However, this term is less common. $\gamma(^1\mathrm{H}) = 267,513 \frac{1}{T \cdot s}$, $\gamma(^{13}\mathrm{C}) = 67,262 \frac{1}{T \cdot s}$

magnetic resonance (NMR) experiments.

Without an external magnetic field the energy levels of $\vec{I}$ are degenerate in m_I. An external magnetic field removes this degeneracy. This effect is called Zeeman-effect. The potential energy of a nuclear magnetic moment $\vec{\mu}_I$ in an external magnetic field $\vec{B_0}$ is described by

$$E = -\vec{\mu}_I \cdot \vec{B_0} = -\gamma m_I \hbar B_0 \,. \tag{2.1.1}$$

By convention the external magnetic field B_0 is always defined in z-direction. Figure 2.1 schematically depicts the splitting of the Zeeman energy levels for a nucleus with spin $I = \frac{1}{2}$.

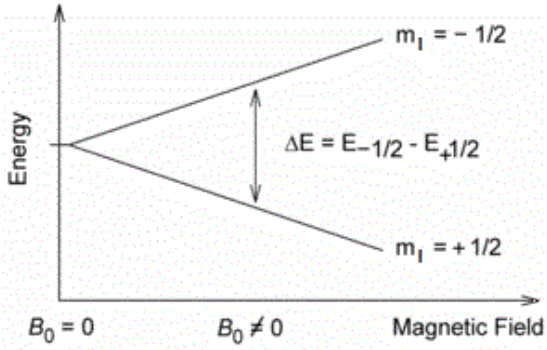

Figure 2.1.: Schematic deptiction of the Zeeman-effect on a nucleus with spin quantum number $I = \frac{1}{2}$.

From equation 2.1.1 it can be derived that if a photon is emitted during the transition between two neighboring Zeeman-levels with $\Delta m = 1$ its frequency is

$$\omega = \gamma B_0 \,. \tag{2.1.2}$$

Equation 2.1.2 is called the central NMR equation. The frequency ω, often also referred to as ω_0 is called Larmor-frequency.
An unequal population of Zeeman energy levels in a spin ensemble is called polarization. If polarization refers to the population of Zeeman levels of a nuclear magnetic moment it is called nuclear spin polarization. Nuclear spin polarization is a measure for the total nuclear magnetic moment or magnetization of a nuclear spin ensemble. The general formula for nuclear spin polarization is

$$P = \frac{1}{I} \frac{\sum_{i=-I}^{I} m_i \cdot N_i}{\sum_{i=-I}^{I} N_i} \,. \tag{2.1.3}$$

N_i is the population number of the Zeeman engergy level with magnetic quantum number m_I. This thesis only deals with NMR on ^{1}H and ^{13}C nuclei, which both have a nuclear spin of $I = \frac{1}{2}$. The polarization of a nucleus with spin $I = \frac{1}{2}$ is given by

$$P\left(I = \frac{1}{2}\right) = \frac{1}{1/2}\frac{(+1/2)\cdot N_{+1/2} + (-1/2)\cdot N_{-1/2}}{N_{+1/2} + N_{-1/2}} = \frac{N_{+1/2} - N_{-1/2}}{N_{+1/2} + N_{-1/2}}. \quad (2.1.4)$$

The basic principle of every NMR experiment is that a sample, containing an ensemble of nuclei with non-zero nuclear spins, is exposed to an external magnetic field B_0 and irradiated with the Larmor-frequency of its nuclear spins. During the irradiation the population of the nuclear spin Zeeman-energy-levels oscillates with the Rabi-frequency Ω. By varying the time of Larmor-frequency irradiaion t the population distribution at the end of irradiation and thus the flip-angle α can be defined. Irradiation times leading to a certain flip-angle α are often accordingly called α-Pulse. While a nuclear spin ensemble that was excited by irradiation of its Larmor-frequency relaxes back to its initial state, it emits electromagnetic radio frequency radiation that exactly corresponds to its Larmor-frequencies. This radiation is detected and recorded as so called Free Induction Decay (FID). Fourier transformation translates the FID into a frequency spectrum where the exact Larmor-frequencies of the sample occur as resonance peaks. The molecular electron shell is able to screen a nuclear spin from the external magnetic field B_0 to different extents within the parts per million (ppm) range. This effect is called chemical shift and causes that Larmor-frequencies of a nucleus depend on its molecular environment. Moreover, nuclear spins within a molecule can couple with intermediation of the electron bonds. This effect is called J-coupling and leads to specific splitting patterns of nuclear magnetic resonance peaks. In total, chemical shift and J-coupling allow for determination of molecular structures from an NMR spectrum. A detailed introduction into NMR experiments in general is given in [6, 8, 9, 7].

A non-zero polarization is required for every NMR experiment, since the NMR signal intensity is proportional to the total nuclear magnetic moment of the sample and thus to the value of polarization. Usually NMR experiments are performed at thermal polarization which refers to the thermal equilibrium polarization in an external magnetic field B_0. If a sample containing an ensemble of $I = \frac{1}{2}$ nuclei is inserted into an external magnetic field B_0 the energetically lower Zeeman level gets overpopulated according to the Boltzmann-distribution

$$\frac{N_{-1/2}}{N_{+1/2}} = exp\left(-\frac{|\Delta E|}{k_B T}\right) = exp\left(-\frac{\hbar\gamma B_0}{k_B T}\right). \quad (2.1.5)$$

From the Boltzmann-distribution in equation 2.1.5 the formula for thermal polarization of an ensemble of nuclei with $I = \frac{1}{2}$ can be derived as

$$P(th, I = \frac{1}{2}) = \frac{N_{+1/2} - N_{-1/2}}{N_{+1/2} + N_{-1/2}} = \tanh\left(\frac{\hbar\gamma B_0}{2k_B T}\right) . \tag{2.1.6}$$

For an external magnetic field of approximately $B_0 = 7\ T$ and a temperature of approximately $T = 300\ K$ equation 2.1.6 yields thermal ^{1}H polarization levels of the order of $\mathcal{O} \sim 10^{-5}$ and ^{13}C thermal polarization levels of the order of $\mathcal{O} \sim 10^{-6}$.
Hence, it is clear that dramatically enhanced polarization values result in dramatically enhanced NMR signal intensities. An artificial strong overpopulation of selected nuclear spin Zeeman energy levels in an ensemble that leads to polarization values of $\mathcal{O} \sim 10^{-1} - 1$ is called nuclear spin hyperpolarization. Nuclear spin hyperpolarization therefore holds an NMR signal enhancement potential of 4-5 orders of magnitude.
Hyperpolarization techniques comprise Dynamic Nuclear Polarization (DNP) [1], Parahydrogen Induced Polarization (PHIP) [2] and hyperpolarization by laser optical pumping at noble gases [3, 4]. The chemically inert noble gases serve as NMR probes and were mostly applied for the investigation of void spaces (e.g. the lung [5]), whereas via DNP and PHIP a large number of different molecules in the gas (PHIP), liquid (DNP, PHIP) and solid (DNP) phase can be hyperpolarized. This work focuses on Parahydrogen Induced Polarization, which is introduced in more detail in section 2.3.
Every polarization value different from the thermal equilibrium polarization $P_{th.eq.}$ described by equations 2.1.5 and 2.1.6 relaxes back to thermal equilibrium in an exponential decay with the spin-lattice-relaxation time constant T_1 .[2]

$$P(t) = P_{th.eq.} + (P_{start} - P_{th.eq.}) \cdot e^{-\frac{t}{T_1}} . \tag{2.1.7}$$

Typical T_1 relaxation times of ^{1}H nuclei are in the order of 1-15 s, of ^{13}C nuclei in the order of 20-100 s. Spin-lattice-relaxation causes that hyperpolarization always has a limited lifetime that in most cases corresponds to T_1 of the hyperpolarized nucleus. In consequence, hyperpolarization, once created, needs to be applied within seconds to minutes in order to exploit its NMR signal enhancement potential. This work focuses on application techniques which aim to prolong the lifetime of PHIP or to reduce the negative effects of its limited lifetime by providing freshly hyperpolarized molecules continuously.

[2] Mathematically the relaxation mechanisms are described by the Bloch-equations. A detailed mathematical description as well as other relaxation mechanisms as the spin-spin-relaxation with time constant T_2 can be looked up in [6].

2.2. Spin Operator Formalism

Due to the quantization of spin angular momentum orientation, which was for the first time observed in the Stern-Gerlach experiment in 1922 [15, 12], the wave function of a spin $I = \frac{1}{2}$ particle can only be described in two complex dimensions

$$|\Psi\rangle = \begin{pmatrix} \Phi_1 \\ \Phi_2 \end{pmatrix} . \tag{2.2.1}$$

The most common base to describe spin wave functions is the so called Zeeman base

$$|\alpha\rangle = |\uparrow\rangle = \begin{pmatrix} 1 \\ 0 \end{pmatrix}, \quad |\beta\rangle = |\downarrow\rangle = \begin{pmatrix} 0 \\ 1 \end{pmatrix} . \tag{2.2.2}$$

Accordingly, the spin density operator $\rho = |\Psi\rangle\langle\Psi|$ is represented by a complex 2×2 matrix.
On the other hand, in experiments the spin vector shows characteristics of an angular momentum vector in real three-dimensional space $\mathbb{R}^3$. The mathematical model in $\mathbb{C}^2$ fulfills this requirement by describing operators for all spin operations, like spacial rotation or spin-flip, with matrices of the special unitary group in two complex dimensions $SU(2)$. $SU(2)$ is homomorphic to the rotation group in $\mathbb{R}^3$ $SO(3)$ and is generated by the three Pauli-matrices $\sigma_1, \sigma_2, \sigma_3$ (eq. 2.2.3) as shown in equation 2.2.4. The real vector $\vec{\alpha}$ denotes spin rotation angles around the axes x,y,z.

$$\sigma_1 = \begin{pmatrix} 0 & 1 \\ 1 & 0 \end{pmatrix}, \quad \sigma_2 = \begin{pmatrix} 0 & -i \\ i & 0 \end{pmatrix}, \quad \sigma_3 = \begin{pmatrix} 1 & 0 \\ 0 & -1 \end{pmatrix} \tag{2.2.3}$$

$$U = exp\left(\frac{1}{2}\vec{\alpha} \cdot \vec{\sigma}\right) \in SU(2), \quad \vec{\alpha} = \begin{pmatrix} \alpha_x \\ \alpha_y \\ \alpha_z \end{pmatrix} \in \mathbb{R}^3, \ \vec{\sigma} = \begin{pmatrix} \sigma_1 \\ \sigma_2 \\ \sigma_3 \end{pmatrix} \tag{2.2.4}$$

The complex spin operators I_x, I_y, I_z (eq. 2.2.5) in the $\mathbb{C}^2$ Zeeman basis are proportional to the Pauli matrices and return the x,y or z component of the spin angular momentum, respectively. The ladder operators $I_{+,-}$ inducing spin flips between the magnetic quantum numbers $m_I = \frac{1}{2}$ (up) and $m_I = -\frac{1}{2}$ (down) are defined in equation 2.2.6.

$$I_{x,y,z} = \frac{1}{2}\ \sigma_{1,2,3} \tag{2.2.5}$$

$$I_{\pm} = I_x \pm iI_y \tag{2.2.6}$$

By the aid of the Kronecker Product the above mathematical model for one spin can be extended onto systems of several spins[6].

The Schroedinger equation allows for a mathematical description of the equation of motion of a spin. Depending on the interaction different Hamilton operators are needed to include the effect in the calculations. H_{Zeeman} describes the Zeeman energy and can be derived from the classical formula for the potential energy of a magnetic moment in an external magnetic field B_0[3]. By considering a slightly different Larmor frequency $\omega_{j,0}$ for each spin j, H_{Zeeman} takes account for the chemical shift effect. H_J describes the energy contribution of the scalar J-coupling between two nuclear magnetic moments[4]. The orientation of the nuclear spins can be manipulated by radio frequency pulses with the Larmor frequency ω_0 and amplitude $\vec{B_1}$, which is oscillating in the x-y-plane orthogonal to the field causing the Zeeman interaction. The corresponding contribution to the Hamiltonian is described by H_{rf}, ϕ denotes the phase between the x-y-plane projection of the nuclear magnetic moment and $\vec{B_1}$ which is fixed in the rotating frame [6].

$$H_{Zeeman} = -\hbar \sum_j \omega_{j,0} I_{j,z} \tag{2.2.7}$$

$$H_J = 2\pi\hbar \sum_{j<k} J_{jk} \vec{I_j} \cdot \vec{I_k} \tag{2.2.8}$$

$$H_{rf} = -\hbar\gamma B_1 \sum_j (\cos(\phi) I_{j,x} + \sin(\phi) I_{j,y}) \tag{2.2.9}$$

2.3. Parahydrogen Induced Polarization

Parahydrogen Induced Polarization (PHIP) is a method to create nuclear spin hyperpolarization by transferring the strongly antiphasic nuclear spin order of enriched parahydrogen into a substrate molecule and was discovered by Bowers and Weitekamp in 1986 to 1987 [16, 17].

Molecular hydrogen exists in four nuclear spin isomers:

$$\begin{aligned} |S_0\rangle &= \frac{1}{\sqrt{2}} \left(|\alpha\beta\rangle - |\beta\alpha\rangle\right) , \\ |T_{+1}\rangle &= |\alpha\alpha\rangle , \\ |T_0\rangle &= \frac{1}{\sqrt{2}} \left(|\alpha\beta\rangle + |\beta\alpha\rangle\right) , \\ |T_{-1}\rangle &= |\beta\beta\rangle . \end{aligned}$$

[3] $H = -\vec{\mu} \cdot \vec{B_0} = -\gamma \vec{I} \cdot \vec{B_0} = -\hbar\gamma \begin{pmatrix} I_x \\ I_y \\ I_z \end{pmatrix} \cdot \begin{pmatrix} 0 \\ 0 \\ B_0 \end{pmatrix} = -\hbar\gamma B_0 I_z = -\hbar\omega_0 I_z$

[4] Its analogon in classical mechanics is the potential energy of a magnetic dipole in the field of another magnetic dipole.

$|T_{+1}\rangle, |T_0\rangle, |T_{-1}\rangle$ are the three nuclear spin triplet state isomers of hydrogen, called orthohydrogen. They have a total nuclear spin of $I_{tot} = 1$. $|S_0\rangle$ is parahydrogen, the nuclear spin singlet state with a total nuclear spin of $I_{tot} = 0$. Parahydrogen stores a strongly antiphasic nuclear spin order.
Since protons are Fermions, the wavefunction of the hydrogen molecule has to be antisymmetric in exchange of the nuclei. This condition can only be fulfilled by the product of the molecular rotational angular momentum $|\Psi_{rot}\rangle$ and the nuclear spin angular momentum $|\Psi_{I_{tot}}\rangle$. Since $|\Psi_{rot}\rangle$ is symmetric for rotational states with even angular momentum quantum number j = even, parahydrogen, whose $|\Psi_{I_{tot}}\rangle$ is antisymmetric, can only exist in the j=even rotational states. Orthohydrogen, whose $|\Psi_{I_{tot}}\rangle$ is symmetric, can on the other hand only exist in the j = odd rotational states. This fact makes it understandable that singlet-triplet transitions are highly suppressed, since they can only be achieved with extremely unlikely two-photon-transitions.[5] In the high temperature limit (T > 250 K), the ratio between ortho- and parahydrogen populations in molecular hydrogen is $N_{ortho}/N_{para} = 3$, hence all nuclear spin isomers are represented equally. In the low temperature limit the vast majority of molecules is in the rotational ground state with j=0 , which implies a symmetrical $|\Psi_{rot}\rangle$ function. Hence, $|\Psi_{I_{tot}}\rangle$ must be antisymmetrical which leads to a strong overpopulation of $|S_0\rangle$ with $N_{ortho}/N_{para} \to 0$.
By cooling hydrogen in the presence of a paramagnetic catalyst as e.g. active charcoal, parahydrogen can be therefore enriched (e. g. to 93% at 35 K). The paramagnetic catalyst provides perturbations in hydrogen's magnetic environment on the scale of the molecular size, which makes singlet-triplet transitions more likely and allows the system to reach the thermodynamical equilibrium much faster than without catalyst. Since the conversion of para- to orthohydrogen in the absence of paramagnetic perturbations is very slow, enriched parahydrogen can be stored at room temperature for days.[18]

The density operator of parahydrogen is given by

$$\rho_{para} = \frac{1}{2}\left(|\alpha\beta\rangle - |\beta\alpha\rangle\right)\left(\langle\alpha\beta| - \langle\beta\alpha|\right) .$$

Using the product operator formalism, this leads to

$$\rho_{para} = \frac{1}{4}\mathbb{1} - \vec{I}_1 \cdot \vec{I}_2 .$$

Since only population differences lead to detectable NMR signals the term proportional to the unity operator can be neglected.

[5] In physics, highly suppressed singlet-triplet transitions are a commonly oberved phenomenon. In literature several other examples for analogous behavior can be found.[12]

Hyperpolarization can be achieved by a pairwise spin order conserving hydrogenation of an unsaturated covalent bond with enriched parahydrogen. This method is called hydrogenative PHIP. Since enriched parahydrogen has a strongly antiphasic spin order the hydrogenation leads to an unequal population of Zeeman levels in the target molecule and thus to hyperpolarization.

There are two major experimental procedures in PHIP. If the hydrogenation is performed in a high magnetic field the two former p-H_2 spins are afterwards usually weakly coupled (AX spin system). The hydrogenation with p-H_2 under high field conditions is commonly called PASADENA (Parahydrogen and Synthesis Allow Dramatic Enhancement of Nuclear Alignment). The density operator of the two former p-H_2 protons can be then given by

$$\rho_{AX,PASADENA} = \frac{1}{4}\mathbb{1} - I_{1z}I_{2z}\,.$$

For $\rho_{AX,PASADENA}$ it can be shown that a 45°-pulse leads to maximum transversal magnetization.

A different spin state is achieved if the reaction is performed at low field followed by an adiabatic transport of the sample into the high field of the NMR system. This experiment is commonly called ALTADENA (Adiabatic Longitudinal Transport After Dissociation Engenders Nuclear Alignment). At low magnetic field, the protons are strongly coupled (AB spin system). Hence, the system stays in the singlet spin state which is an eigenfunction of the strongly coupled spin system. By the adiabatic transfer, the system remains in a state corresponding to an eigenfunction of the Hamiltonian. Thus, only the energetically favored spin states of $|\alpha\beta\rangle$ and $|\beta\alpha\rangle$ become populated in the AX spin system at high field, which leads to the density operator

$$\rho_{ALTADENA} = \frac{1}{4}\mathbb{1} - \left(I_{1z}I_{2z} \pm \frac{1}{2}\left(I_{1z} - I_{2z}\right)\right)\,. \tag{2.3.1}$$

Another possibility to create hyperpolarization from enriched p-H_2 is called non-hydrogenative PHIP, whose most prominent example is Signal Amplification By Reversible Exchange (SABRE)[19]. In this case the spin order of p-H_2 is transferred onto spins in the target molecules though J-couplings in a complex around a metal based catalyst to which both p-H_2 and the substrate molecule are temporarily bound. The polarization transfer happens due to avoided energy level crossings, whose principle is explained in detail in section 2.5. Since substrate molecule and p-H_2 molecule bound to the catalyst complex are constantly exchanged SABRE holds the possibility to re-polarize one substrate molecule for a theoretically infinite number of times, as long as fresh enriched p-H_2 is available in the reaction solution.

2.3.1. Enhancement Factor

The signal enhancement factor is defined by the ratio of the achieved hyperpolarization and the thermal polarization present in a thermal reference experiment in the same apparatus under the same conditions. A formula for the theoretical maximum signal enhancement is given in equation 2.3.2 and was originally published by Natterer and Bargon [2].

$$\eta = \left| \frac{k_B T(1-4a)}{6\hbar\gamma B_0} \right| \tag{2.3.2}$$

a denotes the fraction of parahydrogen in the hydrogen gas used for the experiment. Exemplary, for the ^{1}H signal at 1.5 T using 93% enriched parahydrogen gas a maximum signal enhancement factor of 43 000 is predicted. Full polarization transfer to a ^{13}Cheteronucleus, leads to a four times higher theoretical maximum signal enhancement due to the four times lower gyromagnetic ratio.

The practically achieved signal enhancement factor is usually calculated from the ratio of the acquired hyperpolarized signal intensity and the signal intensity in a thermal reference experiment in the same apparatus under the same conditions. However, since antiphasic hyperpolarized signals often partially cancel each other out it must be taken into account that a signal enhancement value calculated this way will be lower than the actually achieved polarization enhancement. Therefore, in practice polarization enhancement must be distinguished from signal enhancement. In order to calculate the correct polarization enhancement factor from a measured signal the hyperpolarized spectral lines must be corrected for signal cancellation.

2.4. Nuclear Spin Singlet States

If two spins of a molecule are strongly coupled they can form a molecular singlet state. The conditions for strong coupling of two spins 1 and 2 is $J_{12} \gg (\nu_1 - \nu_2)$, meaning that their J-coupling is much bigger than the difference of their chemical shifts or Larmor frequencies. If this condition is fulfilled the singlet spin wave function

$$|\psi_{singlet}\rangle = \frac{1}{\sqrt{2}} \left(|\alpha\beta\rangle - |\beta\alpha\rangle \right) ,$$

corresponding to the singlet spin density operator

$$\rho_{singlet} = \frac{1}{4}\mathbb{1} - \vec{I}_1 \cdot \vec{I}_2$$

is either an eigenfunction of the spin system's Hamiltonian, making the pure singlet state an energy eigenstate of the spin system, or it exists an eigenstate whose wavefunction can be written as a superposition of the kind

$$|\psi\rangle = a\,|\psi_{singlet}\rangle + b\,|\psi_{triplet}\rangle\,, \quad a, b \in \mathbb{C}, \quad |a|^2 + |b|^2 = 1, \quad |a| \gg |b|\,.$$

In the latter case the spin system's energy eigenstate is very close to a singlet state, but it is not a pure singlet state (close-to-singlet eigenstate). Physically this results in a higher probability for singlet-triplet transitions the bigger the difference $1 - |a|$. One singlet-triplet-mixing mechanism that can occur in this case exploits avoided energy level crossings and is described in more detail in section 2.5. Other effects, often summarized as "spontaneous" polarization transfer are described in [20].
Hydrogenative PHIP experiments transfer parahydrogen's singlet spin order into the target molecule and thus always overpopulate the molecule's nuclear spin eigenstate closest to the singlet state.

A characteristic of nuclear spin singlet states is their total nuclear spin $I_{tot} = 0$. Therefore, molecular singlet states can not be detected by NMR, even if they are overpopulated and thus hyperpolarized. They are called NMR-silent. On the other hand the suppressed nature of singlet-triplet transitions makes overpopulated molecular singlet states atypically long-lived. The longevity also applies to eigenstates close to a singlet state.
This combination makes molecular nuclear spin singlet states particularly appealing for applications of parahydrogen induced polarization, since they can be used to "store" hyperpolarization for a time that exceeds the spin-lattice-relaxation constant T_1. Deliberately breaking the singlet-state converts the stored hyperpolarization into strong magnetization that is detectable with NMR spectroscopy as enhanced hyperpolarized signal. A singlet state can be broken and converted to magnetization by exploiting an energy level anticrossing (cf. sec 2.5) or by modifying the molecule chemically in a way that removes the involved spin's strong coupling such that no close-to-singlet eigenstate exists any more.

2.5. Energy Level Anticrossings

The effect of energy level anticrossings, also called avoided energy level crossings or non-adiabatic crossings of energy levels is based on the adiabatic theorem [21]. The adiabatic theorem is a concept in quantum mechanics that was originally stated and proven in 1928 by the famous theoretical physicists Max Born and Vladimir Fock [22].

The basic principle of an energy level anticrossing can be explained as follows. Consider a 2-level spin-system subjected to an external magnetic field. The states, labelled $|1\rangle$ and $|2\rangle$ using bra-ket notation, can be thought of as nuclear spin angular-momentum states, each defined by a particular geometry or configuration. These states will be referred to as the diabatic states. The system wavefunction can be represented as a linear combination of the diabatic states:

$$|\Psi\rangle = a\,|1\rangle + b\,|2\rangle\,, \qquad a, b \in \mathbb{C}\,.$$

With the field absent, the energetic separation of the diabatic states is equal to $\hbar\omega_0$. The energy of state $|1\rangle$ increases with increasing magnetic field (a low-field-seeking state), while the energy of state $|2\rangle$ decreases with increasing magnetic field (a high-field-seeking state). Assuming the magnetic-field dependence is linear, the Hamiltonian matrix for the system with the field applied can be written as:

$$H = \begin{pmatrix} \vec{\mu}\cdot\vec{B}(t) - \hbar\omega_0/2 & c \\ c* & \hbar\omega_0/2 - \vec{\mu}\cdot\vec{B}(t) \end{pmatrix},$$

where $\vec{\mu}$ is the magnetic moment of the nuclear spin configuration, assumed to be the same for the two diabatic states, and c is a time-independent coupling between the two states. The diagonal elements are the energies of the diabatic states ($E_1(t)$ and $E_2(t)$). However, as H is not a diagonal matrix, it is clear that these states are not eigenstates of the Hamiltonian that includes the coupling contribution.

The eigenvectors of the matrix H are the eigenstates of the system, which we will label $|\phi_1(t)\rangle$ and $|\phi_2(t)\rangle$, with corresponding eigenvalues

$$\epsilon_1 = -\frac{1}{2}\sqrt{4c^2 + (\hbar\omega_0 - 2\vec{\mu}\cdot\vec{B}(t))^2}\,,$$
$$\epsilon_2 = +\frac{1}{2}\sqrt{4c^2 + (\hbar\omega_0 - 2\vec{\mu}\cdot\vec{B}(t))^2}\,.$$

The eigenvalues ϵ_1 and ϵ_2 are the only allowed outputs for any individual measurement of the system energy, whereas the diabatic energies $E_1(t)$ and $E_2(t)$ correspond to the expectation values for the energy of the system in the diabatic states $|1\rangle$ and $|2\rangle$.

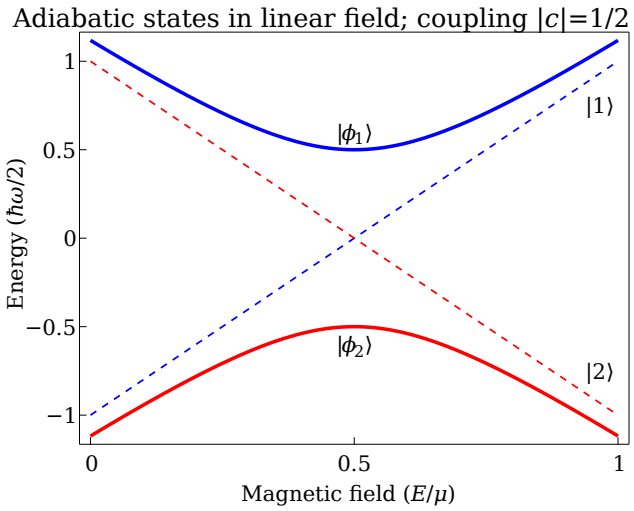

Figure 2.2.: Dependence of the diabatic and adiabatic energies on the value of the magnetic field.

Figure 2.2 shows the dependence of the diabatic and adiabatic energies on the value of the magnetic field. An avoided crossing occurs, which reflects the fact that for non-zero coupling the eigenvalues of the Hamiltonian cannot be degenerate. If an atom is initially in state $|\phi_2(t_0)\rangle$ in zero magnetic field (on the red curve, at the extreme left), an adiabatic, infinitely slow increase in magnetic field $\left(\frac{dB}{dt} \to 0\right)$ will ensure that the system remains in an eigenstate of the Hamiltonian $|\phi_2(t)\rangle$ throughout the process, meaning that it follows the red curve. A diabatic increase in magnetic field $\left(\frac{dB}{dt} \to \infty\right)$ will ensure the system follows the diabatic path, thus the dotted blue line, such that the system undergoes a transition to state $|\phi_1(t_1)\rangle$. For finite magnetic field slew rates $\left(0 < \frac{dB}{dt} < \infty\right)$ there will be a finite probability of finding the system in either of the two eigenstates. The probabilities can be calculated with the Landau-Zener-formula [21].

These results can be used to control the energy-state distribution in a population of molecules. For the case that $|\phi_1(t)\rangle$ corresponds to a close-to-triplet and $|\phi_2(t)\rangle$ corresponds to a close-to-singlet eigenstate (cf. section 2.4) a singlet-triplet-transition can be induced. If in the beginning the ensemble is in a magnetic field higher than the avoided energy-level crossing (e.g. sample at earth magnetic field, level-anticrossing below earth field) and the close-to-singlet eigenstate is overpopulated (red curve, extreme right side in Fig. 2.2), a singlet-triplet transition is achieved by either slowly lowering the magnetic field (most molecules follow red curve) and rapidly increasing it again (most molecules follow dotted blue line), or by rapidly lowering the magnetic field (most molecules follow dotted red line) and

slowly increasing it again (most molecules follow blue curve). In chapter 3 this was experimentally achieved by slowly inserting the sample into a magnetic field shield and quickly pulling it out.
Energy-level anticrossings are also responsible for the polarization transfer in SABRE experiments [23].

2.6. Zero-to Ultralow Field (ZULF) NMR

Zero- to Ultralow Field (ZULF) NMR is a technique to perform nuclear magnetic resonance measurements at zero or microtesla external magnetic fields. Since at near-zero field all major contributions to the nuclear spin Hamiltonian besides the B-field independent J-coupling term are negligible (cf. section 2.2), ZULF NMR is a pure J-coupling spectroscopy method. As explained in more detail in subsection 2.6.1, the ZULF NMR signal depends only on heteronuclear J-couplings within the molecule, which however are sufficient to provide a unique spectrum for each molecule. Thus, ZULF NMR is a suitable technique for chemical analysis and could complement established techniques in niche applications. Since it allows for the detection of internal spin-spin interactions without that they are disturbed by an external magnetic field it is particularly suitable for relaxometry, but can also be useful for quantum information processing or experiments in fundamental physics. The high field homogeneity of zero-field, together with the absence of field dependent relaxation mechanisms enables a very high spectral resolution. ZULF NMR is moreover appealing for imaging and spectroscopy inside of metal objects or in heterogeneous materials, since magnetic susceptibility inhomogeneity, unlike in high-field NMR, has no negative effects. The fact, that without an external magnetic field all nuclear spins in a system are strongly coupled allows for the formation of long-lived heteronuclear singlet-states and for a free spin-order diffusion through J-couplings, which significantly simplifies hyperpolarization of heteronuclear systems and could be used to track slow reactions. Last but not least the absence of an external magnetic field lowers the cost of ZULF NMR spectroscopy and enables a good portability of the experimental setup. On the other hand, low spin precession (Larmor) frequencies make an inductive detection of ZULF NMR signals impossible such that the use of alternative and more elaborate signal detectors like SQIDs (superconducting quantum interference devices) or atomic magnetometers becomes necessary. However, the biggest drawback of the technique is that without an external magnetic field no thermal polarization can build up which leads to a very low sensitivity of the method and makes an external polarization of the sample necessary. The easiest external source of magnetization is to prepolarize the sample with a permanent magnet. Another option is to apply hyperpolarization techniques as e.g. PHIP [24, 25]. Signal Amplification By

Reversible Exchange (SABRE, cf. section 2.3) is particularly appealing, since a zero magnetic field is the trivial solution for the propagation of parahydrogen's singlet spin order throughout the catalyst-based complex thorough J-couplings. This enables to create SABRE hyperpolarization in-situ at zero-field making it a promising source of magnetization for continuous long-term experiments with ZULF NMR, as presented in chapter 4.
Detailed information on ZULF NMR from the theoretical and experimental side can be found in [26, 27, 28, 29].

2.6.1. Origin of the Zero-Field Signal

Consider a sample at zero magnetic field containing a J-coupled spin system of two nuclei with different gyromagnetic ratios γ. The two nuclei are prepolarized such that the state $|T_{+1}\rangle = |\alpha\alpha\rangle$ is overpopulated. By applying a magnetic field B for a short time t (B-pulse), the two spins turn by different angles due do their different gyromagnetic ratios and thus different Larmor frequencies. With a carefully selected B-pulse time t one can achieve a nuclear spin polarization along $|\psi(0)\rangle = |\alpha\beta\rangle = 1/\sqrt{2}\,(|T_0\rangle + |S_0\rangle)$. Since $|T_0\rangle$ and $|S_0\rangle$ are separated in energy by hJ, after the magnetic pulse, quantum beats occur between those two states at precisely the frequency J. Recording the evolving magnetization therefore returns an oscillating signal with freqency J, which constitutes the "ZULF NMR FID". [27]

Chapter 3.

Parahydrogen Induced Polarization of Fumarate

The intrinsically low sensitivity of Nuclear Magnetic Resonance (NMR) also applies to Magnetic Resonance Imaging (MRI). Research on hyperpolarized substrates that can be applied as contrast agents for medical imaging is therefore an important subdomain of hyperpolarization research. Fumarate is a very appealing candidate among potential hyperpolarized MRI contrast agents, since it is enzymatically converted into malate within the citric acid cycle, which provides an insight into cell function. Moreover, fumarate possesses a strongly coupled two-spin system, which is capable of forming a long-lived nuclear spin singlet state at any magnetic field. Nuclear spin singlet states are immune to dipolar coupling relaxation effects and can be applied to sustain hyperpolarization for a longer time than spin lattice relaxation would usually allow. In this work it is presented that both unlabeled fumaric acid disodium salt as well as 1-^{13}C-fumaric acid disodium salt can be produced with hyperpolarized long-lived singlet states by trans-hydrogenation of a chemical precursor with enriched p-H_2. Information on the singlet states' lifetimes can be deduced.

3.1. Introduction

Nuclear Magnetic Resonance (NMR) suffers from an intrinsically low sensitivity, which also affects Magnetic Resonance Imaging (MRI). During the last two decades research on hyperpolarized MRI contrast agents was constantly performed, and lead amongst others to the application of hyperpolarized gases for imaging of the lung [5], metabolic imaging of cancer by observing the conversion of hyperpolarized

^{13}C-pyruvate to ^{13}C-lactate [30, 31] and recently an early-stage detection of cell necrosis in mice by observing the conversion of hyperpolarized [1,4-$^{13}C_2$]-fumarate to [1,4-$^{13}C_2$]-malate [32, 33, 34]. The latter uses the enzymatic conversion of fumarate to malate (cf. Fig. 3.1), which happens within the citric acid cycle, to obtain an insight into cell function.

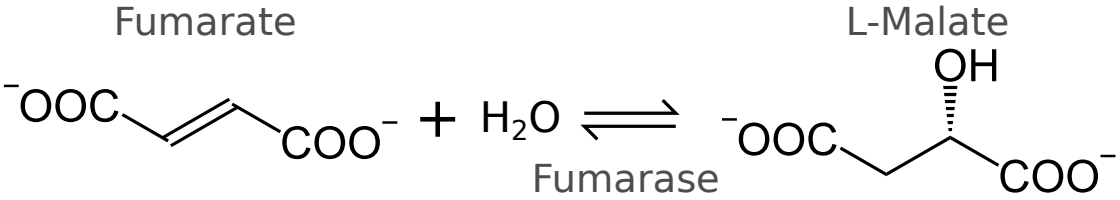

Figure 3.1.: The enzyme fumarase hydrates fumarate to L-malate by *trans*-addition of a hydroxyl group and a hydrogen atom. This reaction takes place in cells within the citric acid cycle.

So far, mostly ^{13}C-imaging was applied in combination with hyperpolarized contrast agents in solution, since ^{13}C T_1 relaxation times exceed ^{1}H T_1 times roughly by an order of magnitude, hereby assuring a longer time to perform the medical application with the hyperpolarized substrate. However, protons provide a 100 times larger NMR sensitivity by natural abundance, therefore research on a hyperpolarized ^{1}H MRI contrast agent is of great interest. To overcome the limitation of short proton T_1 times hyperpolarized nuclear spin singlet-states [35, 36, 37] are a promising approach. Since nuclear spin singlet-states are immune to relaxation via dipolar coupling [38] their lifetime T_S often significantly exceeds T_1. The drawback of hyperpolarized molecular singlet-states is that themselves they are NMR-silent and need to be converted into detectable magnetization in order to release the stored hyperpolarization. The most direct way to break a singlet-state is to remove the chemical equivalence of the involved protons, thus getting a weakly coupled spin system. This can be achieved by modifying the molecule chemically [39, 40]. The enzymatic conversion of fumarate to malate induces a significant chemical shift difference between fumarate's protons thus being able to break a nuclear spin singlet state on fumarate, besides revealing cell function. This makes fumarate a particularly appealing candidate for a hyperpolarized metabolic ^{1}H MRI contrast agent.

In this work, fumaric acid disodium salt in a hyperpolarized nuclear spin singlet-state (PHIP fumarate) is produced by a pairwise *trans*-hydrogenation of acetylene dicarboxylic acid disodium salt with enriched p-H_2 by the aid of the *trans*-catalyst [RuCp*(MeCN)$_3$]PF_6 [41, 42, 43]. It was found that the *trans*-hydrogenation reaction works in water which is a huge benefit for biocompatibility, thus all presented

experiments were performed in D_2O. Experiments were performed with both unlabeled and 1-^{13}C-fumarate. A scheme of the reaction can be found in Fig. 3.2.

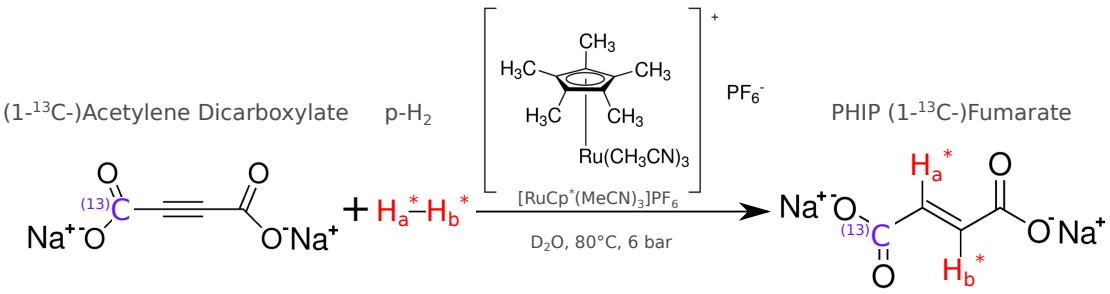

Figure 3.2.: Production of hyperpolarized (1-^{13}C-)fumaric acid disodium salt in long-lived singlet state by pairwise *trans*-hydrogenation of (1-^{13}C-)acetylenedicarboxylic acid disodium salt by the aid of the ruthenium based catalyst $[RuCp^*(MeCN)_3]PF_6$. The reaction was performed in D_2O at 80°C with 6 bar p-H_2 pressure.

For unlabeled PHIP fumarate the only method to break its singlet state that was found is to convert the molecule to non-symmetrical L-malate enzymatically. For PHIP 1-^{13}C-fumarate the ^{13}C label breaks the protons' magnetic equivalence and thus energy level anticrossings between NMR-silent singlet states and NMR-active triplet states appear, one of them at a magnetic field of 417 nT [1] [44]. By exploiting the avoided energy level crossing 1-^{13}C-fumarate's hyperpolarized singlet state can be turned into detectable hyperpolarization either on the ^{13}C label or on protons [45]. Experimentally this can be achieved either with field-cycling experiments [46], which is done in this work, or fully inside an NMR spectrometer with spin-locking radiofrequency sequences [47, 48] like S2M [37] or S2hM [49, 50] [1]. Exploiting energy level anticrossings is a more reproducible technique to gain information on a molecule's singlet state compared to enzymatic conversion. However, singlet states in molecules without avoided energy level crossings are expected to have the longest lifetimes T_S due to even fewer relaxation mechanisms, which justifies the effort to optimize the vulnerable enzymatic conversion of fumarate to L-malate.

3.2. Experimental Setup and Procedure

The *trans*-hydrogenation of acetylene dicarboxylate to PHIP fumarate was performed inside 5 mm OD screw cap NMR tubes by Wilmad (507-TR-7) sealed with a septum screw cap. Samples were prepared under inert atmosphere and consisted of

[1] Work performed by James Eills, PhD student associated to Malcolm H. Levitt's group at the University of Southampton, UK.

40 mg (1-^{13}C-)acetylene dicarboxylic acid disodium salt, 5 mg $[RuCp^*(MeCN)_3]PF_6$ and 1 ml D_2O. For experiments with enzymatic conversion the amount of D_2O was reduced to 0.7 ml and a syringe containing 50 units fumarase from porcine heart (according to 20 μl fumarase suspension F1757 by Sigma-Aldrich) dissolved in 0.3ml D_2O was prepared for each sample. For field cycling experiments the sample volume was reduced with a factor of 0.6 in order to make the whole sample volume fit in the zero-field area of the applied μ-metal shield (Lakeshore Cryotronics 4060 Small zero gauss chamber). Parahydrogen was enriched to 92% with a commercial Bruker BPHG 90 parahydrogen generator and filled at 10 bar into a 1 l aluminum gas bottle. The outlet line of the gas bottle was equipped with a pressure regulator set to 6 bar and a hollow needle at the end to inject parahydrogen into the sample tube through the septum cap. NMR measurements were performed on a Bruker AVANCE II 300 MHz spectrometer.

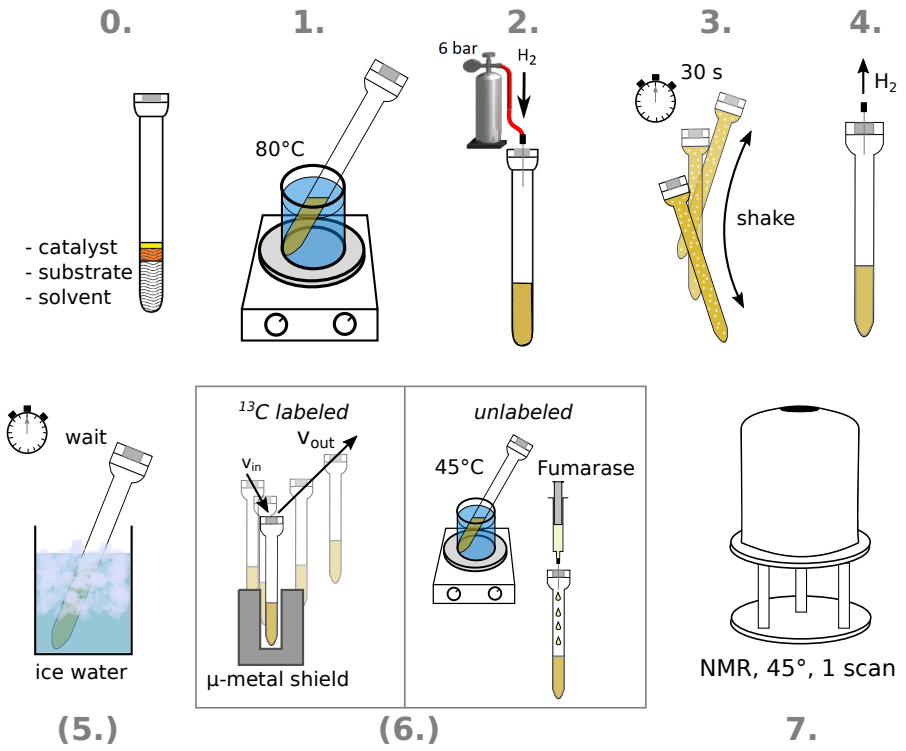

Figure 3.3.: Scheme of the procedure for experiments with PHIP fumarate. 1. The sample tube is heated to 80°C in a heated water bath. 2. p-H_2 at a pressure of 6 bar is injected into the sample tube. 3. The tube is shaken vigorously for 30 s. 4. Pressure is released from the tube with a hollow needle. 5. Optional: The sample is placed in ice water to wait for a defined delay with interrupted hydrogenation reaction. 6. Optional: For ^{13}C-labeled PHIP fumarate: For field cycling the sample tube is slowly (∼5 s) inserted into the μ-metal shield and quickly (<1 s) pulled out. For unlabeled PHIP fumarate: The sample is heated to 45°C in a heated water bath, subsequently fumarase solution at room temperature is injected through the septum, effectuating a mixture at 38°C. 7. An NMR spectrum with 1 scan after applying a 45° pulse is acquired as quickly as possible.

A scheme of the experimental procedure is shown in Fig. 3.3. As a first step the sample tube is heated to 80°C in a heated bath. Then, p-H_2 at a pressure of 6 bar is injected into the sample tube through the septum cap and the tube is shaken vigorously for 30 s. Afterwards, the p-H_2 pressure is released from the tube with a hollow needle. For some experiments, the sample is subsequently placed in an ice water bath to wait for a certain delay with interrupted hydrogenation reaction. This step reveals information about the singlet state lifetime T_S in the hyperpolarized product molecule. For field cycling experiments with ^{13}C-labeled PHIP fumarate the sample tube is slowly (∼5 s) inserted into the μ-metal shield

and quickly (<1 s) pulled out in order to exploit the avoided energy level crossing. For enzyme experiments on unlabeled PHIP fumarate the sample is heated to 45°C in a heated bath before fumarase solution at room temperature is injected through the septum, effectuating a mixture at 38°C. The enzymatic activity of fumarase is maximal between 37°C and 40°C. In the last step an NMR spectrum with one scan using a 45° pulse is acquired as quickly as possible. All steps from heating the sample to acquisition constitute one shake cycle. Up to ten shake cycles can be performed with one sample. At the end of each experiment, after all hyperpolarization had decayed a 90° one-scan thermal reference was acquired under the same conditions.

3.3. Results and Discussion

3.3.1. PHIP 1-^{13}C-Fumaric Acid Disodium Salt

Figure 3.4 shows resulting hyperpolarized proton NMR spectra of 1-^{13}C-fumaric acid disodium salt for NMR acquisition directly after shaking the sample and pressure relase, as well as after field cycling, which was performed directly after pressure release. In comparison with the thermal reference it can be observed that the directly acquired spectrum in Fig. 3.4 a) is hyperpolarized with the typical antiphasic PHIP pattern, although it is expected to form an NMR-silent singlet state. This effect is based on spontaneous polarization transfer due to singlet-triplet mixing in the three-spin system (^{13}C label and two PHIP protons). [20] Moreover, singlet-triplet transitions can occur during the *trans*-hydrogenation reaction process. However, the spectrum after field-cycling in Fig. 3.4 b) shows a factor ∼2 bigger 1-^{13}C-fumarate signal intensity, which proves that the majority of 1-^{13}C-fumarate molecules must have been in an undetectable hyperpolarized singlet state, whose hyperpolarization has been converted into detectable ^{1}H magnetization during field cycling. Quantitative comparison with the thermal reference reveals signal enhancement factor of 75 after field cycling. Compared to the theoretically possible enhancement on protons of $\sim 2 \cdot 10^4$ this value is low. The reason for this is that only a small fraction of molecular singlet states in the sample is converted into observable hyperpolarization during the manual field cycling procedure. This could be significantly improved by performing the field cycling step several times in a row within the time limitation of fumarate's proton T_1 relaxation time. Moreover, more than half (∼53%) of the yielded observable hyperpolarization is lost due to T_1 relaxation during the 10 s delay between field cycling and acquisition. (table of T_1 times cf. appendix A).

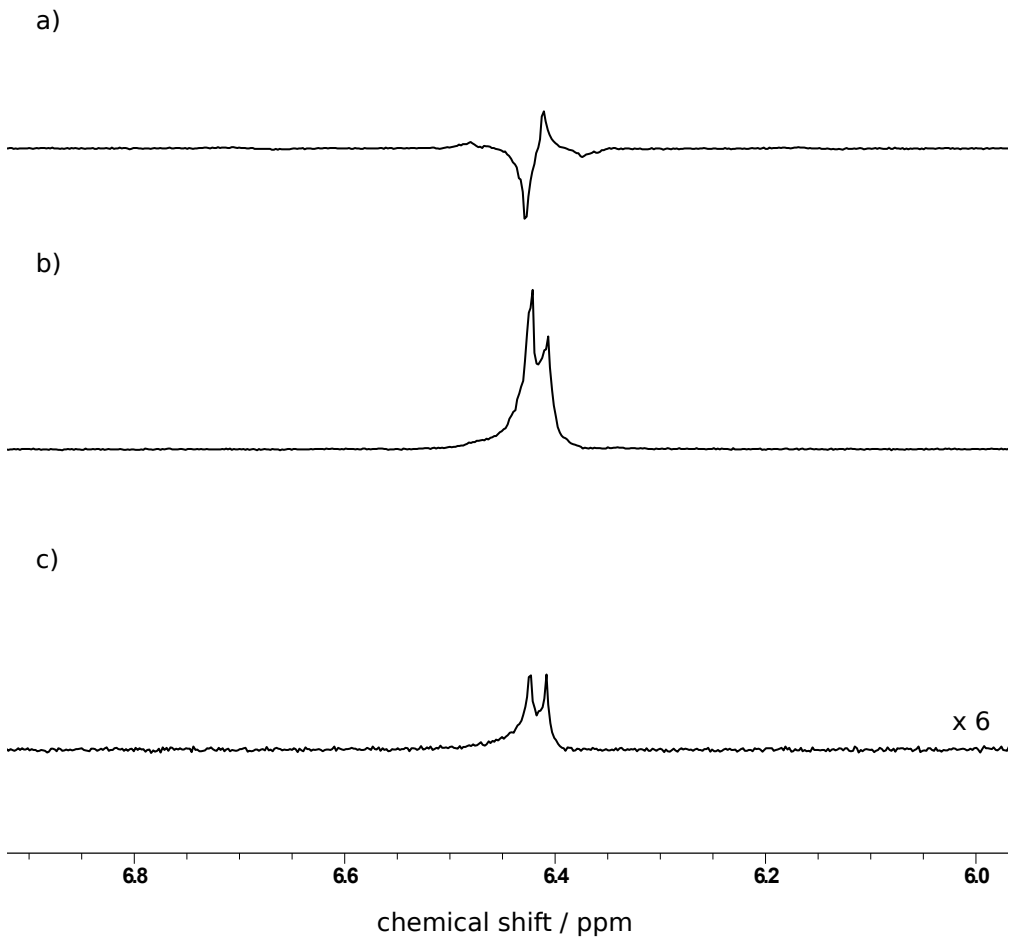

Figure 3.4.: Resulting proton NMR spectra of PHIP 1-^{13}C-fumaric acid disodium salt: a) for NMR detection directly after shaking the sample tube and pressure release, b) after field cycling in μ-metal chamber. Comparison with the thermal reference reveals a signal enhancement factor of 75. c) Thermal reference spectrum after 6 shake cycles, scaled $\times$6.

Accordingly, Fig. 3.5 depicts hyperpolarized ^{13}C NMR spectra of 1-^{13}C-fumaric acid disodium salt for acquisition directly after shaking the sample and pressure relase, as well as after field cycling, which was performed directly after pressure release. Again, the directly acquired spectrum appears hyperpolarized with the typical antiphasic PHIP pattern, which is due to singlet-triplet mixing, either spontaneous [20] or during *trans*-hydrogenation and consistent with the observation on ^{1}H. After field cycling the 1-^{13}C-fumarate signal intensity is again $\sim$2 times higher than after direct acquisition without field cycling. This confirms that a majority of 1-^{13}C-fumarate molecules must have formed an unobservable nuclear spin singlet

state after the hydrogenation reaction. In comparison with the thermal reference the 1-^{13}C-fumarate signal after field cycling is enhanced with a factor of 1900. The theoretical maximum enhancement on ^{13}C at a magnetic field of 7 T and a temperature of 290 K amounts to a factor of $\sim 8 \cdot 10^4$, which is again significantly more than observed and can be explained with an only partial exploitation of the energy level anticrossing. During the 10 s delay between field cycling and acquisition about 27% of the ^{13}C polarization is lost.

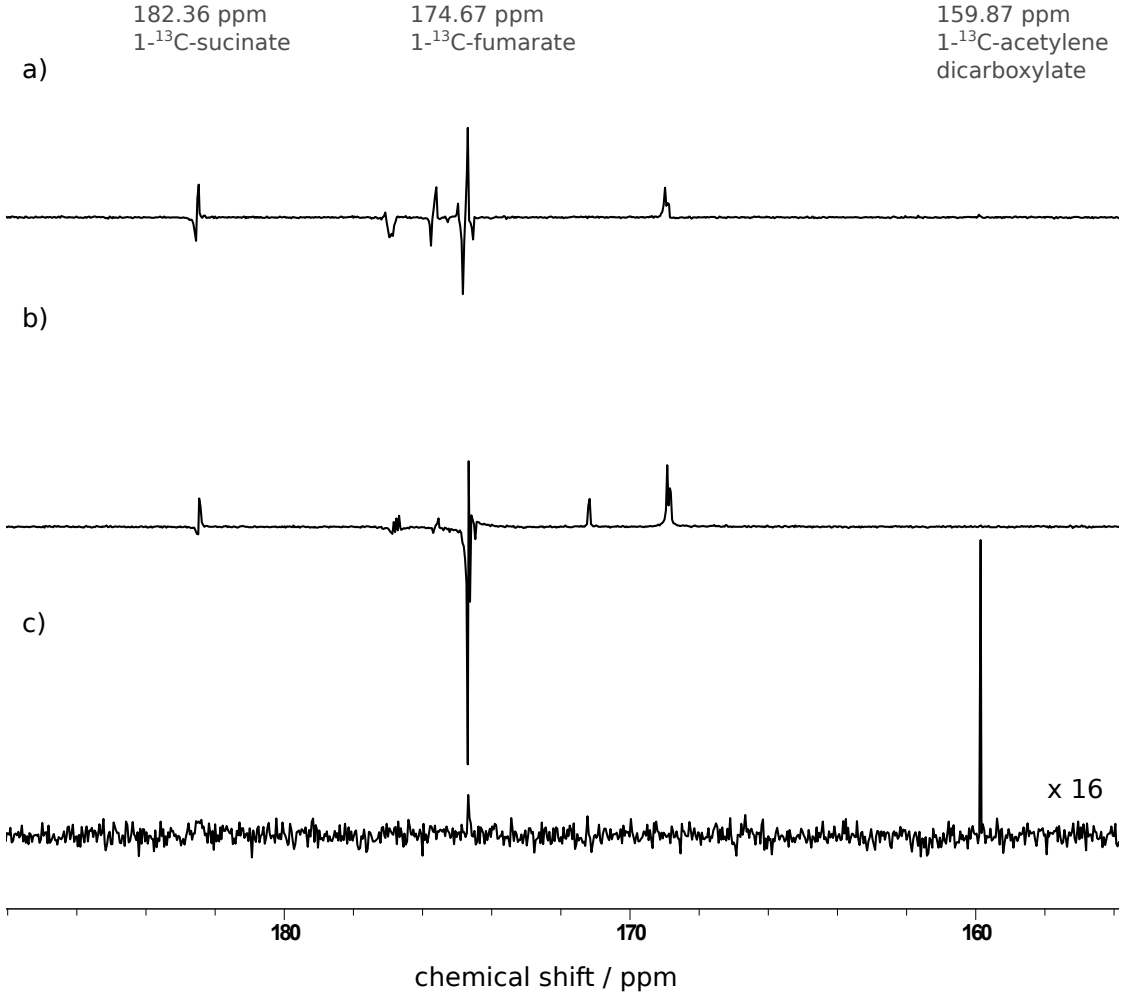

Figure 3.5.: Resulting ^{13}C NMR spectra PHIP 1-^{13}C-fumaric acid disodium salt: a) for NMR detection directly after shaking the sample tube and pressure release, b) after field cycling in μ-metal chamber. Comparison with the thermal reference reveals a signal enhancement factor of 1900. c) Thermal reference spectrum after 10 shake cycles, scaled $\times$16.

Summarizing up, the above results prove that a long-lived nuclear spin singlet state exists on 1-^{13}C-fumarate. In cooperation with the University of Southampton the proton singlet state lifetime T_S of 1-^{13}C-fumaric acid disodium salt in D_2O was determined to be (46±7) s at 11.4 T [2], which exceeds the ^{13}C T_1 relaxation time of 32 s. This finding makes 1-^{13}C-fumaric acid disodium salt a promising candidate for hyperpolarized metabolic magnetic resonance imaging on ^{1}H as well as on ^{13}C.

3.3.2. PHIP Fumaric Acid Disodium Salt

Unlabeled fumaric acid disodium salt posesses a pair of strongly coupled protons that are fully chemically and magnetically equivalent, therefore no physical means for transitions into another quantum mechanical state exists within the molecule. Hence, unlabeled fumarate is expected to form a proton spin singlet state with a significantly longer lifetime T_S compared to 1-^{13}C-fumarate. Due to the lack of energy level anticrossings the equivalence of the two protons must be broken chemically in order to convert hyperpolarization stored in its singlet state into detectable magnetization. To achieve this the enzymatic conversion of fumarate into L-malate by the aid of the enzyme fumarase is applied (see Fig. 3.1). In order to gain information about unlabeled fumarate's singlet state lifetime PHIP hyperpolarized samples were stored in an ice water bath for different delays between the *trans*-hydrogenation reaction and fumarase injection. (cf. Fig. 3.3)

Figure 3.6 shows resulting ^{1}H NMR spectra of unlabeled PHIP fumaric acid disodium salt for NMR acquisition directly after shaking the sample tube and pressure release, after fumarase injection that was performed directly after the *trans*-hydrogenation and pressure release and after fumarase injection that was performed 30 min after the *trans*-hydrogenation. For comparison there is a thermal one-scan reference spectrum. In comparison with the thermal reference it can be observed that already PHIP fumarate without fumarase injection (Fig. 3.6 a)) is signal enhanced, although it is expected to form an NMR silent singlet state. In the thermal one-scan reference the fumarate peak is within the noise. This effect is too strong to be explained by spontaneous singlet-triplet mixing in the molecules with natural abundance ^{13}C and confirms the assumption that some detectable hyperpolarization is created during catalysis. After fumarase injection that is performed directly after hydrogenation (Fig. 3.6 b)) an aniphasically enhanced L-malate peak occurs at 4.20 ppm, which exceeds the former fumarate signal by a factor of ∼5. This proves that a majority of the fumarate molecules after hydrogenation must have formed an undetectable singlet state whose hyperpolarization was transformed into detectable magnetization by the enzymatic

[2] Work performed by James Eills, PhD student associated to Malcolm H. Levitt's group at the University of Southampton, UK. To be published soon in cooperation.

conversion. When fumarase is added 30 min after the hydrogenation reaction was stopped by pressure release and temperature decrease (ice water bath) there is still a detectable antiphasic PHIP L-malate signal at 4.20 ppm. Since singlet state relaxation follows an exponential decay with time constant T_S back to thermal polarization it is supposed that relaxation is practically complete after the 5-fold relaxation constant T_S, which in Fig. 3.6 c), after a delay of 30 min, is apparently not the case. Hence, it can be deduced that $T_S \geq 6$ min, which exceeds fumarate's ^{1}H T_1 time of (13.3±0.6) s by a factor ≥27. The findings on fumarate's proton singlet state lifetime T_S are in accordance with findings by Zhang et al. on T_S of dimethyl fumarate with deuterated methyl groups (T_S= 5.48±0.29 min) [40]. Deuterated methyl groups result in a significant prolongation of the singlet-state lifetime compared to protonatec methyl groups, since relaxation mechanisms are truncated. A complete absence of methyl groups is expected to result in an even longer proton singlet state on fumarate. Several hyperpolarized *trans*-hydrogenation side product resonances were detectable in the spectra, which is discussed in detail in section 3.3.3

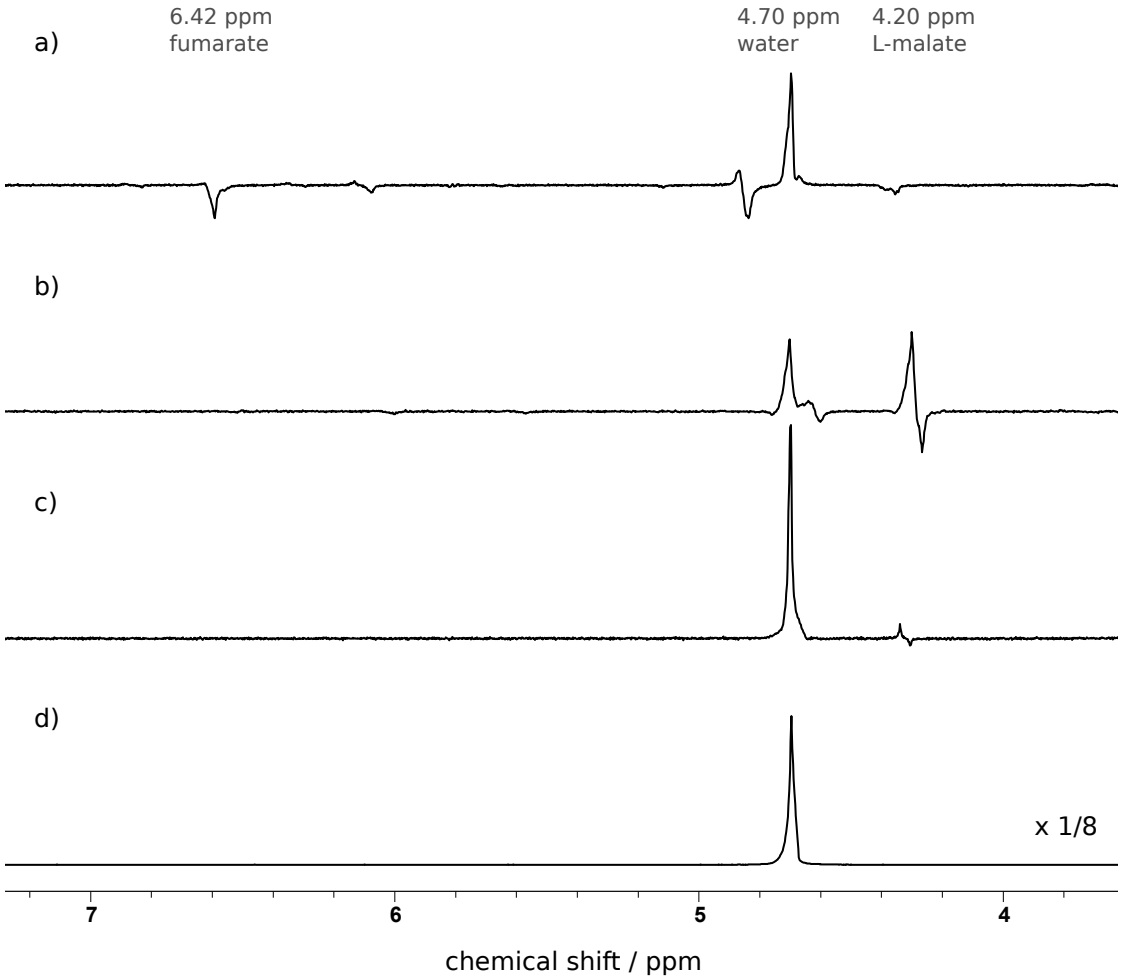

Figure 3.6.: Resulting ^{1}H NMR spectra of PHIP-fumaric acid disodium salt: a) for NMR detection directly after shaking the sample tube and pressure release, b) after fumarase injection that was performed directly after the *trans*-hydrogenation and pressure release, c) after fumarase injection that was performed 30 min after the *trans*-hydrogenation. d) Thermal reference spectrum after one shake cycle, scaled $\times 1/8$

In order to determine the exact singlet state relaxation constant T_S of fumaric acid disodium salt in D_2O the enzymatic conversion into malic acid disodium salt needs to be optimized in terms of conversion rate per units time and reproducibility. It was found that the enzymatic conversion is 1.8-fold faster in a D_2O-based monopotassium phosphate buffer at pH 7.6,[3] compared to the conver-

[3] 100 mM solution of monopotassium phosphate in D_2O, adjusted to pH 7.6 at 25°C with a 100 mM solution of potassium hydroxide in D_2O.

sion in pure D_2O. On the other hand, experiments have shown that 10 mM of $[RuCp^*(MeCN)_3]PF_6$ *trans*-PHIP-catalyst in the buffer solution slows the enzymatic conversion of fumarate to malate down by a factor of approx. 3 and stops the conversion at 39%. Adding 17 mM of ethylenediaminetetraacetic acid (EDTA), which according to literature reverses the inhibition of enzyme activity by metal ions [51], was not able to increase the speed of the enzymatic conversion, however it was able to stop the conversion at 52%. Without $[RuCp^*(MeCN)_3]PF_6$ in the buffer solution the enzymatic conversion reached its equilibrium at approx. 68% malate. All optimization experiments described above were performed with 25 units fumarase enzyme from porcine heart (according to 10 μl fumarase suspension F1757 by Sigma-Aldrich) per 1 ml D_2O or buffer solution, respectively. The only reliable method that was found to increase the velocity of the enzymatic conversion of fumarate to malate despite the presence of $[RuCp^*(MeCN)_3]PF_6$ is to increase the amount of enzyme significantly. Despite the high cost of this method it will be chosen for further experiments. In order to increase the reproducibility of results after enzymatic conversion of fumarate in the nuclear spin singlet state into hyperpolarized malate it is crucial to control delay times during the experiment very precisely. The experimental method presented in Fig. 3.3 has an inaccurate timing, because all steps are carried out manually and delays are determined with a stopwatch. Hence, it is only appropriate for proof-of-principle experiments. In order to perform accurate experiments for a quantitative analysis of T_S, an experimental setup is planned where the PHIP reaction is performed by bubbling p-H_2 through the sample solution, which afterwards is transported through a flexible tube to another NMR tube that contains buffer solution and enzyme. The sample transport is going to be realized with pressure differences within the experimental setup which will be computer-controlled.

3.3.3. *trans*-Hydrogenation Side Products

In all *trans*-hydrogenation PHIP reactions with $[RuCp^*(MeCN)_3]PF_6$ as catalyst hydrogenation side products including overreduction to succinate did occur, which is consistent with literature findings [52, 53, 41, 43].

Figure 3.7 shows a selection of PHIP hyperpolarized NMR spectra after the *trans*-hydrogenation of acetylenedicarboxylate to fumarate together with according thermal references. Several hyperpolarized peaks that do not originate from fumarate can be observed in each spectrum. These resonances belong to side products of the *trans*-hydrogenation reaction with $[RuCp^*(MeCN)_3]PF_6$ as catalyst. From high resolution thermal reference spectra that were recorded after the experiments for this chapter (cf. appendix A) it can be derived that between 40% and 50% of the precursor is turned into side products, which exceeds the average detected fumarate yield of 19.4% by factor $\sim$2.5.

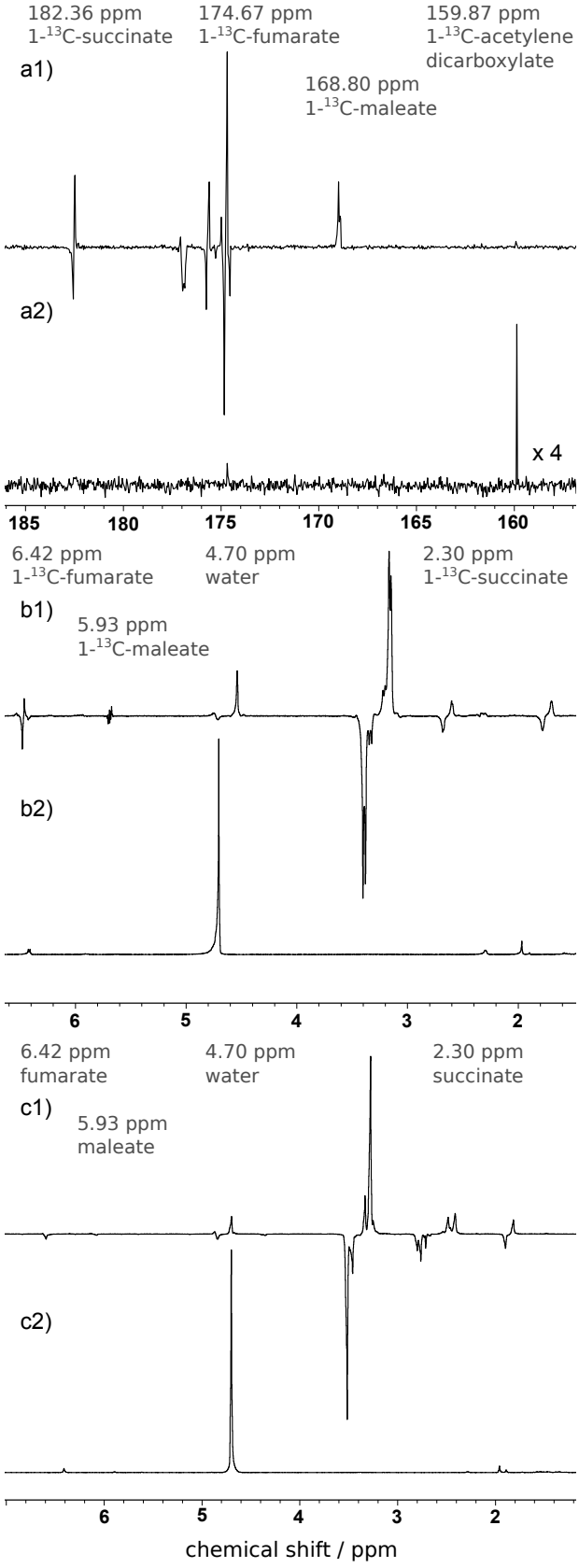

Figure 3.7.:
NMR spectra after the *trans*-hydrogenation of (1-^{13}C-)acetylenedicarboxylic acid disodium salt with enriched parahydrogen with according thermal references. Every PHIP spectrum shows hyperpolarized resonances which belong to *trans*-hydrogenation side products.
a1) ^{13}C NMR spectrum after PHIP *trans*-hydrogenation of ^{13}C labeled substrate. Hyperpolarized side products can be found at 168.8 ppm (1-^{13}C-maleate) and 175-180 ppm.
a2) Thermal reference spectrum for a1) acquired after 10 shake cycles, scaled $\times 4$.
b1) ^{1}H NMR spectrum after PHIP *trans*-hydrogenation of ^{13}C labeled substrate. Hyperpolarized side products can be found at 3.0-3.5 ppm, 5.5-6.0 ppm and 1.2-2.9ppm.
b2) Thermal reference spectrum for b1), acquired after 6 shake cycles.
c1) ^{1}H NMR spectrum after PHIP *trans*-hydrogenation of unlabeled substrate. Hyperpolarized side products occur at the same frequencies as in b1).
c2) Thermal reference spectrum for c1), acquired after 7 shake cycles.

In the first place the *cis*-hydrogenation side product maleic acid disodium salt needs to be mentioned. Maleate is the *cis*-byproduct of the reaction path that produces the *trans*-alkene fumarate. In the experiments presented in this chapter maleic acid disodium salt was produced with an average yield of 2.3% and occurs in the proton NMR spectra of Fig. 3.7 at 5.93 ppm, and at 168.80 ppm in the ^{13}C NMR spectra. Thus, the average ratio of maleate to fumarate was 0.12. Markus Leutzsch and colleagues have recently published that [RuCp*(MeCN)$_3$]PF$_6$ and other [Cp*Ru]-based catalysts lead to the formation of ruthenium carbenes by geminal hydrogenation of the triple bond of alkynes.[52, 53] These findings directly explain the strongly hyperpolarized side product that occurs at 3.2 ppm, which by far dominates the PHIP proton NMR spectra in Fig.3.7 with respect to signal amplitude. The *trans*-hydrogenation side product at 3.2 ppm is produced with 9% yield in average and shows a signal enhancement factor of 4000 on protons for NMR acquisition directly after shaking the sample and pressure release, e.g. in Fig. 3.7 b1), c1). Indirectly, the formation of ruthenium carbenes leads as well to the side product NMR peaks that occur between 1.2 ppm and 2.9 ppm in the proton NMR spectra of Fig. 3.7 including the overreduced alkane succinic acid disodium salt, whose average yield in the presented experiments was 12.5% and which occurs at 2.30 ppm in ^{1}H and at 182.36 ppm in ^{13}C spectra (succinate to fumarate ratio is 0.64). Despite numerous efforts the exact chemical structure of the side products could not be determined yet. Although the creation of side products does not affect the reaction path that produces hyperpolarized fumarate in its nuclear spin singlet state, it constitutes a significant drawback because it consumes a large fraction of the precursor, thus reducing the fumarate yield. Since many of the hydrogenation side products, as maleate or ruthenium carbenes, are toxic, their formation is a huge issue for possible *in vivo* applications. Therefore, before seriously attempting applications of PHIP fumarate, the reaction must be modified to strongly reduce or eliminate the formation of side products while increasing the fumarate yield.

A approach to reduce the formation of side products and to increase the fumarate yield, that was recently found within this work, is adding sodium sulfite (E 221) to the sample solution. Fig. 3.8 a) shows a thermal ^{1}H NMR spectrum after the *trans*-hydrogenation reaction of 250mM acetylenedicarboxylic acid disodium salt with 10 mM [RuCp*(MeCN)$_3$]PF$_6$ as catalyst in D$_2$O. Fig. 3.8 b) shows a thermal ^{1}H NMR spectrum after the same reaction, but with 100 mM sodium sulfite additive in the sample solution.

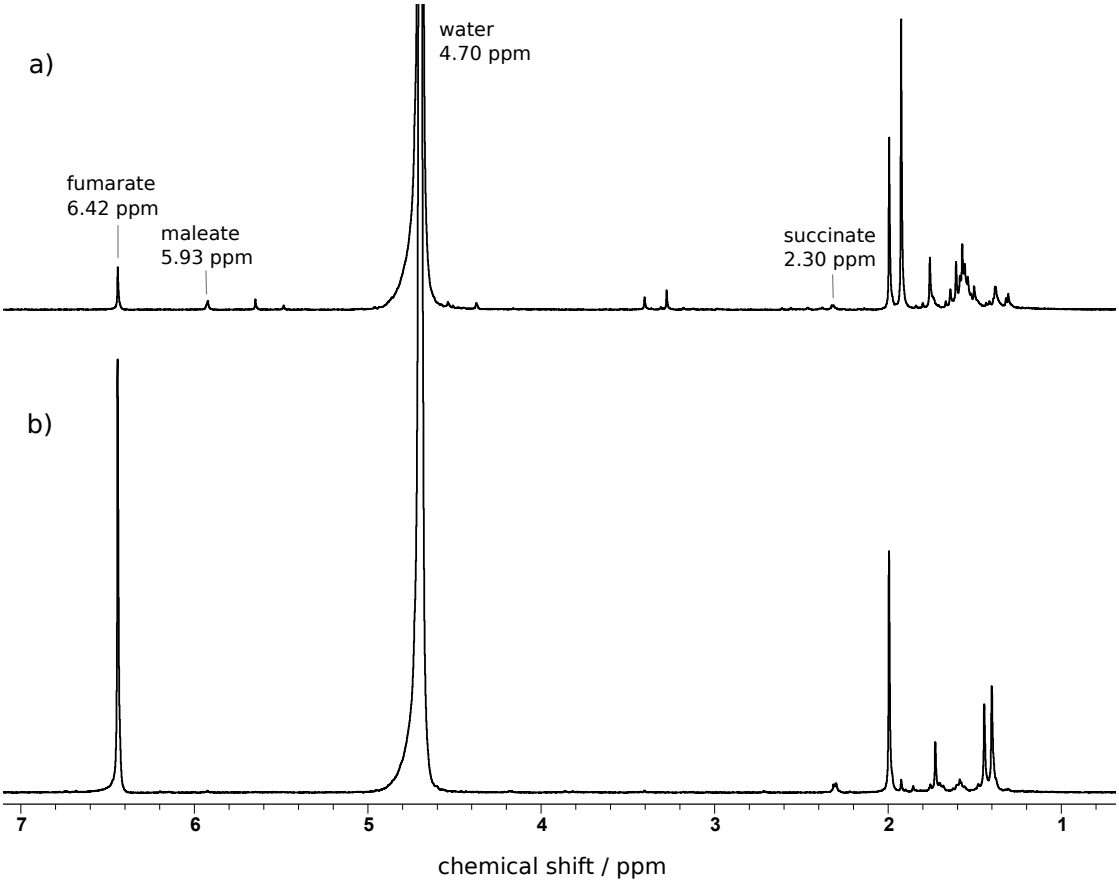

Figure 3.8.: Thermal ^{1}H NMR spectra a) after the *trans*-hydrogenation reaction of 250 mM acetylenedicarboxylic acid disodium salt with 10 mM $[RuCp^{*}(MeCN)_3]PF_6$ as catalyst in D_2O. The sample was reacted with hydrogen for 300 s under 5 bar pressure and 80°C. b) as a) but with 100 mM sodium sulfite additive in the sample solution.

It can be deduced that the sodium sulfite additive increases the fumarate yield by factor 7.3, while reducing the maleate to fumarate ratio by factor >30 from 0.12 to 0.0036 and the succinate to fumarate ratio by factor > 10 from 0.64 to 0.050. Thermal ^{13}C NMR spectra after the same reaction with 1-^{13}C-acetylene dicarboxylate as substrate (see app. A) reveal that the total yield of *trans*-hydrogenation side products is reduced by factor 2.5 to 18% in average.

Fig. 3.9 shows a selection of proton NMR spectra after PHIP-experiments (procedure see Fig. 3.3) with (1-^{13}C-)acetylene dicarboxylate as substrate and sodium sulfite additive in the sample solution. Fig. 3.9 a) shows the result of a PHIP reaction on unlabeled acetylene dicarboxylate as substrate. In contrary to Fig. 3.6 a),

which shows the same reaction without sodium sulfite, no hyperpolarized fumarate signal occurs. This indicates that sodium sulfite helped to eliminate singlet-triplet mixing during catalysis. Fig. 3.9 b) shows the PHIP spectrum after *trans*-hydrogenation of 1-^{13}C-acetylene dicarboxylate. In this case a significantly hyperpolarized antiphase 1-^{13}C-fumarate signal can be observed. Since singlet-triplet mixing during catalysis was proven to be negligible with sodium sulfite additive this signal must be due to spontaneous polarization transfer to ^{13}C spins in symmetric molecules [20]. In Fig. 3.9 c) the result of the PHIP *trans*-hydrogenation of 1-^{13}C-acetylene dicarboxylate after cycling using a zero gauss chamber is shown. Field cycling in a μ-metal chamber converts a part of the singlet magnetization in the sample into observable magnetization by exploiting the molecule's energy level anticrossing at 417 nT.(cf. section 2.5) The result is a strong in-phase hyperpolarization of the fumarate resonance, which exceeds the fumarate polarization in Fig. 3.9 b) by factor 3 in magnitude and proves that a majority of the fumarate polarization was stored in an NMR-silent singlet state. A quantitative comparison with the thermal reference (Fig. 3.9 d)) reveals an NMR signal enhancement factor of 270, which is 3.6 times higher than the proton signal enhancement factor without sodium sulfite additive in Fig. 3.4. As far as hyperpolarized side products are concerned, ruthenium carbenes at 3.2 ppm are still detectable, but in comparison with experiments without sodium sulfite additive like in Fig. 3.7 their intensity and amount are reduced by factor 8.

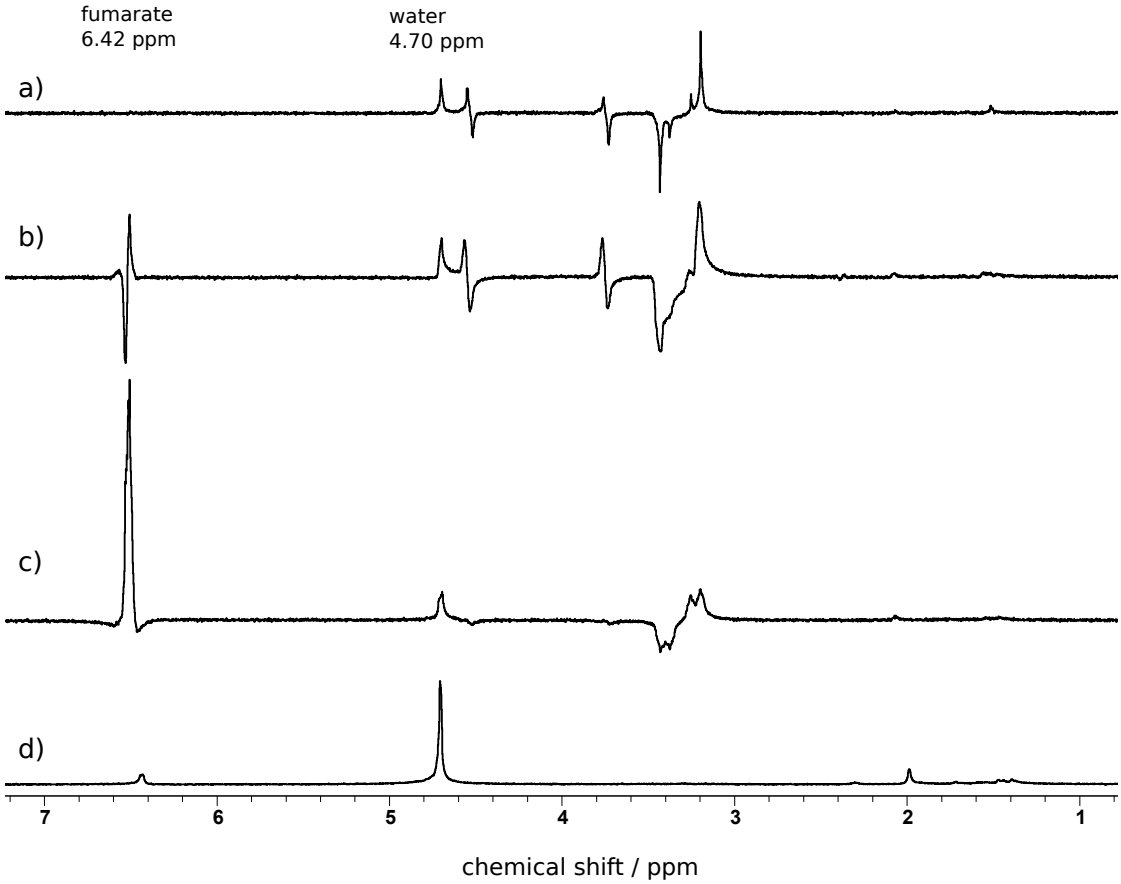

Figure 3.9.: ^{1}H NMR spectra (1 scan) after *trans*-hydrogenation of 250 mM (1-^{13}C-) acetylene dicarboxylic acid disodium salt with enriched p-H_2 (92%) in D_2O with 10 mM $[RuCp^*(MeCN)_3]PF_6$ as catalyst and with 100 mM sodium sulfite additive in the sample solution. a) For unlabeled substrate and NMR detection (45°-pulse) directly after shaking the sample tube and pressure release. b) For ^{13}C labeled substrate and NMR detection (45°-pulse) directly after shaking the sample tube and pressure release. c) For ^{13}C labeled substrate and NMR detection (90°-pulse) after field cycling in μ-metal chamber. Comparison with the thermal reference reveals a signal enhancement factor of 270. d) Thermal reference (90°-pulse) acquired after 6 shake cycles with labeled substrate.

Fig. 3.10 shows a selection of ^{13}C NMR spectra after PHIP-experiments using 1-^{13}C-acetylene dicarboxylate as substrate and sodium sulfite additive in the sample solution. Fig. 3.10 a) shows the PHIP spectrum right after the *trans*-hydrogenation. A hyperpolarized antiphase 1-^{13}C-fumarate signal can be observed, which again arises from spontaneous polarization transfer to ^{13}C spins in symmetric

molecules.[20] After field cycling in a zero gauss chamber (Fig. 3.10 b)) a strongly hyperpolarized in-phase 1-^{13}C-fumarate resonance can be observed, that exceeds the spontaneous polarization transfer by factor 2. Quantitative comparison with the thermal reference spectrum (Fig. 3.10 c)) reveals a signal enhancement factor of 2500, which is 1.3 times higher than the ^{13}C signal enhancement factor without sodium sulfite additive in Fig. 3.5. Hyperpolarized *trans*-hydrogenation side products are still detectable, but in comparison to experiments without sodium sulfite additive, like in Fig. 3.7, their intensity is strongly reduced.

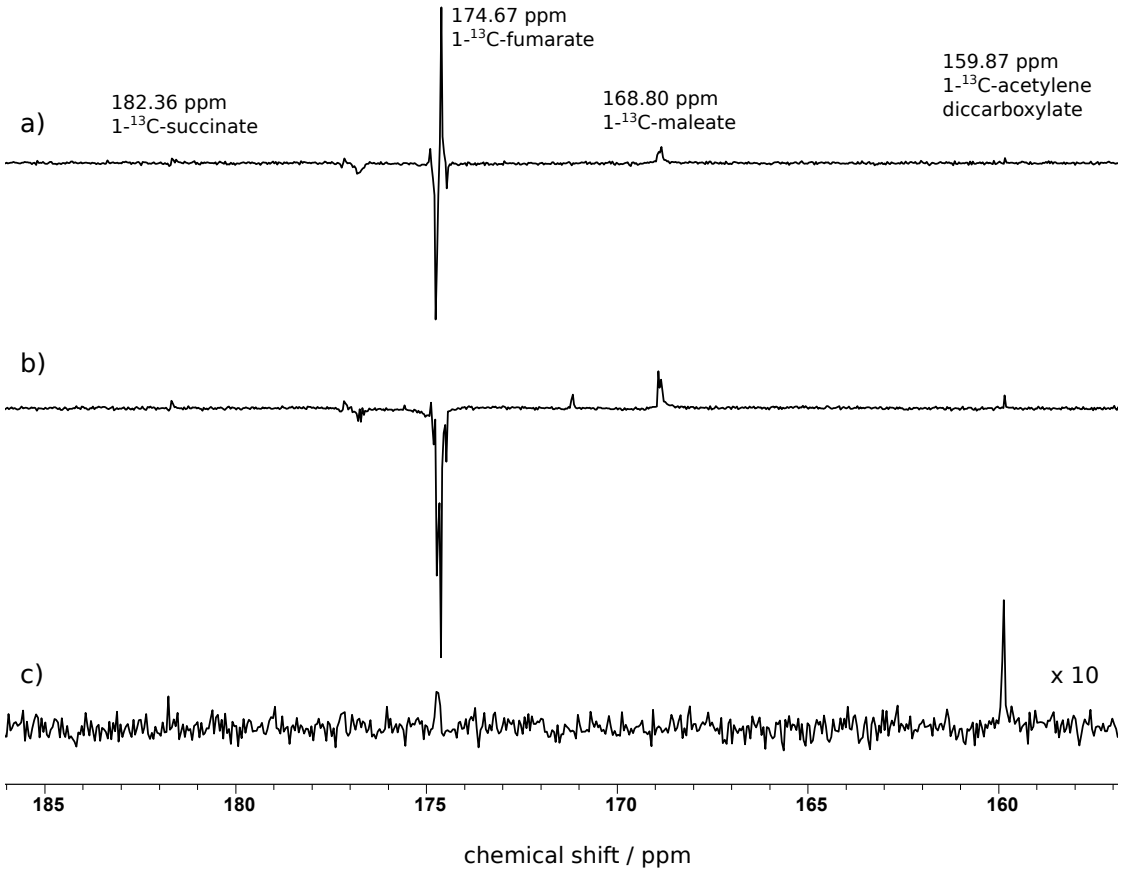

Figure 3.10.: ^{13}C NMR spectra (1 scan) after *trans*-hydrogenation of 250 mM 1-^{13}C-acetylene dicarboxylic acid disodium salt with enriched p-H_2 (92%) in D_2O with 10 mM $[RuCp^*(MeCN)_3]PF_6$ as catalyst and with 100 mM sodium sulfite additive in the sample solution. a) For NMR detection (45°-pulse) directly after shaking the sample tube and pressure release. b) For NMR detection (90°-pulse) after field cycling in μ-metal chamber. Comparison with the thermal reference reveals a signal enhancement factor of 2500. c) Thermal reference (90°-pulse) acquired after 6 shake cycles, scaled $\times$10.

Overall it can be stated that adding sodium sulfite to the sample solution increases the fumarate yield and the signal enhancement values while significantly reducing the production of unwanted side products. Other tests have proven that sodium sulfite does not affect the activity of the fumarase enzyme. Thus, the addition of sodium sulfite is a promising approach to optimize the *trans*-hydrogenation reaction with $[RuCp^*(MeCN)_3]PF_6$ as catalyst. Further research is required in order to determine how the addition of sodium sulfite influences the hydrogenation

reaction chemically.

The findings presented in this section confirm that the *trans*-hydrogenation catalyst $[RuCp^*(MeCN)_3]PF_6$ has several drawbacks which however can be significantly reduced by addition of sodium sulfite to the reaction solution. For a medical application of PHIP fumarate the *trans*-hydrogenation of acetylene dicarboxylate with $[RuCp^*(MeCN)_3]PF_6$ as catalyst should be made even faster and the production of side products should be fully eliminated. Therefore, a chemical optimization of $[RuCp^*(MeCN)_3]PF_6$ should be considered in the long run. The addition of sodium sulfite can indicate a direction here.

3.4. Conclusion and Outlook

It has been proven that both 1-^{13}C-fumaric acid disodium salt as well as unlabeled fumaric acid disodium salt possess a long-lived proton nuclear spin singlet state. This long-lived state can be overpopulated by parahydrogen induced polarization with acetylene dicarboxylate as precursor compound and $[RuCp^*(MeCN)_3]PF_6$ as catalyst. The pairwise *trans*-hydrogenation reaction can be performed in water, which is biocompatible and thus beneficial for possible future medical applications of hyperpolarized fumarate. The enzymatic conversion of fumarate into l-malate is able to break fumarates NMR-silent hyperpolarized proton singlet state and thus to reveal the stored hyperpolarization as observable signal enhancement, which has been previously shown by Bornet et al. [54] Using this method it has been shown that the proton singlet state lifetime T_S of unlabeled fumaric acid disodium salt exceeds 6 min, which is very promising for medical applications where time is needed to build up significant amounts of the hyperpolarized agent and for catalyst removal. The enzymatic conversion of fumarate into l-malate is furthermore a promising method for the exact determination of fumarate's proton singlet state lifetime T_S, however this step requires further optimization and a specialized experimental setup to ensure faster enzymatic conversion and an exact reproducibility of experimental results. The pairwise *trans*-hydrogenation catalyst $[RuCp^*(MeCN)_3]PF_6$ has several drawbacks like slow reaction conversion, the formation of toxic side-products during hydrogenation and significantly slowing down the enzymatic conversion of fumarate into l-malate. Speeding up the conversion and overcoming the formation of side products will probably require a chemical modification of $[RuCp^*(MeCN)_3]PF_6$, for which the addition of sodium sulfite to the sample solution indicates a direction. The catalyst $[RuCp^*(MeCN)_3]PF_6$ is toxic as well, therefore a method to remove it quickly and entirely from the reaction solution must be developed, before medical applications of hyperpolarized fumarate can be attempted. A basic approach for catalyst removal might be to im-

mobilize the $[RuCp^*(MeCN)_3]PF_6$ molecules e.g. to silicone pellets. Fortunately, catalyst removal will automatically solve the problem that $[RuCp^*(MeCN)_3]PF_6$ reduces the enzyme acitivity of fumarase. From theory and observations on other singlet state molecules it is expected that fumarate's proton singlet state lifetime T_S will be significantly reduced in an oxygen-rich environment like blood, due to paramagnetic relaxation.[36, 55] However, the preparation of PHIP fumarate for medical applications can be performed in a degassed environment, within the longer time limitations of $T_S \geq 6$ min. Moreover, with $T_S \geq 6$ min in a degassed sample chances are given that T_S in an oxygen-rich environment like blood will still be in the order of minutes.

Chapter 4.

In Situ Detection of Continuous Spin Hyperpolarization by Reversible Exchange of Parahydrogen at μT Fields

Zero- to Ultralow Field (ZULF) NMR can precisely detect undisturbed nuclear spin-spin couplings, which is potentially useful for precision measurements of weak physical interactions. However, without a magnetic field it requires an external source of nuclear spin polarization, which for long-time precision measurements under stable conditions should be produced continuously and in situ . Signal Amplification by Reversible Exchange (SABRE) is a continuous nuclear spin hyperpolarization technique based on parahydrogen, that works at μT and zero magnetic fields. Its major limitation is sample evaporation through continuous contact with fresh parahydrogen gas. In this work it is shown that saturating parahydrogen with methanol vapor before sample contact decreases evaporation effects by factor >8, allowing for >5h of continuous SABRE measurement in situ at zero-field. Experimental parameters are easily optimized for a maximum SNR. The optimized technique is applied to confirm a recently published polarization transfer characteristic for heteronuclear SABRE at μT fields in situ with ZULF NMR.

4.1. Introduction

Nuclear Magnetic Resonance (NMR) spectroscopy is a powerful tool in analytical chemistry, however it suffers from an intrinsically low spin sensitivity. This problem can be directly overcome by hyperpolarization techniques, which maximize the sample's total magnetization by strongly overpopulating selected Zeeman eigenstates. Compared to the thermal overpopulation of energetically lower

Zeeman eigenstates in an external magnetic field ($\mathcal{O} \sim 10^{-6}$) hyperpolarization techniques hold a signal enhancement potential of up to 6 orders of magnitude. Para-Hydrogen Induced Polarization (PHIP) is a technique to create hyperpolarization by transferring the antiparallel singlet-state nuclear spin order of enriched para-hydrogen into a molecule. From the exact way how this is achieved, PHIP experiments can be divided into two subgroups. Hydrogenative PHIP transfers the nuclear spin order into the target molecule by a pairwise, spin-orientation conserving hydrogenation reaction of an unsaturated bond with enriched para-hydrogen. In non-hydrogenative (NH) PHIP enriched para-hydrogen molecules and the substrate molecule to be polarized are bound to short-lived complexes by the aid of a catalyst. While the complex persists, nuclear spin polarization can be transferred to the substrate molecule, if the external magnetic field fulfills a resonance condition. As long as fresh enriched para-hydrogen is available in the sample solution, the process can be repeated for a theoretically unlimited number of times. The most prominent example of NH PHIP is Signal Amplification By Reversible Exchange (SABRE) [19] with maximum proton-proton spin order transfer at mT fields [23]. Despite SABRE is a theoretically continuous technique for creating nuclear spin polarization, there are technical limitations, in the first place evaporation of the sample solution. The longest period of a continuous SABRE experiment, published so far, was 2500 s (= 25 min) [56]. We present an approach that can reduce sample evaporation significantly. Zero- to Ultralow Field NMR (ZULF NMR) [26, 57] enables a high resolution detection of undisturbed nuclear spin-spin couplings, due to the absence of an external magnetic field as a coupling partner. Herewith, ZULF NMR is a potentially suitable instrument to perform precision measurements for the detection and determination of weak physical interactions. One target experiment of this kind is the detection of Dark Matter by ZULF NMR. However, the lack of an external magnetic field produces a vanishing equilibrium nuclear spin polarization which leads to no measurable magnetization. Therefore, ZULF NMR requires an external source of spin polarization. The easiest way to solve this problem is to use a prepolarizing magnet, in which the sample is placed and magnetized before each measurement [29]. The main drawback of this method is a regular removal of the sample from its measurement environment, which would disturb long-time precision measurements significantly. Moreover, a prepolarizing magnet can only reach polarization values of $\mathcal{O} \sim 10^{-6}$, which is insufficient for many tasks. Therefore, a method to create a high nuclear spin polarization *in situ* at ZULF that is stable over a long time is of great interest.

A low-field version of SABRE called SABRE-SHEATH (SABRE in SHield Enables Alignment Transfer to Heteronuclei) [58, 59] has been recently developed. Here, polarization transfer from protons to ^{15}N takes place at magnetic fields in the range of few microtesla. However, in order to exploit SABRE-SHEATH hy-

perpolarization so far, it was necessary to move the sample between a shield for spin order transfer and the spectrometer for detection. Besides that moving the sample for each measurement is not convenient, it is challenging to achieve reproducible results with this method. Since the used ZULF NMR instrumentation has the ability to apply a microtesla magnetic field inside the ZULF-shield during polarization transfer [29], SABRE-SHEATH can be used to create nuclear spin polarization *in situ* , at the measurement environment, therefore moving the sample is not required any more. It has been demonstrated as well that SABRE spin order transfer can occur at zero-field ($\ll$nT) [25]. Zero-field, where all Zeeman states are degenerate, constitutes the trivial solution to the resonance condition for parahydrogen spin order propagation. In this case the nuclear spin singlet order is transferred into the substrate molecule. In this work a SABRE process was maintained continuously for more than 5 hours, allowing for an easy optimization of reaction conditions and an *in situ* confirmation of a characteristic for SABRE-SHEATH magnetization transfer in depencence of magnetic field strength recently published by Colell et al. [60]. Applying SABRE-SHEATH in situ at ZULF NMR is extraordinarily useful, since it simplifies current SABRE-SHEATH applications significantly and moreover constitutes a step towards ZULF NMR long-time precision measurements for the determination of weak physical interactions and possibly detection of dark matter.

4.2. Materials and Methods

ZULF NMR was performed in a home-built apparatus as described in [29, 26, 57], where zero-field is achieved with a cylindrical multilayer mu-metal shield and the sample's evolving nuclear spin magnetization at zero-field is captured with an atomic magnetometer based on a rubidium vapor cell. The experimental setup depicted in Fig. 4.1 b) was composed from $\frac{1}{4}$" OD stainless steel tubing, as well as from flexible 6 mm OD Festo PU tubing (PUN-H-6x1-NT). Computer controlled valves by Swagelok are employed parallel to manual ones in order to enable computer-controlled, as well as manual p-H_2 bubbling. The sample adapter was connected with flexible Festo polyurethane tubes in order to enable removing the sample from the ZULF shield without disconnecting it from the setup. The sample was contained in a 5mm OD valved glass NMR tube, p-H_2bubbling was achieved with a 1/16" OD x .030" ID PEEK tube which extended to the bottom of the sample tube. The presaturator bottle was composed of a 100 ml Schott flask with GL 45 thread, closed with a screw cap with two hose connections. For bubbling the gas flow through methanol, the gas inlet connection was equipped with four parallel 1/16" OD x .030" ID PEEK tubes which extended to the bottom of the flask. The presaturator bottle was heated to $\sim$65°C in a sand bath. The sample's

temperature inside the ZULF shield was regulated and stabilized with a temperature controlled nitrogen gas flow. The setup's gas inlet was equipped with a three way valve to choose between nitrogen and parahydrogen gas flow. Nitrogen was provided from the in-house nitrogen supply, parahydrogen was enriched to 92% (36 K) using a Bruker BPHG 90 parahydrogen generator. A 1 l aluminum gas bottle was attached to the p-H_2 gas cycle in order to buffer pressure fluctuations. Samples, consisting of 0.3 ml of a mixture of Pyridine as substrate, anhydrous methanol as solvent and Ir(COD)(IMes)Cl as catalyst were prepared under inert atmosphere in a 5 mm OD valved glass NMR tube. Details on the used chemicals and experimental materials can be found in appendix B. The sample was attached to the bubbling setup outside the ZULF shield while the setup was intensively purged with nitrogen, in order to avoid air contact. Next, the gas supply was switched to parahydrogen. For activating the SABRE catalyst, parahydrogen was bubbled through the sample until its color changed from yellow to clear. In order to speed up the activation process, the sample was heated to approximately 60°C in a water bath. For measurements the attached and activated sample was inserted into the ZULF shield. Parahydrogen bubbling is achieved by closing the short valve and opening the vent valve of the setup in Fig. 4.1 b). The bubbling period is stopped by first closing the vent valve and then, after a short bubbling recovery delay d1, opening the short valve which definitely ends any bubbling. Between the short B-field pulse in y-direction or the sudden magnetic field turn-off and acquisition there is a dead time of 10 ms. Controlling of the ZULF NMR setup and data acquisition were performed with an in-house controlling software written in Labview. Data processing and analysis were performed with Wolfram Mathematica (Wolfram Research, Long Hanborough, UK). Processing included polynomial background subtraction, backwards prediction of the time-evolution signal in a few ms range in order to ensure physically meaningful spectral phases and exponential apodization.

4.3. Results and Discussion

A reaction scheme for the SABRE mechanism with pyridine as substrate, as used in this work, is depicted in Fig. 4.1 a). The general experimental setup, used for all experiments described constists of a gas cycle with the options to be supplied either with parahydrogen for the SABRE reaction or nitrogen for purging. A scheme of the setup can be found in Fig. 4.1 b) Parahydrogen gas flowing though the cycle is bubbled through heated Methanol with ∼65°C in the presaturator bottle first and secondly through the SABRE sample. This way the dry p-H_2 gas becomes saturated with methanol vapor before it reaches the sample and sample evaporation is reduced by a factor >8, resulting in continuous SABRE experiments lasting more

than 5 hours. The actual signal acquisition is performed with a rubidium vapor magnetometer that is placed inside the ZULF shield. A measurement follows the scheme of the "pulse sequence" shown in Fig. 4.1 c) for each scan. In the beginning p-H_2 is bubbled though the sample for 5-15 s. During this period a magnetic field in y-direction can be optionally applied, that is suddenly turned off. If no magnetic field is applied during bubbling, a short B-field pulse in y-direction follows after another optional delay d2. Acquisition of the sample's evolving magnetization follows the short B-field pulse and lasts 8-10 s. After a break of flexible duration the next scan is performed. The total duration from beginning of bubbling until the end of the scan was 28-40 s. Fig. 4.1 d) shows the ZULF NMR time evolution signal of SABRE enhanced pyridine's magnetization. Fig. 4.1 e) shows the according ZULF NMR spectrum, which only depends on pyridine's J-couplings.

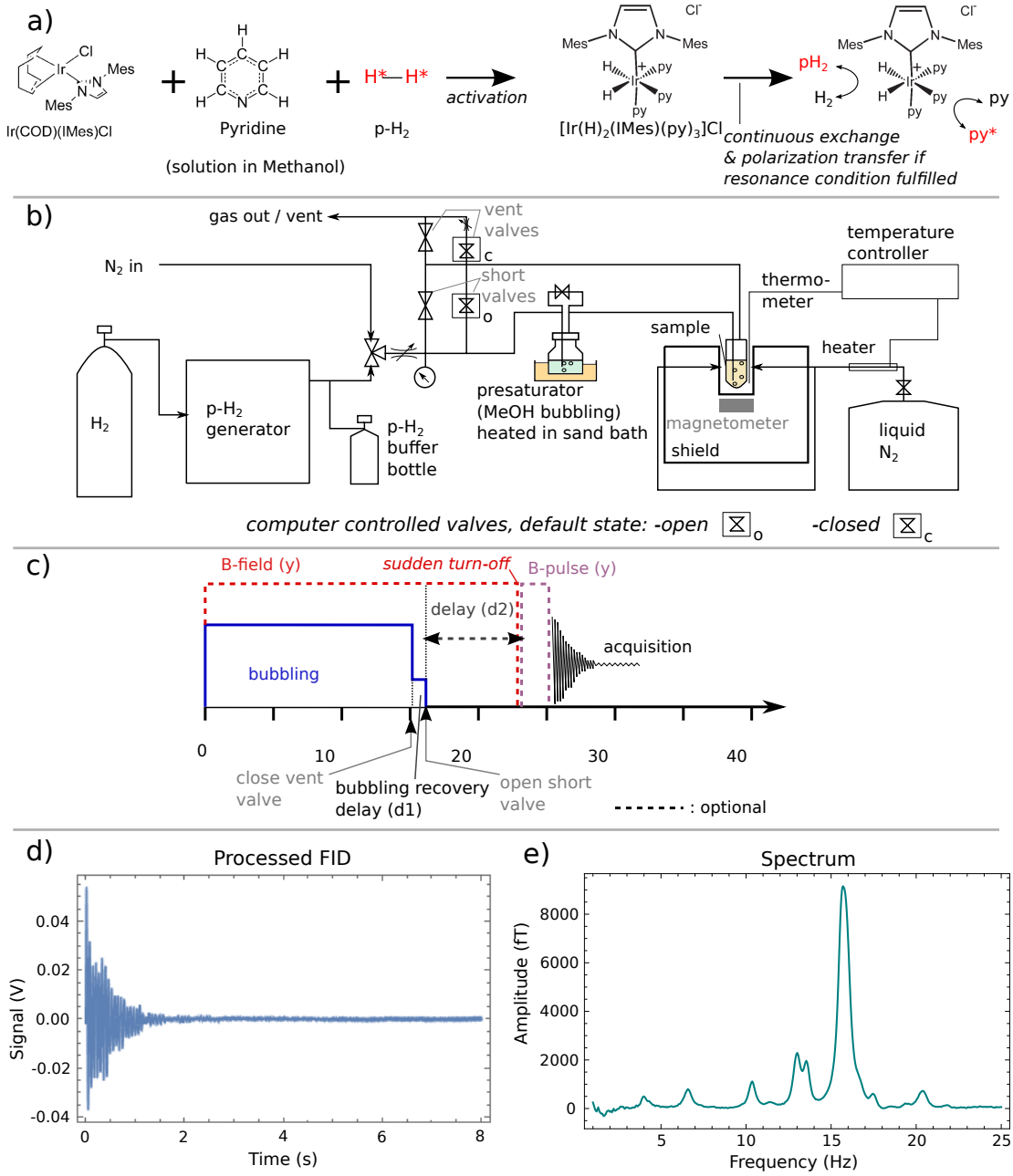

Figure 4.1.: a) SABRE reaction scheme with pyridine as substrate. b) Scheme of the experimental setup for computer controlled p-H_2 bubbling through a SABRE sample, including a heated methanol presaturator that prevents sample evaporation by saturating the p-H_2 gas with methanol vapor before contact with sample solution. The sample is temperature controlled. c) Scheme of the ZULF NMR "pulse sequence", consisting of a time interval for p-H_2 bubbling with a magnetic field in y-direction during it, that is abruptly switched off, a delay between bubbling and the ZULF magnetic field pulse in y- direction, which is followed by acquisition. Dashed lines mark optional elements that were incorporated in different combinations for different experiments. d) ZULF NMR time evolution signal of SABRE enhanced pyridine. e) ZULF NMR spectrum obtained from d). A ZULF NMR spectrum depends only on the sample molecule's J-couplings.

For the described experiments it was first necessary to optimize the SABRE reaction for a maximum signal to noise ratio (SNR) per units time. Optimization experiments were performed for sample composition, pressure-flow-balance, reaction temperature, duration of bubbling and the delay between bubbling and acquisition. The optimal sample was found to be composed of 1.9 M pyridine in methanol (15 vol%) with 1.3 mol% of Ir(COD)(IMes)Cl catalyst [61] with respect to pyridine. Since only molecules with a ^{15}N are hyperpolarized with the SABRE-SHEATH method, 0.04 M ^{15}N-Pyridine was added to increase the SNR additionally. The optimal pressure-flow-balance within the possibilities of the parahydrogen generator was found to be at 6-7 bar of p-H_2 pressure with the maximum flow possible to keep this pressure stable. Best SNR was reached at a temperature of 310 K and a bubbling duration of 15 s with a 1 s delay between end of bubbling and start of acquisition.

Results of a long-time *in situ* SABRE experiment can be found in Fig. 4.2. For this experiment no magnetic field was applied during p-H_2 bubbling, the bubbling recovery delay d1 was set to 1 s and no d2 delay was incorporated (d2=0). Immediately after d1 a short B-field pulse in y-direction was applied in order to convert the nuclear spin singlet state order that was transferred to pyridine at zero-field into evolving magnetization which was acquired (cf. Fig. 4.1 c)). SABRE enhanced ZULF NMR spectra of pyridine were continuously recorded every 30 s for more than 5 hours' time. Over time the signal amplitude decreased exponentially with a decay constant of $T_{evap} = (2.79 \pm 0.10)$ hours (Fig. 4.2 a)), which can be explained by an increasing pyridine concentration in the sample solution, while methanol evaporates gradually. The gradually changing sample composition also influences pyridine's J-couplings [62, 63], which is visible as a frequency shift in the recorded ZULF NMR spectra (Fig. 4.2 b)).

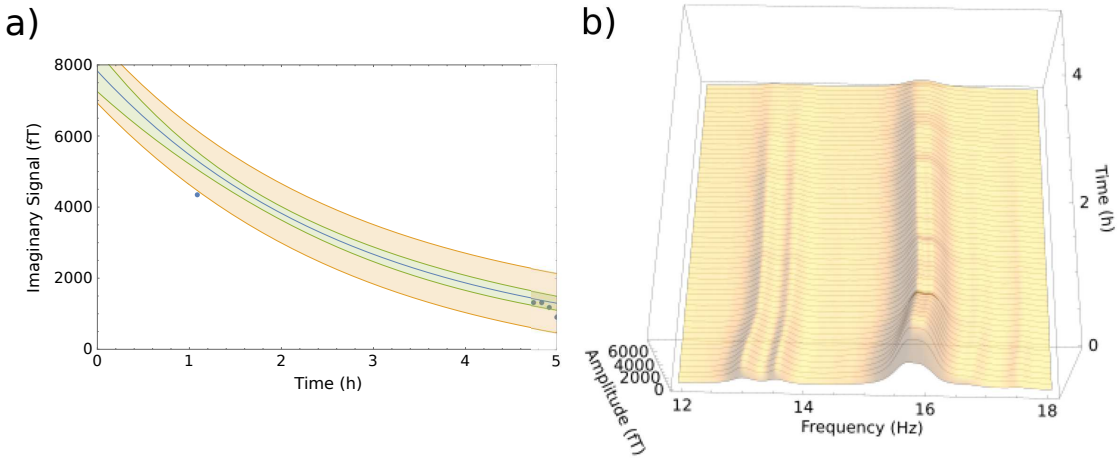

Figure 4.2.: Results of a continuous long-time SABRE experiment detected *in situ* at ZULF. The signal was continuously detected for over 5 hours. a) The maximum signal amplitude is plotted over time. A decay occurs due to a changing substrate concentration, since the solvent methanol evaporates gradually. An exponential fit gives a decay constant of $T_{evap} = (2.79 \pm 0.10)$ hours. 2σ prediction bands are shown in red, 3σ confidence bands are shown in green. b) A frequency shift arises in the acquired ZULF NMR spectra over time, since pyridine's J-couplings shift with its changing concentration in the sample while methanol evaporates [62, 63].

Without a methanol presaturator in the experimental setup the solvent methanol evaporated fully in about 40 min, so that the presaturator prolonged the measurement's time by a factor >8. The remaining sample evaporation could be further diminished or even avoided by cooling the upper part of the sample tube, so that sample vapors are re-condensated before leaving the sample container. The observed decay in signal intensity is not related to the decreasing sample volume, since the total sample volume exceeded the magnetometer's sensitivity area throughout the whole experiment.

In order to discover the magnetic field dependency of the magnetization transfer during in situ ZULF-SABRE experiments, a variable magnetic field in the range from -3μT to 3μT was applied during bubbling, and thereby during polarization transfer. In the applied sequence, compare to Fig. 4.1 c), delay d1 was set to 250 ms and d2 to 10 ms. The magnetic field was abruptly turned off right after d2, after a dead time of 10 ms acquisition was started. No short B-field pulse was applied. A plot of the maximum signal amplitude over the applied magnetic field strength can be found in Fig. 4.3. A pair of antiphase Lorentz curves was fitted into the data points, the fit's 5σ confidence bands are shown in yellow.

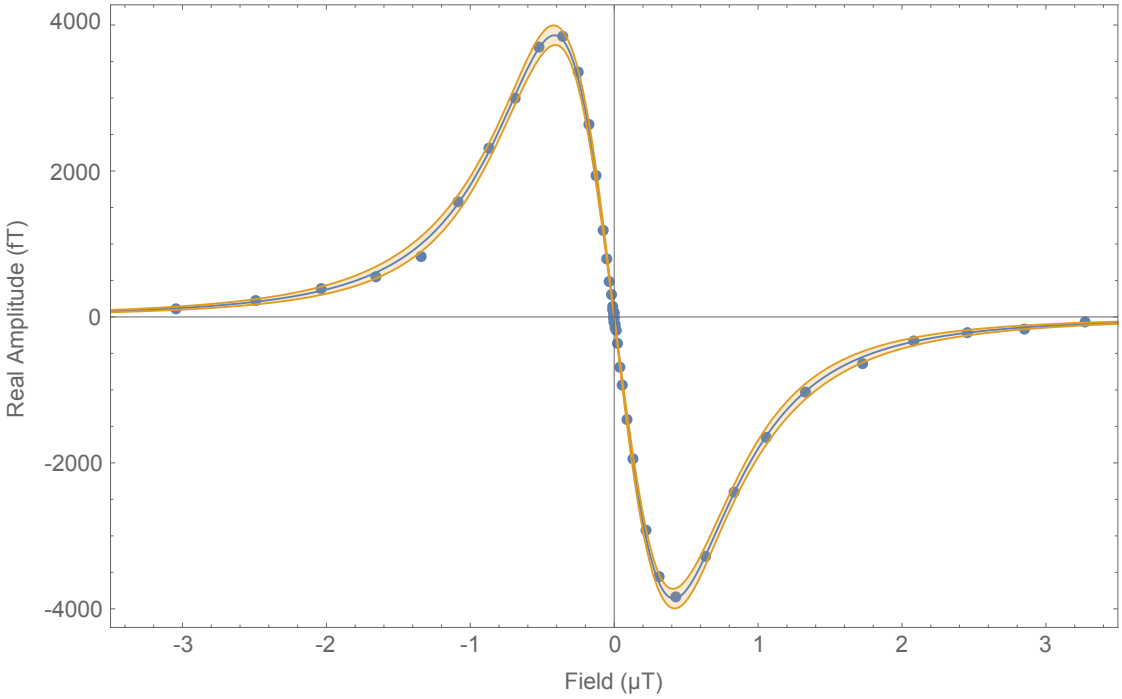

Figure 4.3.: Results of the B-field variation during polarization transfer, maximum signal amplitude is plotted over the magnetic field strength applied during p-H_2 bubbling and SABRE polarization transfer. Two antiphase Lorentz curves were fitted into the results. 5σ confidence bands are shown in yellow.

The abrupt turn-off of the magnetic field does not allow for a transfer of the energy eigenstates from the μT regime to the corresponding ZULF regime energy eigenstates. Therefore, during acquisition only the magnetization which was transferred to pyridine at the respectively applied magnetic field during bubbling was measured. Transferred singlet state order cannot be detected due to a missing B-field pulse. The results confirm the SABRE-SHEATH polarization transfer characteristic measured by Colell et al. [60] at high-field after polarization transfer in a μT shield. Since the results in Fig. 4.3 were measured *in situ* at ZULF, it is proven that transporting the SABRE-SHEATH sample from μT shield through earth field into high-field for acquisition has no influence on the experimental results. Hence, all the measured magnetization was transferred to pyridine by the energy level anticrossings according to SABRE-SHEATH polarization transfer theory [58].

4.4. Conclusion and Outlook

It was accomplished to maintain a SABRE signal *in situ* at zero- to ultralow field continuously for more than 5 hours, which shows that the limitation of sample evaporation has been largely overcome. Cooling the gas that leaves the sample tube after bubbling is proposed for further improvement and could even lead to overcoming sample evaporation fully. Performing long-time SABRE experiments *in situ* at zero- to ultralow field significantly increases the reproducibility of ZULF NMR results, since it is not further required to remove the sample from its measurement environment during the experiment for re-polarization. Moreover, continuous *in situ* experiments enabled an easy optimization of experimental parameters for maximizing the signal to noise ratio per units time. The ability to perform reproducible *in situ* long-time experiments with a high signal to noise ratio constitutes the first step towards performing long-time precision measurements for the detection and determination of weak physical interactions with ZULF NMR, which could in the long run result in the detection of dark matter. For now, continuous *in situ* long-time SABRE experiments at ZULF were applied to confirm a recently published SABRE-SHEATH polarization transfer characteristic [60] and to exclude that transporting the sample from the SABRE SHEATH shield through earth field into high field for NMR acquisition has any effect on the observed results.

Chapter 5.

Hyperpolarization Enables Fast Reaction Monitoring in Diluted Systems with Compact NMR Devices

The application of compact medium-field NMR spectrometers for chemical engineering purposes is rapidly growing. Compared to common high-field NMR spectrometers, medium-field NMR spectrometers are flexible and easily applicable in every day laboratories because of their small size and no need of cryogenic media. The inherent drawbacks of medium-field spectrometers are their lower sensitivity and chemical shift resolution compared to high-field NMR instruments. However, the sensitivity issue can be overcome by applying hyperpolarization methods. Parahydrogen Induced Polarization (PHIP) is a hyperpolarization method that is easy to implement and cost efficient. Here, the applicability of Parahydrogen Induced Polarization for fast reaction monitoring with a medium-field NMR spectrometer is evaluated. Two setups are investigated, shake and continuous flow experiments, respectively. Shake experiments are performed to deduce the $^{1}\mathrm{H}$ *and* $^{13}\mathrm{C}$ *signal enhancements available for different chemicals by PHIP in a benchtop NMR setup. Continuous flow experiments are conducted to derive the reaction kinetics of the hydrogenation reaction in a low concentration regime from the enhanced product peaks.*

5.1. Introduction

NMR spectroscopy is an important analytical tool with a wide range of applications in chemistry, biology, and chemical engineering. [64] It is non-invasive and has a high chemical resolution, thus complex fluid mixtures can be investigated without sampling or even under flow conditions. Since the NMR spectrum

offers inherent quantitative information without the need for calibration measurements, NMR spectroscopy is an appropriate analysis method for monitoring of reactions and processes. [65, 66, 67, 68, 69, 70] The drawback of well-established high-field NMR spectrometers is the utilization of super-conducting magnets that require a dedicated laboratory infrastructure, constant supply of cryogenic media, and climatisation. In recent years, medium-field NMR spectrometers (often called Benchtop NMR spectrometers) employing a Halbach array of small permanent magnets with high stability and homogeneity of the magnetic field have been developed. They allow an acquisition of quantitatively evaluable spectra, are small in size, do not require cryogenic media and have almost no stray field, which makes them easily applicable in every day laboratories. However, medium-field NMR spectrometers have much lower magnetic field strengths of 1-2 T (corresponding to proton Larmor frequencies of 42.5-80.0 MHz) [71], which gives rise to a lower sensitivity and chemical resolution compared to high-field NMR spectrometers (9.4-20 T) and leads to longer acquisition times. When employing NMR spectroscopy under flow conditions the signal intensity further decreases because of incomplete premagnetization of the samples. This is especially important for nuclei with long T_1 relaxation times (e.g. ^{13}C). Successful approaches overcome the loss of premagnetization with prior external magnetic fields or with loopy flow cells to increase the residence time of the fluid in the magnetic field. [72, 73, 74] Hyperpolarization techniques overcome the issues of low sensitivity and incomplete premagnetization, by creating a magnetization that exceeds thermal polarization by several orders of magnitude and does not depend on the magnetic field strength anymore. In this work, hyperpolarization enables a quick acquisition of medium-field NMR spectra with high signal to noise ratio (SNR) on ^{13}C and in diluted samples, even under flow conditions.

Several applications of hyperpolarization in combination with medium-field NMR are reported in literature. The most relevant among them are the detection of low concentrated unsaturated C-C bonds enhanced by PHIP [75] or acquisition of SABRE-hyperpolarized 15N spectra [60], which would have been impossible to measure or would have taken weeks to acqire, whereas using hyperpolarization techniques they could be detected within a single scan. Moreover, sampling of hyperpolarized signals from the enzymatic or cell conversion of DNP hyperpolarized 1-^{13}C-pyruvate to 1-^{13}C-lactate at medium-field is reported. This application benefits from longer T_1 relaxation times at 1T compared to high-field [76]. Other interesting application examples are a continuous detection of SABRE enhanced compounds in diluted samples, that were hyperpolarized in a continuous-flow setup with a membrane reactor to bring substrate-catalyst solution and parahydrogen in contact [77] and data analysis on systems with a multitude of overlapping signal contributions or a dominant background signal with DNP enhanced fast field

cycling relaxometry [78].

In this work, we employ ALTADENA PHIP shake measurements detected with a medium-field NMR spectrometer on three substrates (2-hydroxyethyl acrylate (HEA), 1-hexyne, and dimethyl acetylenedicarboxylate (DMAD)) in combination with appropriate solvents (acetone d_6, methanol d_4 and D_2O). Thereby, we address the question whether signal enhancement is accessible in ^1H as well as in ^{13}C spectra in benchtop NMR experiments and to which extent. Magnetic field inhomogeneities broaden NMR spectral lines and low magnetic fields reduce the frequency gaps between them. Therefore, the extent of signal cancellation in PHIP enhanced antiphasic medium-field NMR spectra must be investigated. In the next step the hydrogenation of HEA is chosen for continuous measurements. For these experiments a flow setup was employed where a membrane module based on semipermeable hollow fiber membranes was used to bring gas and liquid into contact. NMR detection was performed in a medium-field NMR spectrometer under flow conditions. The reaction kinetics is deduced from the measured time dependent PHIP signal intensity of the reaction product.

5.2. Experimental Section

5.2.1. Reaction Systems

The pairwise homogeneous hydrogenation reactions used in this work are listed in Fig. 5.1. Enriched parahydrogen (92%) was prepared with a commercial parahydrogen-generator (Bruker BPHG 90) and filled into 1 liter aluminum bottles with a pressure of 10 bar.

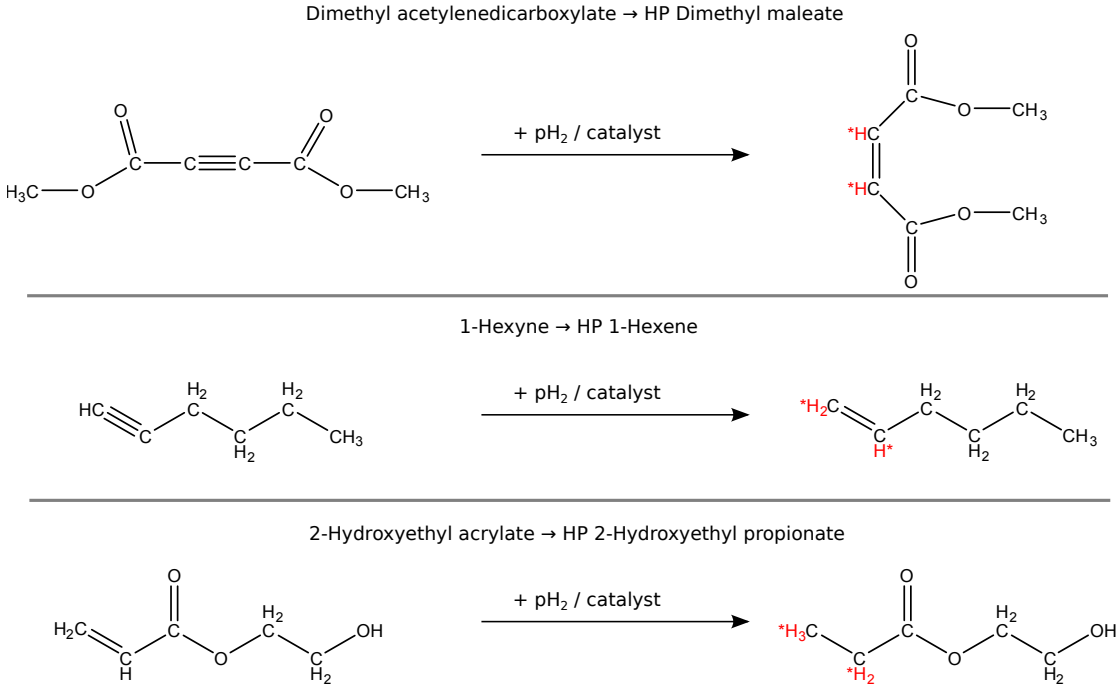

Figure 5.1.: Pairwise homogeneous hydrogenation reactions used to create Parahydrogen Induced Polarization. The reactions were performed at a parahydrogen pressure of 5 bar and at a temperature of 65°C for organic solvents and 80°C for water. Details on solvents and catalysts can be found in Table 5.1.

substrate	**catalyst**	**solvent**	**hyperpolarized product**
dimethyl acetylenedicarboxylate (2.03 M)	$[Rh(dppb)(COD)]BF_4$ (0.2 mol% w. resp. to substrate)	acetone d_6	dimethyl maleate
1-hexyne (2.18 M)	$[Rh(dppb)(COD)]BF_4$ (0.2 mol%)	acetone d_6	1-hexene
2-hydroxyethyl acrylate (2.18 M)	$[Rh(dppb)(COD)]BF_4$ (0.2 mol%)	methanol d_4	2-hydroxyethyl propionate
2-hydroxyethyl acrylate (2.18 M)	$[Rh(nbd)(ppbs)]BF_4$ (0.2 mol%)	D_2O	2-hydroxyethyl propionate

Table 5.1.: Investigated combinations of substrates and solvents.

5.2.2. Experimental setup and procedure

Shake measurements

The shake experiments were carried out in pressure-resistant 5 mm diameter glass NMR tubes by Wilmad (length 7 inch) closed with a screw-cap with septum. The substrate solution was prepared as follows: 3 mg of catalyst was weighed in the NMR tube under inert conditions. Then, 0.25 ml substrate and 0.75 ml solvent were filled in the tube using a syringe. Finally, the NMR tube with substrate solution was heated in a water bath to 65°C for organic solvents and 80°C for water as solvent. Table 5.1 lists the investigated combinations of substrate and solvent with the appropriate catalyst. A shake cycle consists of the following steps: (i) Parahydrogen at a pressure of 5 bar is injected in the preheated NMR tube, (ii) hydrogenation reaction is initiated by shaking the tube vigorously, (iii) the NMR tube is inserted into the benchtop NMR spectrometer, (iv) acquisition of ^{1}H and ^{13}C 1-scan NMR spectra after 45° pulse in alternating order is performed, (v) pressure is released from the NMR tube, (vi) the NMR tube is reheated to target temperature. Up to eight shake cycles were performed on every sample. Parahydrogen was provided from a 1 liter aluminum gas bottle filled with 10 bar parahydrogen equipped with a pressure regulator set to 5 bar and a hollow needle at the end of the gas outlet line. After the experiment, ^{1}H and ^{13}C thermal reference spectra of each sample were acquired at medium-field as well as high-field. ^{13}C reference spectra were acquired without ^{1}H decoupling.

Continuous Measurements

The continuous measurements were performed using the flow setup shown in Fig. 5.2. The setup consists of a closed loop where substrate solution is constantly pumped from the feed container through an in-house built membrane module, which is permeable to gas, to the NMR spectrometer and back. The flow rate of the employed pump (Wadose Plus, Wagner MSR, Offenbach, Germany) is regulated with a Coriolis flow sensor (Mini Cori-Flow, Bronkhorst, Ruurlo, Netherlands). In the membrane module Celgard X40 hollow fiber membranes by Membrana, Germany are integrated. The module is placed in a heated bath of 60°C to initiate the hydrogenation reaction with parahydrogen diffusing through the membranes. This way dissolution of parahydrogen can be achieved without bubbles and foam formation [79]. All feed lines of the loop are capillaries made of PEEK, the corresponding inner diameter is indicated in the scheme in Fig. 5.2.

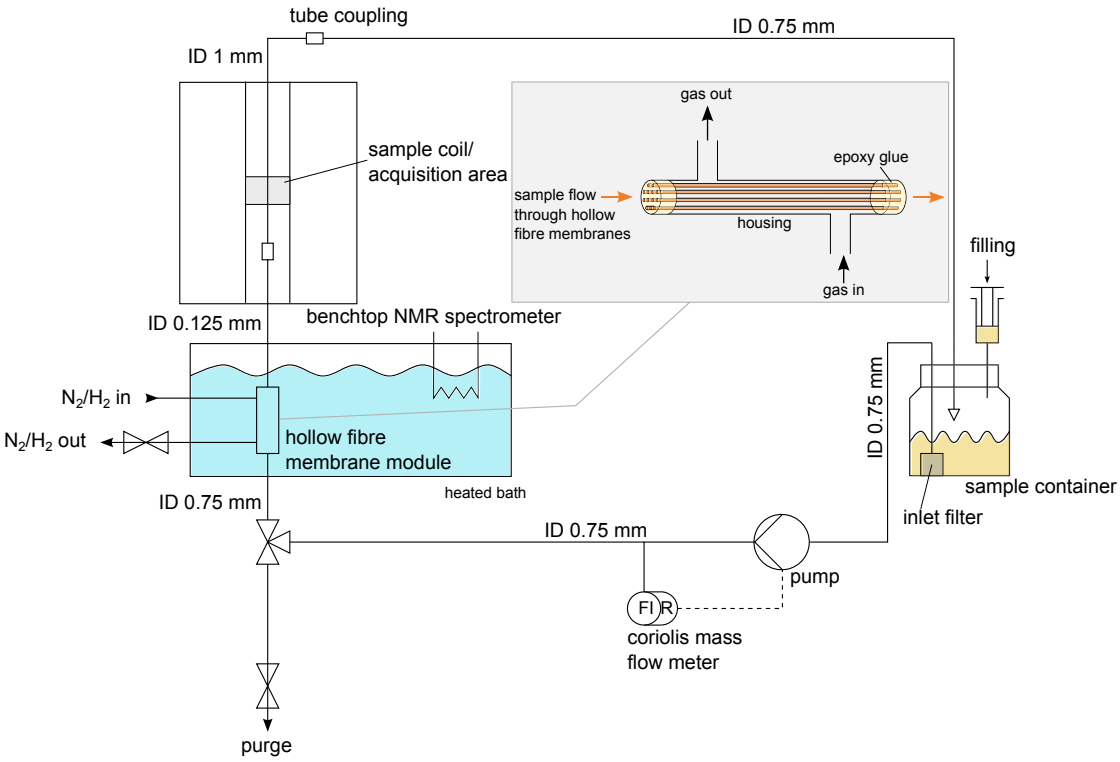

Figure 5.2.: Scheme of the flow setup for continuous ALTADENA measurements.

The feed lines for gas are made of PU (FESTO, PUN-H-3X0,5-NT) and were supplied with up to 5 bar nitrogen or parahydrogen depending on demand. The feed container is equipped with a safety cap with two inlets for filling and reflux as well as one outlet for sample intake. Several three port valves are installed to change the flow direction in the setup depending on the mode that was performed. A continuous measurement consists of three modes: flushing the setup with nitrogen, filling the setup with reaction mixture and the continuous measurement during application of parahydrogen. Initially the membrane module and the setup were flushed for 10 minutes with nitrogen to ensure an oxygen free atmosphere. Therefore the purge line was used as outlet. Under inert conditions 50 ml of reaction mixture were prepared consisting of 45 ml water, 5 ml HEA, and approximately 30mg of catalyst $[Rh(nbd)(ppbs)]BF_4$. The reaction mixture was inserted into the sample container with a syringe. While the circulation was initiated by the pump, nitrogen pressure in gas- as well as in sample flow cycle was increased to 5 bar. After a constant flow rate of 2 ml/min was reached, the continuous NMR measurement that acquired one spectrum every 60s was started. After 5 min the membrane module was placed in the heated bath and after another 5 min the 5 bar nitrogen in the gas cycle were exchanged by 5 bar parahydrogen, initiating the pairwise hydrogenation reaction. With the used flow rate transport from mem-

brane module to NMR coil takes about 2s. After the reaction was completed, the gas cycle was flushed with nitrogen again. Reference measurements were taken on the fluid at rest, on the flowing fluid, and on the heated flowing fluid before and after the continuous measurement during hydrogenation. Nitrogen was provided from the in-house nitrogen supply line and parahydrogen was provided from two connected 1 liter aluminum bottles filled with 10 bar parahydrogen and equipped with a pressure regulator set to 5 bar. Additionally, thermal high-field NMR ^{1}H reference spectra were acquired for each completed experiment.

5.2.3. NMR Instruments and Methods

The medium-field NMR measurements were carried out on a Magritek Spinsolve Carbon NMR spectrometer (Magritek, Aachen, Germany) with a field strength of 1 T corresponding to a Larmor frequency of 42.5 MHz for ^{1}H. The optimization of the magnetic field homogeneity (shimming) was performed with the respective setup (NMR pressure tube or PEEK capillary) on the measured sample solution. All spectra were acquired without addition of reference compounds. The shake measurements were performed with the standard ^{1}H and ^{13}C pulse sequences provided by Magritek with one scan per spectrum and a 45° pulse. Thermal reference spectra were acquired with the same parameters, but a larger number of scans between 16 and 1276. During the continuous measurements 1-scan-spectra employing a 45° pulse were acquired every 60 s. The number of spectra acquired was chosen depending on the target length of experiment. Prior to integration post processing of the obtained NMR spectra was carried out with the Mnova software (MestReLabs, Santiago de Compostela, Spain). For baseline correction, a Whittaker smoother algorithm was used. Integration was performed on magnitude spectra in order to obtain positive magnitude integral values from antiphasic peaks. For enhancement determination and following calculations the Spinsolve spectra were imported to Wolfram Mathematica. High-field NMR reference spectra were acquired with a Bruker avance300 spectrometer with an external magnetic field of 7.0460 T, corresponding to a proton Larmor frequency of 300 MHz.

5.3. Data Analysis

5.3.1. Shake Measurements

For each PHIP hyperpolarized ^{1}H spectrum the average signal enhancement was determined by the aid of medium-field thermal reference spectra. It was assumed that conversion rates per shaking cycle in one sample were approximately constant. The average enhancement value was determined from the ratio of the magnitude

integral over all hydrogenation product peaks in the hyperpolarized spectrum and the integral over all hydrogenation product peaks in the thermal reference spectrum, divided by the number of scans of the thermal reference and the number of shaking cycles that were performed with this sample. The enhancement value is defined as the ratio of the maximum PHIP signal intensity, which occurs after a 45°pulse, and the maximum thermal signal intensity, which occurs after a 90° pulse with the same acquisition parameters and under the same conditions.

$$Enh = \frac{I(PHIP, 45°)}{I(therm., 90°, norm.)}$$

The error of the enhancement values was calculated from the SNR and from the uncertainty of the conversion per shake cycle, where the latter was the dominant contribution. For the analysis of the medium-field PHIP spectra on ^{1}H high-field NMR references were only consulted to reassure a correct assignment of J-couplings and chemical shift values. On ^{13}C it was not possible to acquire medium-field thermal reference spectra with clearly visible hydrogenation product resonances within less than 24 hours, due to low sensitivity. Therefore, for the PHIP hyperpolarized spectra on ^{13}C only a lower bound for the signal enhancement was determined by the aid of high-field ^{13}C thermal references.

5.3.2. Continuous Measurements

The main experimental data consist of ^{1}H spectra of PHIP hyperpolarized 2-hydroxyethyl propionate, constituting snapshots at a defined time during the pairwise hydrogenation reaction. For the data analysis a numerical integration over the complex magnitude of the hyperpolarized peaks of 2-hydroxyethyl propionate was performed in each spectrum, in order to determine the PHIP signal intensity over time. In order to keep offset-effects as small as possible a noise-threshold was defined. Points, whose magnitude did not exceed the noise-threshold were not taken into account for the numerical integration. For the reaction performed in H_2O a clearly distinguishable water peak occurs in each acquired spectrum. The obtained PHIP signal intensities were normalized with the signal intensity of the water peak in the same spectrum, in order to correct them for possible fluctuations in the spectral amplitude, for instance resulting from micro bubbles. Errors were determined with the variance formula for error propagation from the level of noise. A reaction kinetics describes the reaction conversion in dependency of time. It can be safely assumed that the PHIP signal enhancement is constant throughout the reaction. Therefore the intensity of PHIP signals is considered proportional to the conversion during the preceding time interval Δt, for which the hyperpolarization that was created during hydrogenation has not yet decayed. Hence, PHIP signal intensities over time describe a curve that is proportional to the time derivative

of the reaction kinetics. In order to calculate the conversion over time the time dependent PHIP signal intensities were numerically integrated. Additionally the values were scaled with a constant factor so that the last data point in time corresponds to the total conversion U_{tot}, which was determined from thermal high-field NMR reference spectra. The errors were determined with the variance formula for error propagation. It is considered that parahydrogen was supplied abundantly throughout the whole reaction. Hence, according to theory the homogeneous pairwise hydrogenation reaction has to be considered as a reaction of pseudo-first order, whose conversion over time U(t) is a saturation curve.

$$U(t) = 1 - e^{-kt}$$

To take account for the fact that the reaction might stop at a lower conversion level than 100% and for technical offset effects, the fit function is complemented with two more parameters.

$$U(t) = a \cdot e^{-kt} + f \tag{5.3.1}$$

The amplitude parameter a depends on the catalyst activity, that is changing over the time of reaction. Therefore parameter a was modeled as a third degree polynomial. Signal enhancement values during the continuous flow experiment were calculated analogously to the average enhancement values for the shake experiments.

5.4. Results and Discussion

5.4.1. Shake Measurements

Fig. 5.3 shows a selection of highly enhanced ^{1}H and ^{13}C spectra superimposed with the according thermal reference, together with the average enhancement value for ^{1}H or a lower bound for the average enhancement value for ^{13}C respectively.

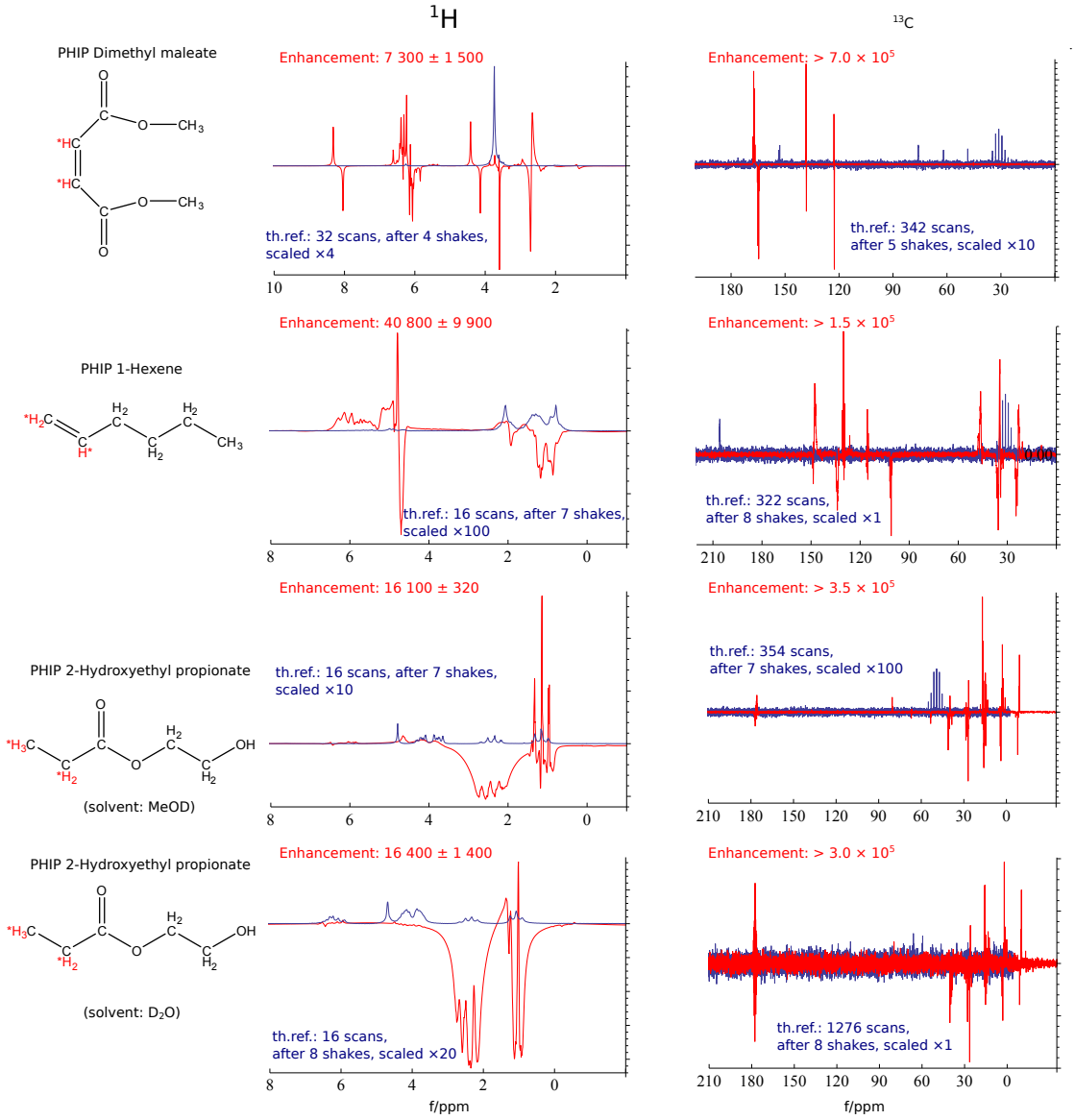

Figure 5.3.: Selection of highly enhanced ^{1}H and ^{13}C spectra superimposed with the according thermal reference acquired at medium-field. Average ^{1}H enhancement values and lower bounds for average ^{13}C enhancement values are noted. All PHIP spectra were acquired with one scan. A detailed explanation of the spectral peaks can be found in appendix C.

All resulting average enhancement values for ^{1}H are in the order of $10^4 - 10^5$ which is close to the theoretical maximum enhancement of $2.96 \cdot 10^5$ at 1 T. For ^{13}C the theoretical upper limit for hyperpolarization enhancement is $1.16 \cdot 10^6$, the measured enhancement values are in the order of 10^5. Enhancement values

one order of magnitude below the theoretical maximum prove an efficient experimental procedure and a high parahydrogen percentage. It is remarkable that signal enhancements achieved with the simple shake setup enable acquisition of ^{13}C spectra with high SNR with only one scan without isotopic labeling. Furthermore it is observed that the hyperpolarization is distributed over several protons, as well as ^{13}C nuclei in the reaction product molecule. A detailed assignment of the hyperpolarized peaks can be found in appendix C. During the transport into the spectrometer's external magnetic field B_0 hyperpolarization spreads from the two former parahydrogen protons over all strongly coupled nuclei with nonzero spin in the molecule. This effect is based on energy level anticrossings (LAC, cf. section 2.5) that occur at magnetic field strengths between earth field and B_0. It must be noted, that polarization transfer by energy LAC automatically breaks the NMR-silent hyperpolarized nuclear spin singlet state on dimethyl maleate, which is overpopulated right after the hydrogenation reaction of DMAD. A detailed quantum mechanical explanation of energy LAC effects especially in DMAD can be found in [80, 81, 46, 45, 82, 83]. Alternatively, nuclear spin polarization can be transferred on specific heteronuclei by applying polarization transfer sequences like e.g. INEPT [84, 85, 86, 87]. This is especially attractive for experiments in PASADENA mode, where the hydrogenation reaction takes place inside the spectrometer and field cycling, which is necessary for addressing LACs, does not take place. Since the acquisition of thermal ^{13}C reference spectra with clearly visible reaction product peaks was not possible within an acquisition time of 24h, it can be stated that PHIP is an enabling technology for acquisition of high SNR ^{13}C spectra of diluted samples within short acquisition times without isotopic labeling. In this experiment substrate concentrations were between 0.9 M and 2.2 M and the acquisition time for ^{13}C spectra was about 1s. Although ^{13}C polarization within the hydrogenation product molecule was non-uniform and antiphasic, which disables a quantitative spectral analysis, J-couplings can be clearly derived from the resulting PHIP spectra on ^{13}C (cf. PHIP peak assignment in appendix C), in some cases even clearer than from high-field NMR ^{13}C reference spectra without proton decoupling. The measured PHIP signal intensity is reduced by T_1relaxation during the 2 s time gap between hydrogenation reaction (tube shaking) and data acquisition. This effect reduces proton signal intensity by an average factor of 0.45 when supposing an average proton T_1 of 2.5 s. For ^{13}C where the average T_1 is approximately 50 s, the effect of T_1 relaxation is almost negligible, with an average reducing factor of 0.96. Exact T_1values can be found in appendix C. The detected PHIP signal intensity is further reduced by signal cancellation due to the antiphasic nature of PHIP. The extent of this effect can be determined quantitatively by fitting antiphase Lorentz curves into the spectral resonances. Due to complex coupling patterns this method could not be applied here. Instead, sig-

nal cancellation effects were roughly estimated to reduce PHIP signal intensity on protons by a factor of 0.4 and by a factor of 0.7 on ^{13}C. This estimation is based on the effective enhancement values, the theoretical maximum enhancement and the known intensity reduction from T_1 relaxation.

5.4.2. Continuous measurements

In Fig. 5.4 a plot of the PHIP signal intensity of 2-hydroxyethyl propionate over reaction time is shown. It is visible that the intensity of the hyperpolarized signals first rises and later decays again. Since parahydrogen was available abundantly, this behavior can be interpreted as a buildup process of the catalyst's activity. Exemplary a ^1H spectrum during reaction is shown, superimposed with a 1-scan thermal reference without flow after the reaction. The average PHIP enhancement is noted. In Fig. 5.4 the PHIP signal intensity curve after numerical integration and scaling is shown. The last data point corresponds to the total conversion U_{tot}= 69.64% at the end of the reaction. As expected the distribution is dominated by a saturation curve. The fit function U(t) (cf. equation 5.3.1) was plotted through the conversion data points and the value of the saturation curve's asymptote is noted. The fit function predicts 70.9% ± 1% for parameter f, the level of saturation for the conversion. This is above the measured conversion U_{tot} at the end of the experiment, but significantly below 1, which implies that the reaction's theoretically predicted run was additionally restricted. One possible reason for additional restriction can be sediments of the catalyst which build up on the inside of the hollow fiber membranes during reaction. The rate of reaction fit parameter k is $(0.1583 \pm 0.0191)\ min^{-1}$. For the same experiment performed in D_2O (cf. appendix C) parameter k was $(0.1400 \pm 0.0027)\ min^{-1}$ and hence both results overlap within errors. This confirms that the experiment is reproducible and that the solvent has no effect on the rate of reaction. Signal enhancement values during the continuous flow experiment were determined to be in average 6666 ± 934. For the data analysis it was assumed that the signal enhancement value was constant throughout the reaction, so that the PHIP signal intensity in one spectrum depends only on the conversion during a short time interval before acquisition. Since the results are well described by the fit function derived from theory, it is confirmed that this assumption was correct. In a continuous flow measurement of this kind without hyperpolarization the reaction product's NMR signal vanishes in the noise. Hence, PHIP is an enabling technology for the measurement of a reaction kinetics under flow conditions in diluted solutions. The huge difference of PHIP and thermal signal intensities can be retraced from the exemplary PHIP spectrum in Fig. 5.4 which is superimposed with a thermal reference spectrum, recorded from the flow setup without flow at a total conversion U_{tot}=69.64%. For comparison, the much bigger PHIP signals in the spectrum originate from a conversion of

about 5%.

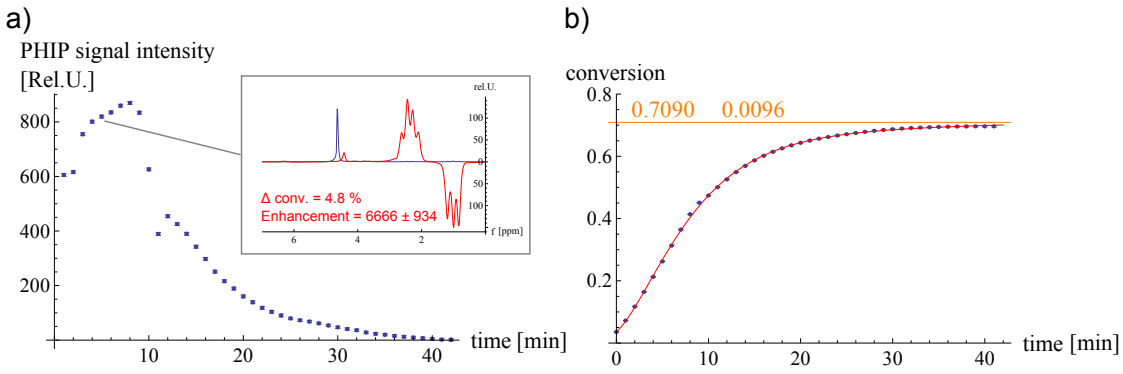

Figure 5.4.: Results of the continuous flow measurement of the pairwise hydrogenation reaction 2-hydroxyethyl acrylate to 2-hydroxyethyl propionate in H_2O. a) PHIP signal intensity of 2-hydroxyethyl propionate over reaction time. For one data point the underlying spectrum is exemplary shown, superimposed with a 1-scan thermal reference acquired without flow after the reaction. The average PHIP enhancement and the reaction conversion that the hyperpolarized spectrum originates from are noted. b) Numerically integrated PHIP intensities, scaled such that the last data point corresponds to the total reaction conversion $U_tot = 69.64\%$ after the experiment. A saturation curve with polynomial amplitude is fitted through the data. The value of the curve's asymptote is noted.

5.5. Conclusions

In the present work PHIP experiments are analyzed with medium field NMR spectroscopy. Two setups are investigated, shake and continuous flow experiments, respectively. The shake experiments have resulted in dramatical NMR signal enhancements both on ^{1}H as well as on ^{13}C. Especially the results for ^{13}C PHIP spectra are a huge benefit, since the acquisition of ^{13}C spectra with high SNR is impossible within a reasonable acquisition time at medium-field for diluted non isotopically enriched samples. PHIP spectra are able to provide an SNR that is high enough for reliable determination of J-couplings in the hydrogenation product molecule in only one scan. In some cases J-couplings could be identified clearer from a 1-scan hyperpolarized medium-field spectrum than from a thermal spectrum acquired with 256 scans at 7 T. Moreover, PHIP hyperpolarized spectra enable an extraordinary chemical selectivity, since only the reaction product resonances appear enhanced. The discussed problem of signal cancellation in PHIP hyperpolarized spectra with antiphasic peaks can be avoided with J-spectroscopy [88, 89]. J-spectroscopy methods allow to exploit the full signal

enhancement potential of PHIP by narrowing spectral lines significantly. Continuous flow experiments with PHIP allow to measure a ^{1}H reaction kinetics under flow conditions. Here as well PHIP has proven to be an enabling technology, since the acquisition of thermal snapshot spectra from a 1 mm ID capillary during flow is not possible for substrate concentrations below 70%. Even after full T_1 buildup a thermal 1-scan snapshot spectrum was hardly able to detect a substrate concentration below 10%. Altogether this work has demonstrated the feasibility of PHIP in a medium-field NMR spectrometer. The quality of the gained results proves that medium-field spectrometers can be used for studies on Parahydrogen Induced Polarization in the same way as high field spectrometers. A big advantage of using medium-field NMR spectrometers for scientific studies is the lower cost of purchase and maintenance, as well as the aspect of space saving. The applications of PHIP in medium-field can be further extended by incorporating polarization transfer sequences like e.g. INEPT or other substrates. For instance the industrially relevant homogeneous hydrogenation of adiponitrile to hexamethylendiamine could become subject of online monitoring by the aid of medium-field NMR spectrometers. Hexamethylenediamine is an important precursor for the production of polymers, whose most prominent example is nylon 66. [90]

Chapter 6.

Conclusion and Outlook

Different applications of Parahydrogen Induced Polarization have been presented. This chapter summarizes the obtained results and provides an outlook on potential future applications. Specific questions that remain unanswered until present and require further research are addressed.

In chapter 3 Parahydrogen Induced Polarization was applied for hyperpolarization of the biocompatible molecule fumaric acid disodium salt dissolved in water. The production of PHIP hyperpolarized fumarate was achieved by *trans*-hydrogenation of acetylene dicarboxylate with the catalyst $[RuCp^*(MeCN)_3]PF_6$. Difficulties with slow conversion and large amounts of unwanted *trans*-hydrogenation side products could be overcome by adding 100mM sodium sulfite (E 221) to the sample solution. It was shown that 1-^{13}C-fumarate has a long-lived molecular singlet state of $T_S = (46\pm7)$ s, whereas the lifetime T_S of unlabeled fumarate's singlet-state exceeds 6 minutes. The singlet state on 1-^{13}C-fumarate can be efficiently broken by the aid of a S2hM NMR pulse sequence, unlabeled fumarate's singlet state can be broken by the enzymatic conversion to L-malate which is part of the Krebs cycle. These are remarkable results, firstly, because fumarate in water is biocompatible and thus of great interest for future medical applications as hyperpolarized metabolic MRI contrast agent. Secondly, the existence of long-lived nuclear spin singlet states provides more time to build up significant amounts of hyperpolarized material for medical application than fumarate's spin-lattice relaxation constants $T_1(^1H) = \sim13$ s and $T_1(^{13}C) = \sim32$ s. The investigated approach for the production of PHIP fumarate with overpopulated singlet state is very promising, since it is cheaper than hyperpolarization via DNP and can gain higher polarization levels

and singlet yield. Further research is required in order to remove the toxic catalyst from the hyperpolarized reaction solution before medical application.

In chapter 4 Signal Amplification By Reversible Exchange was applied to provide hyperpolarization *in situ* at zero-field continuously for more than 5 hours. ZULF NMR is superior to traditional high-field NMR when it comes to chemical analysis or imaging inside metal objects or of heterogeneous materials. The ability to measure undisturbed internal spin-spin couplings makes it appealing for applications in quantum information processing and fundamental physics. However, the most serious drawback of ZULF NMR is its lack of thermal polarization which makes external sources of magnetization inevitable. With *in situ* SABRE an approach was investigated which allows to provide polarization continuously over a long time without the necessity to remove the sample from the experimental environment for re-polarization. This is a first step towards creating suitable conditions for long-time precision measurements with ZULF NMR. Long-time ZULF NMR experiments could be applied e.g. for fundamental dark matter research. Further research is required to widen the range of substrate molecules that can be polarized with the presented approach. For now the achieved continuous *in situ* polarization was used to explore a SABRE polarization transfer characteristic in dependence of external magnetic fields in the microtesla range.

In chapter 5 PHIP was used for signal enhancement in a continuous flow setup with NMR detection during flow by the aid of a mid-field NMR spectrometer. Parahydrogen for the pairwise hydrogenation was fed into the flowing sample solution though gas-permeable hollow fiber membranes. The achieved signal enhancement enabled to record a reaction kinetics of the pairwise hydrogenation reaction during flow. In order to achieve the same with thermal polarization multiple times higher sample concentrations would have been required in combination with slower flow rates, such that PHIP was proven to be an enabling technology for reaction-monitoring in diluted samples during flow.

Summarizing up PHIP was proven to be a versatile and promising technique that can help to overcome the drawback of low sensitivity in NMR. Its applications are likely to prove useful in the near future for different branches of science ranging from life sciences over engineering to fundamental physics.

Appendix A.

Parahydrogen Induced Polarization of Fumarate

A.1. Enzymatic Conversion of Fumarate to L-Malate

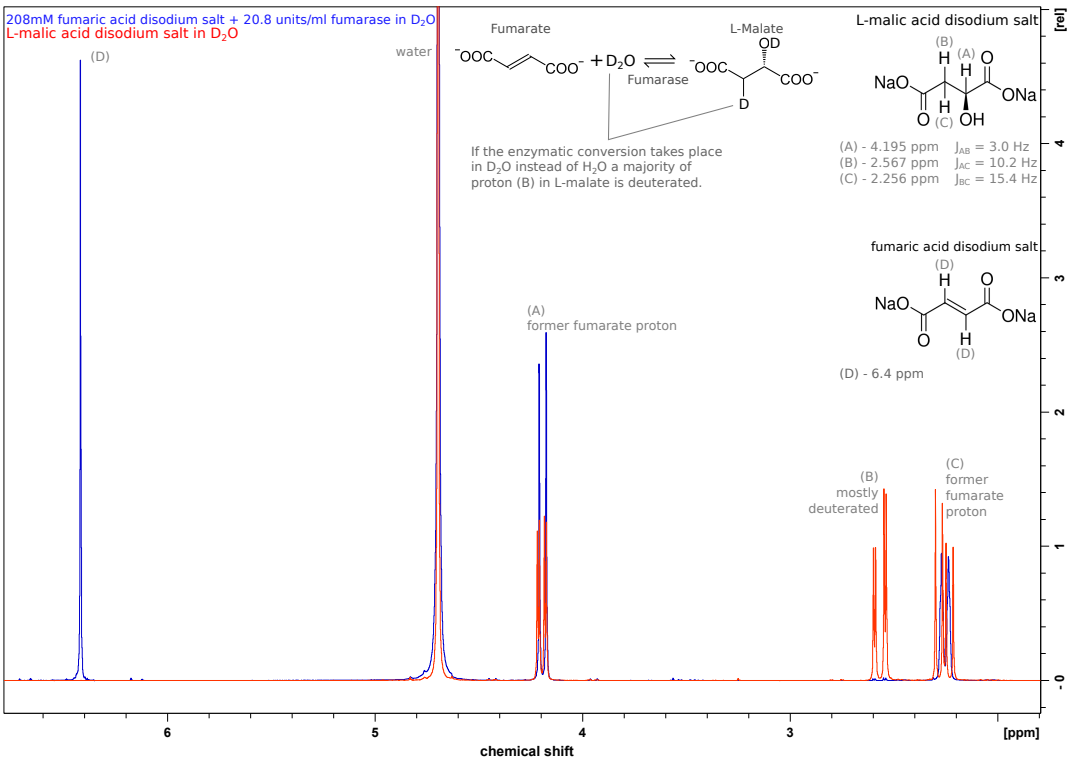

Figure A.1.: ^{1}H NMR spectra of pure L-malic acid disodium salt in D_2O (red) and of 208mM fumaric acid disodium salt with 20.8 units/ml enzyme fumarase in D_2O after complete enzymatic conversion (blue), acquired at 7 T.

A.2. Chemical Shift Values and T_1 Relaxation Times

	Chemical Shift [ppm]	
Molecule	^{1}H	^{13}C
acetylenedicarboxylic adic disodium salt	-	-
1-^{13}C-acetylenedicarboxylic adic disodium salt	-	159.87
fumaric acid disodium salt	6.42	-
1-^{13}C-fumaric acid disodium salt	6.42 (doublet with 4.7 Hz splitting)	174.67 (triplet w. 4.7 Hz splitting)
succinic acid disodium salt	2.30	-
1-^{13}C-succinic acid disodium salt	2.30	182.36
L-malic acid disodium salt	4.195, 2.567, 2.256	-
^{13}C-L-malic acid disodium salt	4.195, 2.5772, 2.256	1-^{13}C-L-malate (^{13}C on CHOH side): 181.02 4-^{13}C-L-malate (^{13}C on CH_2 side): 179.84
maleic acid disodium salt	5.925	-
1-13C-maleic acid disodium salt	5.925	168.80

Table A.1.: Chemical shift values of relevant molecules, determined at 7 T (300 MHz) and 15°C.

	T_1 [s]	
Molecule	^{1}H	^{13}C
1-^{13}C-acetylenedicarboxylic adic disodium salt	-	(63±3) s
fumaric acid disodium salt	13.3±0.6 (degassed: 20±1)	-
1-^{13}C-fumaric acid disodium salt	13.3±0.6	32±2
succinic acid disodium salt	2.4±0.2	-
1-^{13}C-succinic acid disodium salt	2.9±0.2	49.2±0.2
L-malic acid disodium salt	(4.195) 8±1, (2.567) 1.5±0.1, (2.256) 1.6±0.1 B-mostly deuterated: (4.195) 9.2±1.5, (2.567) 20±2, (2.256) 8.0±0.3	-
^{13}C-L-malic acid disodium salt (B mostly deuterated)	(4.195) 10±1, (2.572) 20±5, (2.256) 8.0±0.3	1-^{13}C-L-malate (^{13}C on CHOH side): 32±2 4-^{13}C-L-malate (^{13}C on CH_2 side): 34±2

Table A.2.: T_1 relaxation times of relevant molecules, determined at 7 T (300 MHz) and 15°C.

A.3. Thermal Reference Spectra of Pure 1-^{13}C-Fumaric Acid Disodium salt

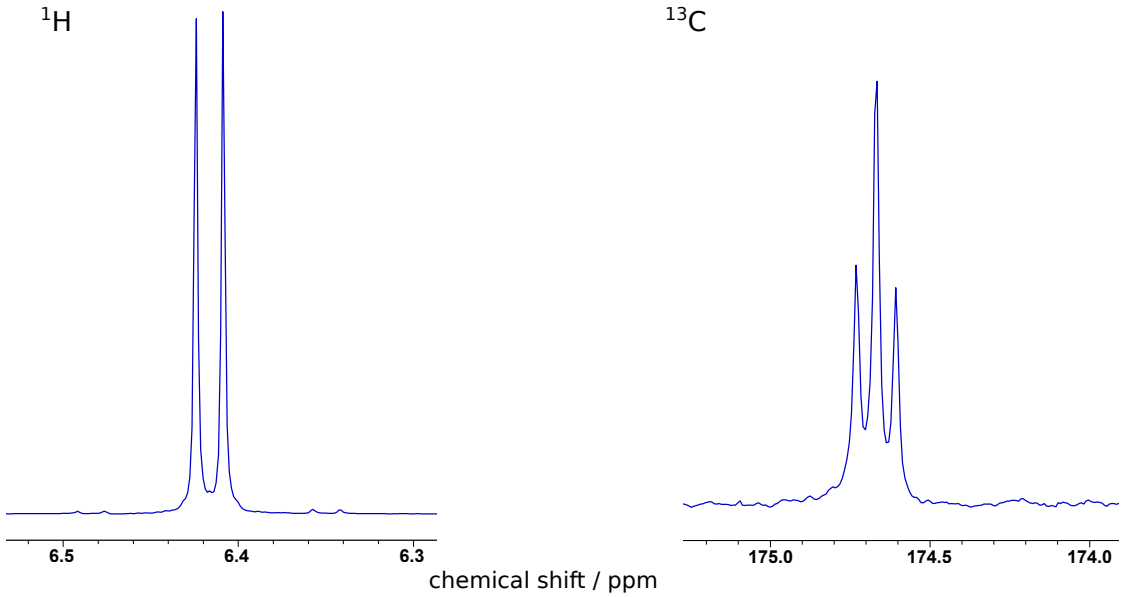

Figure A.2.: Thermal ^{1}H and ^{13}C spectra of 1-^{13}C-fumaric acid disodium salt.

A.4. Thermal Reference Spectra after *trans*-hydrogenation of 1-^{13}C-Acetylenedicarboxylic Acid Disodium Salt

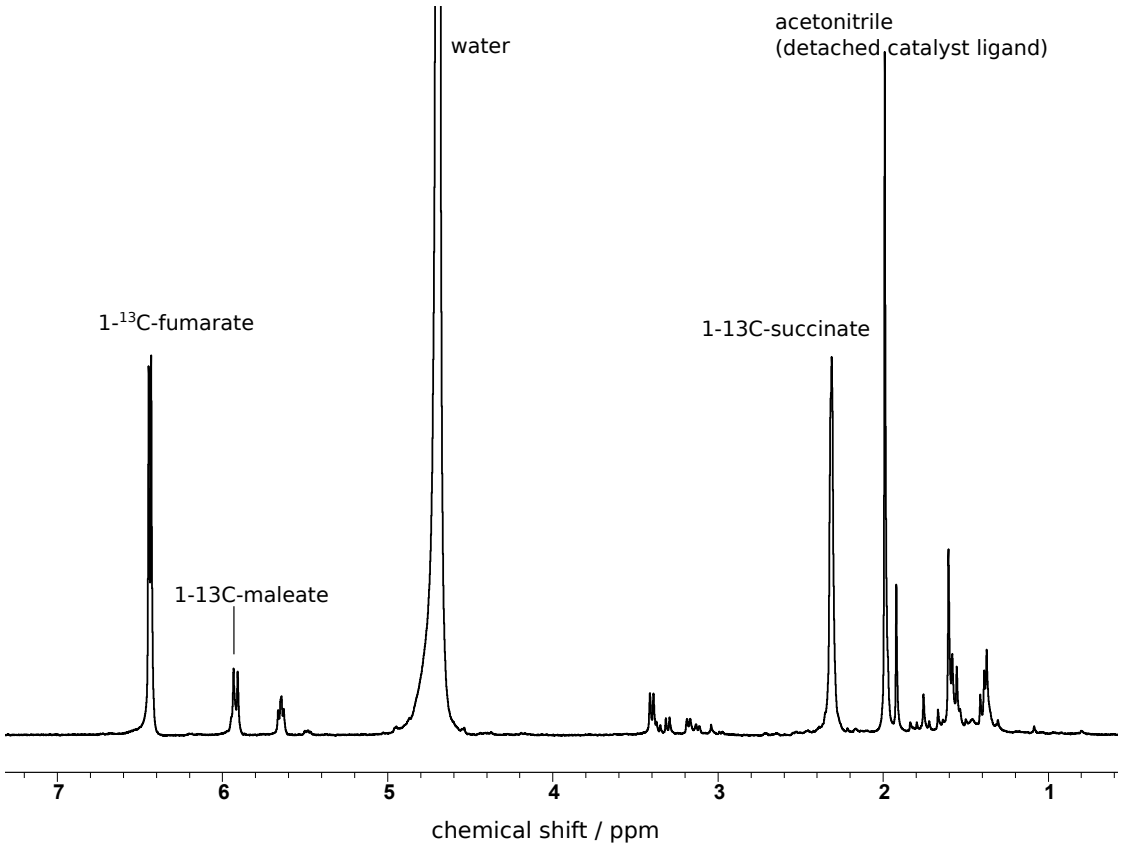

Figure A.3.: Thermal ^{1}H NMR spectrum after *trans*-hydrogenation of 1-^{13}C-acetylene dicarboxylate to 1-^{13}C-fumarate. Hydrogenation side products are visible.

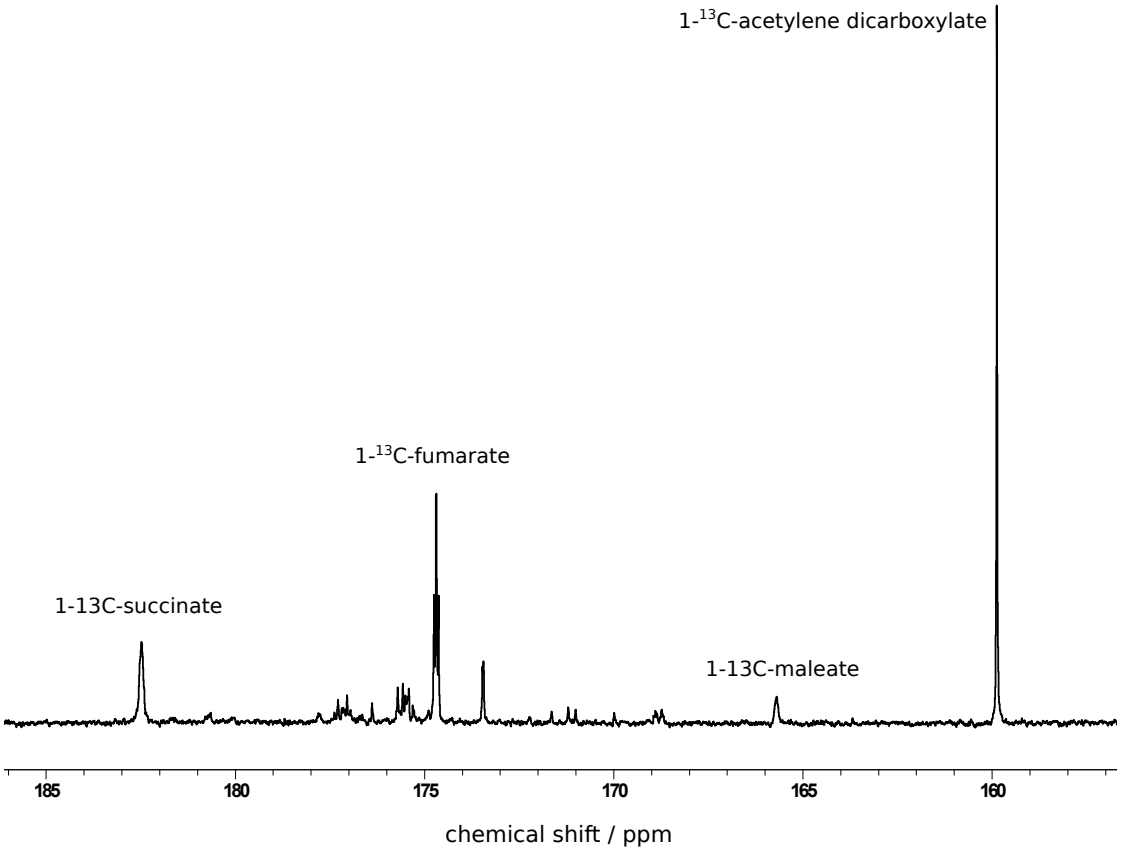

Figure A.4.: Thermal ^{13}C NMR spectrum after *trans*-hydrogenation of 1-^{13}C-acetylene dicarboxylate to 1-^{13}C-fumarate. Hydrogenation side products are visible.

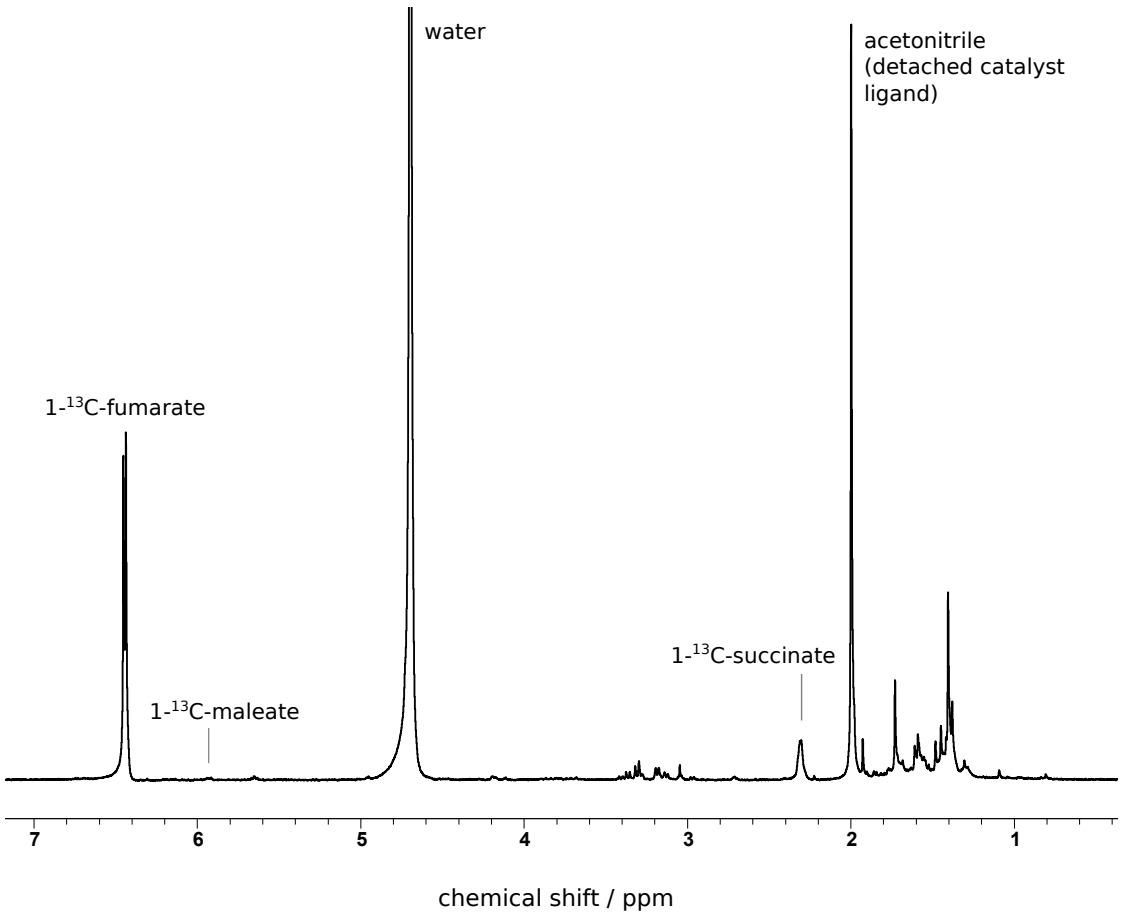

Figure A.5.: Thermal ^{1}H NMR spectrum after *trans*-hydrogenation of 1-^{13}C-acetylene dicarboxylate to 1-^{13}C-fumarate with 100 mM sodium sulfite additive in the reaction solution. Hydrogenation side products are strongly reduced.

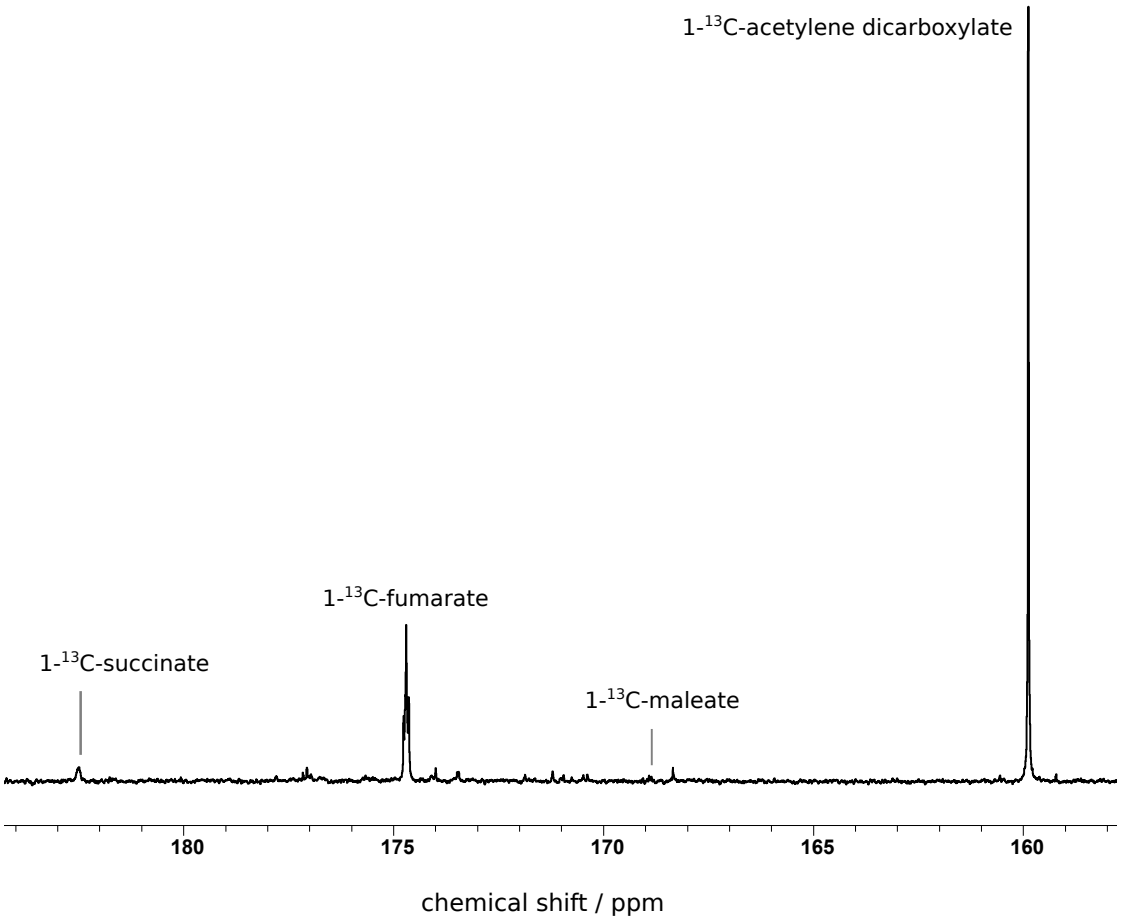

Figure A.6.: Thermal ^{13}C NMR spectrum after *trans*-hydrogenation of 1-^{13}C-acetylene dicarboxylate to 1-^{13}C-fumarate with 100 mM sodium sulfite additive in the reaction solution. Hydrogenation side products are strongly reduced.

Appendix B.

Continuous SABRE at Zero- to Ultralow Field

B.1. Optimization of Reaction Parameters

In order to maximize the signal intensity the sample composition, meaning the concentration of Pyridine in the sample solution, as well as the catalyst to Pyridine mass ratio were optimized. Moreover experiments for optimization of the pressure-flow-balance, reaction temperature, duration of bubbling and delay between bubbling and acquisition were performed. During all optimization experiments no magnetic field was applied during bubbling, the sequence is shown in Fig. B.1. For the optimization of the concentration of Pyridine in the sample solution, samples with a Pyridine concentration of 0.1 M (1 vol%), 0.6 M (5 vol%), 1.2 M (10 vol%), 1.9 M (15 vol%), 2.5 M (20 vol%), 3.7 M (30 vol%), 5.0 M (40 vol%), 6.2 M (50 vol%), 9.9 M (80 vol%) and 12.4 M (100 vol%) were tested, the catalyst concentration was 1:10 mass ratio (1.3 mol%) for each sample. For the optimization of the concentration of catalyst Ir(COD)(IMes)Cl with respect to Pyridine, samples with catalyst:Pyridine mass ratios of 1:100 (0.1 mol%), 1:50 (0.3 mol%), 1:20 (0.6 mol%), 1:10 (1.3 mol%), 3:20 (1.9 mol%), 1:5 (2.5 mol%) were tested, the Pyridine concentration was 1.9 M (15 vol%) for each sample. Each sample was measured for approximately 30 min (60 scans) after full activation of the catalyst. The optimization of reaction temperature, pressure-flow-balance, duration of bubbling and delay between bubbling and acquisition were performed during continuous long-time experiments for 2-4h with one sample. The reaction temperature was scanned from 320K to 295K. The parahydrogen pressure was varied from 5 bar to 7 bar, with the maximum flow rate that allowed for keeping the pressure stable with the Bruker parahydrogen generator BPHG 90, respectively. The duration of bubbling was varied from 1s to 19s in steps of 3s. For the variation of the delay between bubbling and acquisition d1 was set to 250ms and d2 was varied from 10ms to 4s in steps of 200ms, at a bubbling duration of 15 s. The sample for these experiments consisted of 0.3 ml of 1.9M solution of

Pyridine in anhydrous Methanol, with a catalyst to Pyridine concentration of 1.3 mol% and a small Pyridine-15N additive (0.04 M). For all experiments, besides the optimization of the named parameter and unless specified differently the sample temperature inside the shield was kept stable at a temperature between 295K and 320K, the delay between bubbling and acquisition d1 was set to 1s and d2 was set to zero, the parahydrogen pressure was 6-7 bar and the bubbling duration 5s.

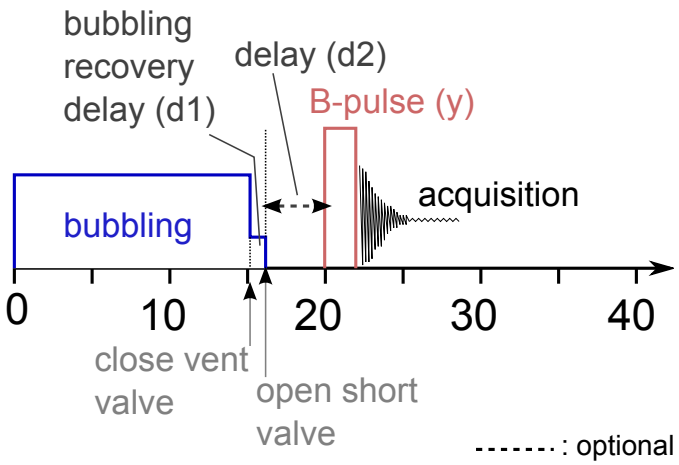

Figure B.1.: Sequence for optimiztation measurements.

For all optimized parameters, the average signal intensity was plotted over the respective parameter. Other aspects, like noise level, time for catalyst activation or experimental feasibility were also taken into account in order to decide on the optimal parameter setting for the following experiments. Table B.1 gives an overview over all optimized parameters with observations and resulting optima used for further experiments.

Parameter	**Observation**	**Optimum used for further experiments**
Pyridine concentration in M	Optimum between 1.9M and 3.7M. 1.9M and 2.5M give almost equal SNR. 3.7M slightly better, but much longer catalyst activation time.	1.9M (15 vol%) Py in MeOH with small (0.04M) ^{15}N-Pyridine additive to increase SNR
Catalyst concentration w.resp. to Pyridine	The higher the catalyst concentration the better the SNR.	Higher catalyst concentrations require significantly longer catalyst activation times. 1.3 mol% (mass ratio 1:10) gave a sufficient SNR with the possibility to activate the catalyst within minutes.
Reaction Temperature	Optimum around 310K.	310K
Pressure-flow-balance	Within the capability of the Bruker BPHG 90 the best results were achieved at 6-7 bar pH2 and a flow rate that allows to keep up this pressure.	6-7 bar pH2, flow rate adjusted to keep the pressure stable.
Duration of bubbling	The signal intensity keeps increasing following a saturation curve with increasing duration of bubbling. At 15s the saturation is almost reached.	15s
Delay between bubbling and acquisition	The signal intensity decreases with an exponential decay with increasing delay between bubbling and acquisition. Delays shorter than 1s however lead to an unsteady signal intensity and more noise, due to residual bubbling.	1s

Table B.1.: Optimized parameters with observation and result.

B.2. Continuous Long-time ZULF-SABRE Hyperpolarization

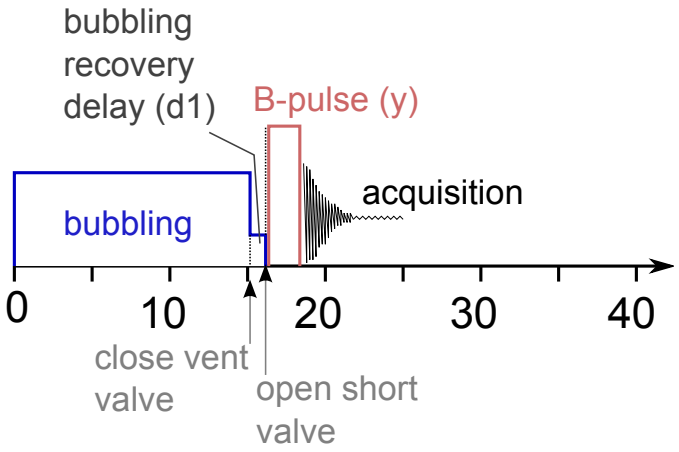

Figure B.2.: Sequence for continuous long-time ZULF-SABRE measurements. No B-field was applied during bubbling. d1 was set to 1s.

The sample for continuous long-time ZULF-SABRE experiments consisted of 0.3 ml of 1.9M solution of Pyridine in anhydrous Methanol, with a catalyst to Pyridine concentration of 1.3 mol% and a small ^{15}N-pyridine additive of 0.04M. The sample temperature was kept stable at 310K. The applied pulse sequence can be found in Fig. B.2.

B.3. Variation of B-field during Polarization Transfer

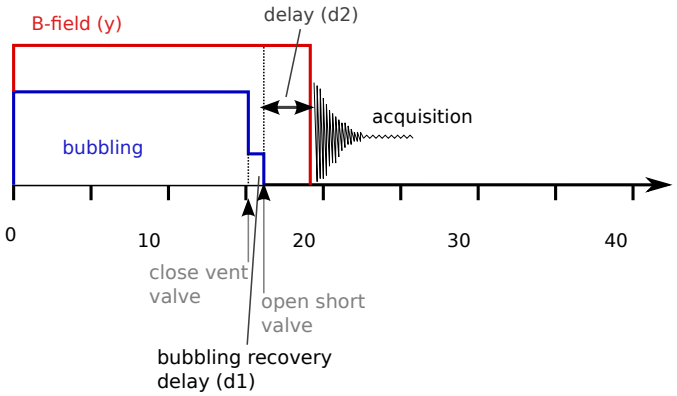

Figure B.3.: Sequence for experiments on the B-field dependency of spin order transfer in ZULF-SABRE. The magnetic field during bubbling and polarization transfer ist turned off abruptly just before acquisition. No more B-field-pulse is applied.

In order to discover the magnetic field dependency of the spin order transfer during in situ ZULF-SABRE experiments, the sequence in Fig. B.3 was used. A variable magnetic field in the range from -3μT to 3μT was applied during bubbling, and thereby during polarization transfer. 52 points were acquired within this magnetic field range, each point was acquired with four scans. The abrupt turn-off of the magnetic field was achieved with compensating currents to disable Lentz's law, d1 was set to 250 ms and d2 to 10 ms. The magnetic field was suddenly turned off, right after delay d2. After a dead time of 10ms acquisition began. No short B-field pulse was applied. One full scan lasted 30s.

Appendix C.

Hyperpolarized Reaction Monitoring

C.1. T1 Times of the Hydrogenation Product Molecules at 1T

in Acetone d_6

	T1 (s)
DMM (6.25ppm)	3,78
DMM (3.60ppm)	3,18
Hex (5.8ppm)	3,80
Hex (4.9ppm)	3,74
Hex (2.05ppm)	3,47
Hex (1.3ppm)	3,35
Hex (0.8ppm)	3,24

in MeOD

	T1 (s)
HEP (4.2ppm)	7,04
HEP (3.7ppm)	2,39
HEP (3.2ppm)	2,29
HEP (2.0ppm)	3,84
HEP (0.7ppm)	4,85

in D_2O

	T1 (s)
HEA (6.2ppm)	2,20
HEP (4.1ppm)	1,46
HEP (3.7ppm)	1,39
HEP (2.2ppm)	2,29
HEP (1.0ppm)	2,76

in H_2O

	T1 (s)
HEA (6.2ppm)	1,66
HEP (4.1ppm)	1,19
HEP (3.7ppm)	1,09
HEP (2.2ppm)	1,96
HEP (1.0ppm)	2,30

C.2. Explanation of PHIP Peaks (Shake Measurements)

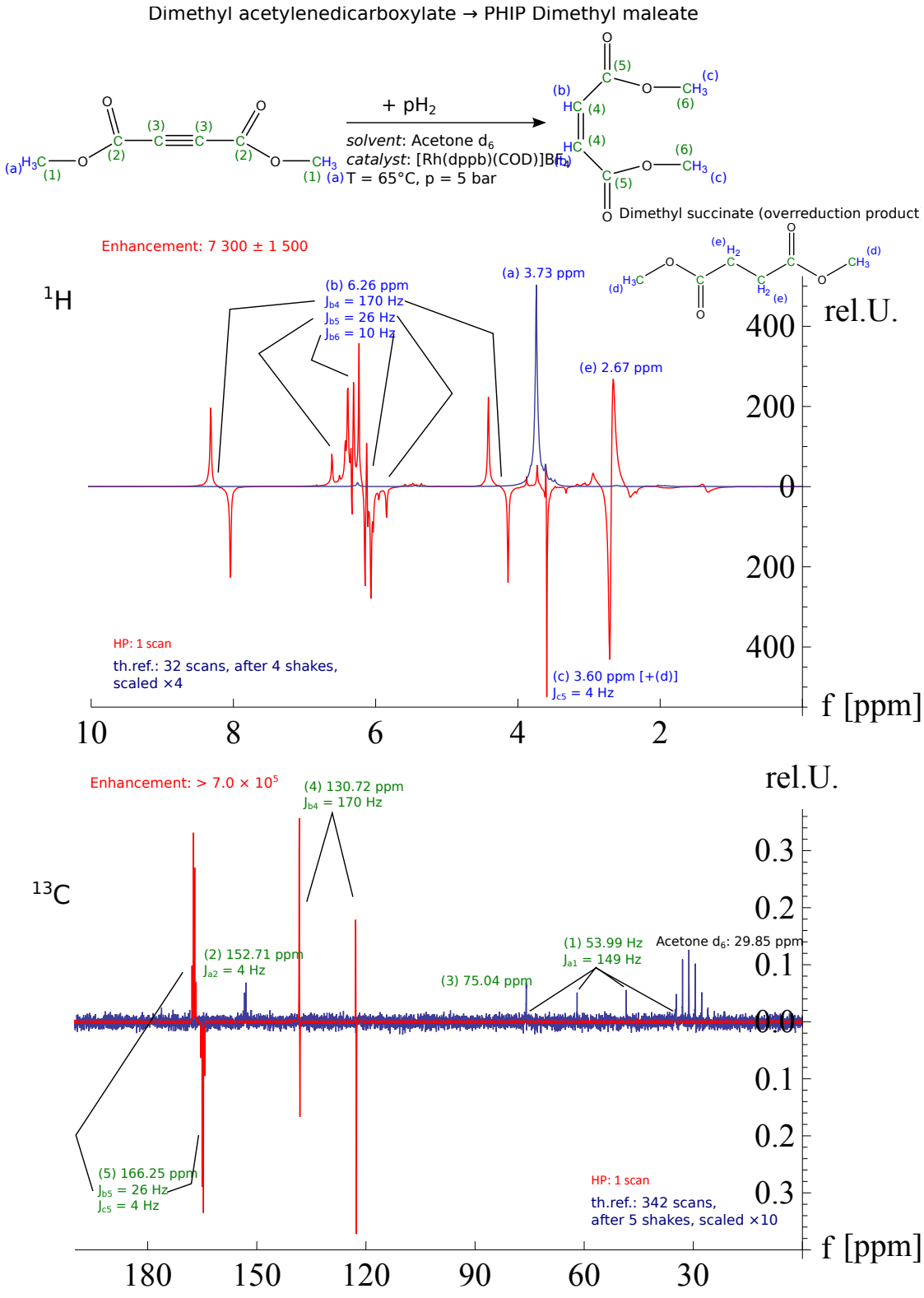

Figure C.1.: Explanation of hyperpolarized resonances in the ^{1}H and ^{13}C spectra of PHIP Dimethyl maleate in Acetone d_6.

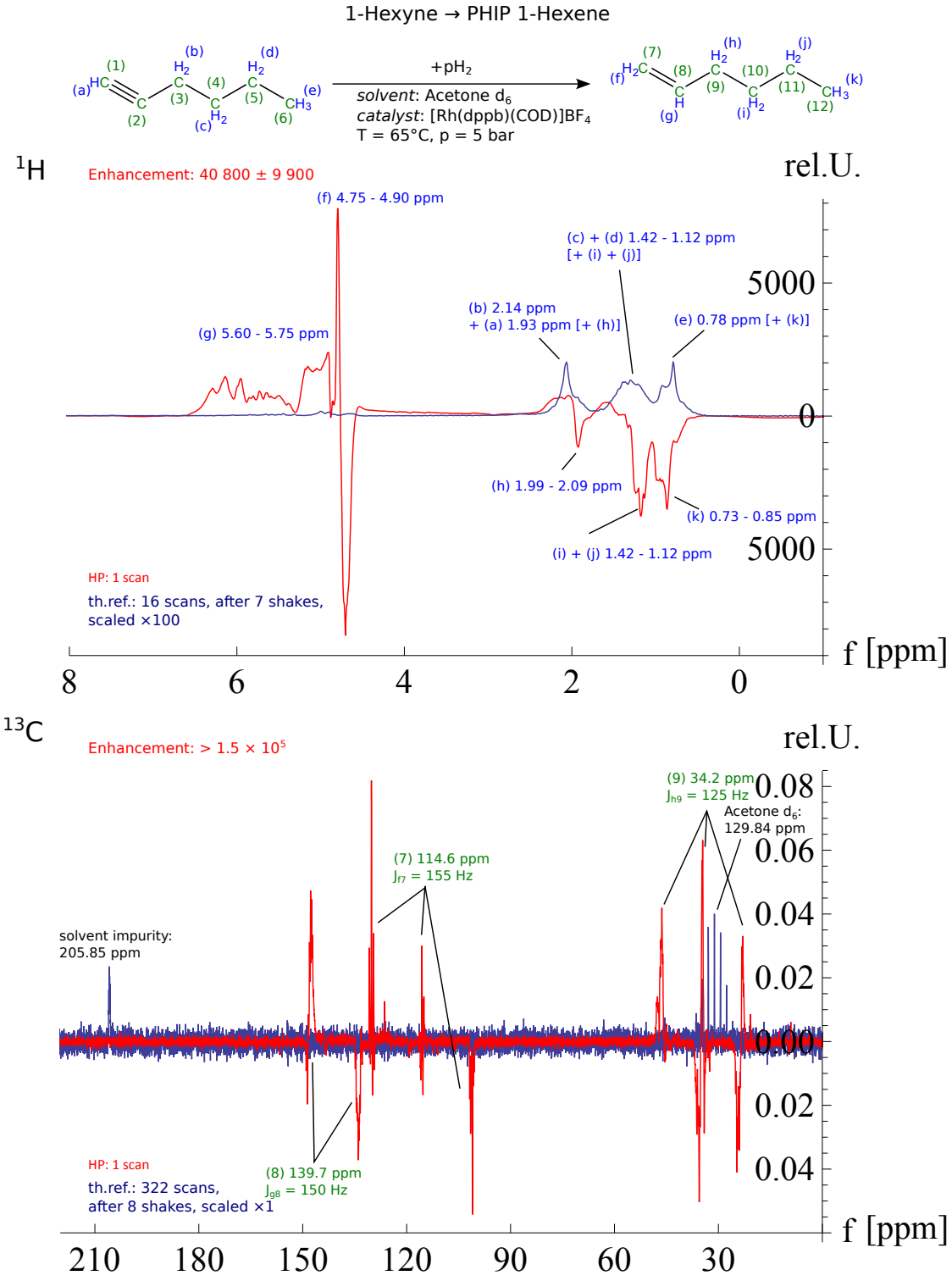

Figure C.2.: Explanation of hyperpolarized resonances in the ^{1}H and ^{13}C spectra of PHIP 1-Hexene in Acetone d_6.

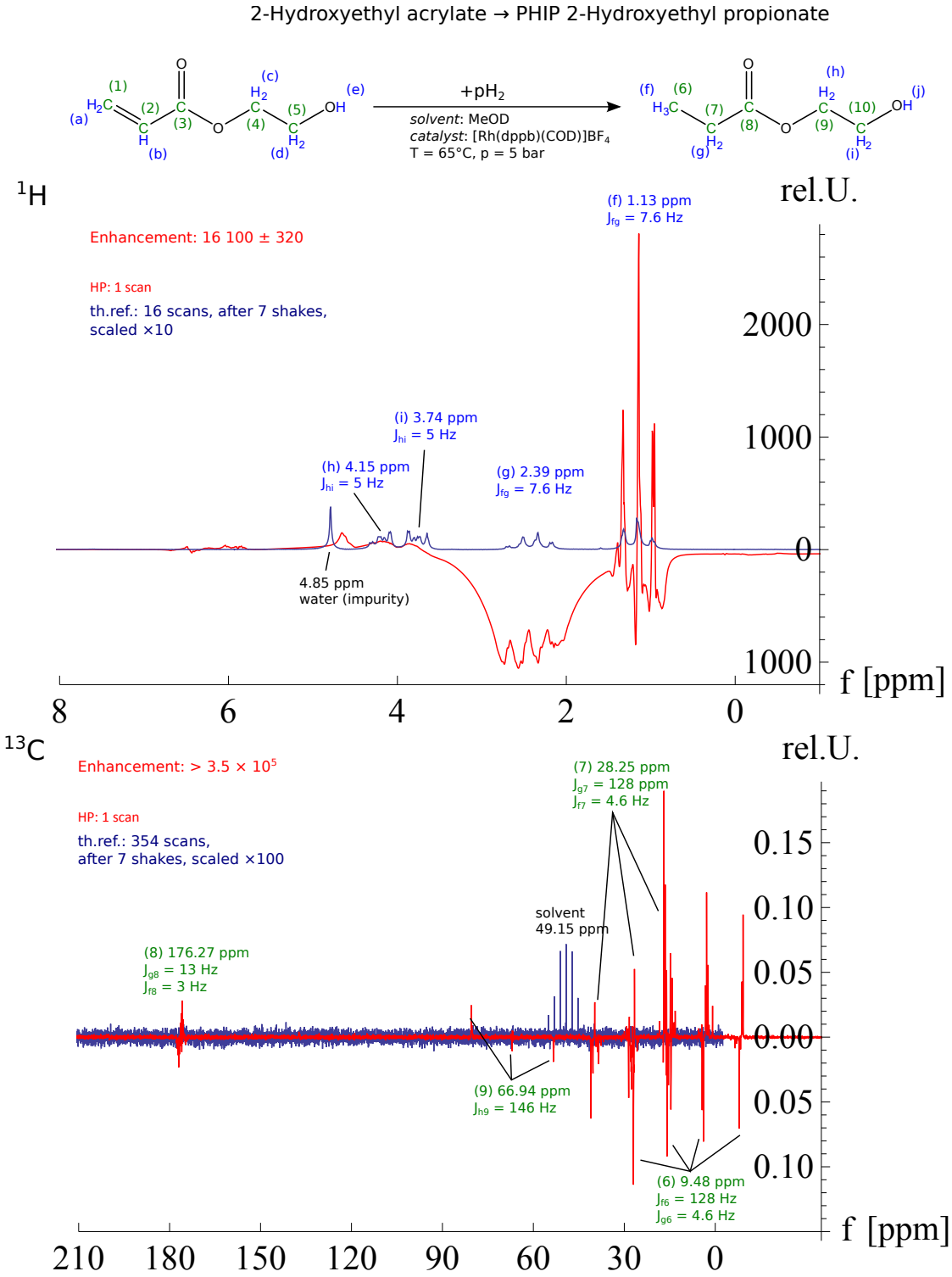

Figure C.3.: Explanation of hyperpolarized resonances in the ^{1}H and ^{13}C spectra of PHIP 2-Hydroxyethyl propionate in MeOD.

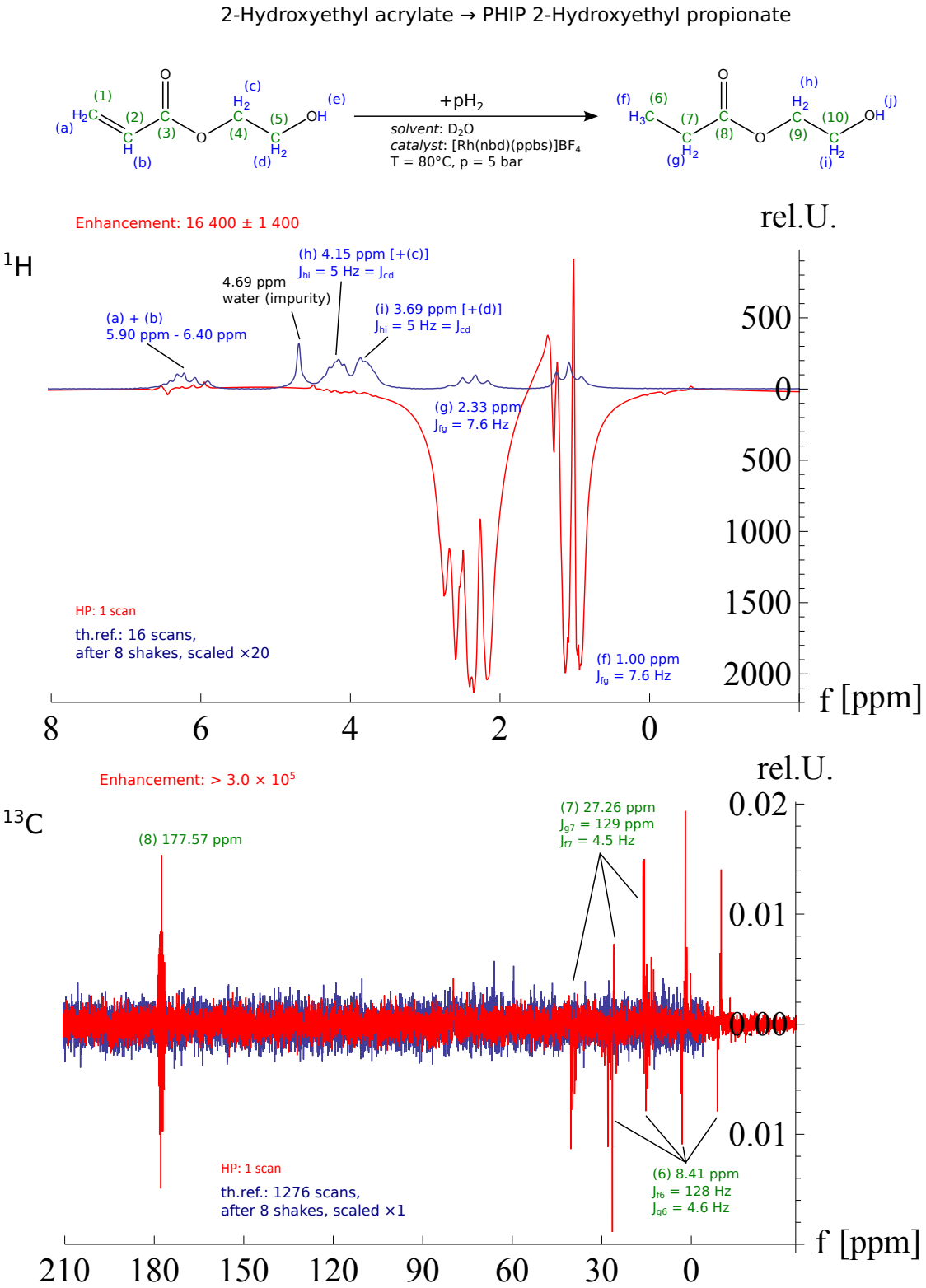

Figure C.4.: Explanation of hyperpolarized resonances in the ^{1}H and ^{13}C spectra of PHIP 2-Hydroxyethyl propionate in D_2O.

C.3. Continuous Measurements

The same experiment as in H_2O was also performed in D_2O. The total conversion at the end of the experiment in D_2O was Utot=77.67% . For reaction in D_2O the spectral amplitudes on the water peak was not possible due to a missing water peak. However, this did not affect further analysis, since amplitude fluctuation effects were negligible. The numerically integrated datapoints of PHIP signal intensity over time were fitted with the function

$$U(t) = (a + bt + ct^2 + dt^3) \cdot e^{-kt} + f$$

Results are shown in Fig. C.5

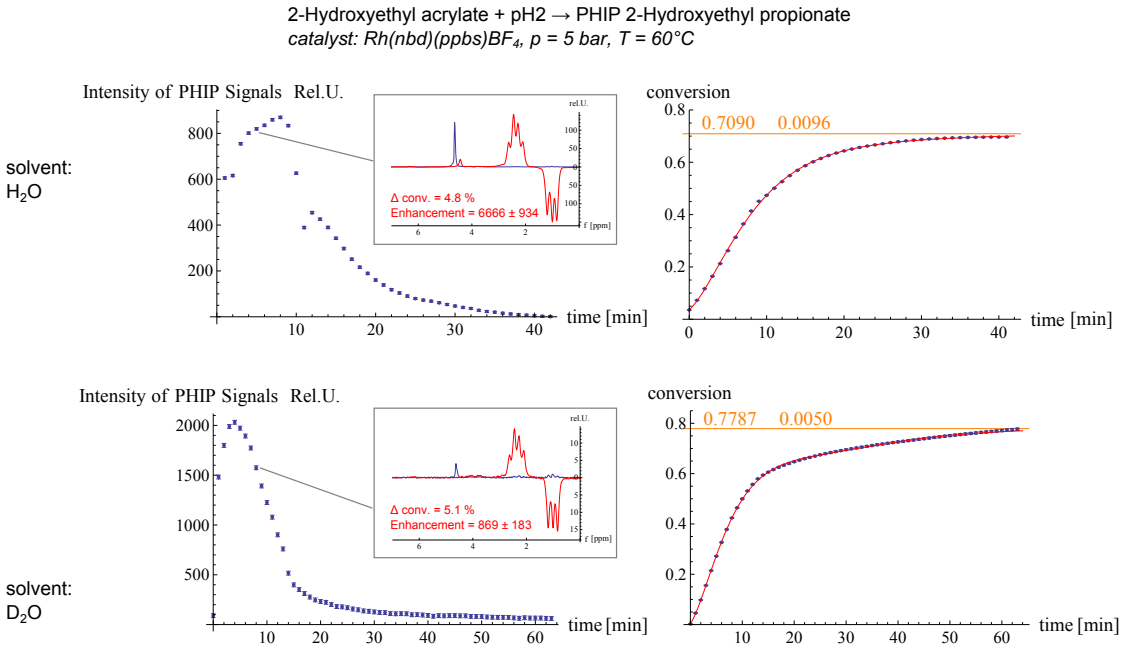

Figure C.5.: Results of the continuous flow measurement of the pairwise hydrogenation reaction 2-hydroxyethyl acrylate to 2-hydroxyethyl propionate in H_2O (top) and D_2O (bottom). Left: PHIP signal intensity of 2-hydroxyethyl propionate over reaction time. For one data point per dataset the underlying spectrum is exemplary shown, superimposed with a 1-scan thermal reference acquired without flow after the reaction. The average PHIP enhancements and the reaction conversions that the hyperpolarized spectra originate from are noted. Right: Numerically integrated PHIP intensities, scaled such that the last data point corresponds to the total reaction conversion after the experiment, U_{tot} = 69.64% in H2O and U_{tot}=77,67% in D_2O. A saturation curve with polynomial amplitude is fitted through both datasets. The value of the curves' asymptotes are noted.

The lower enhancement values of 869 ± 183 in D_2O, compared to 6666 ± 934 in H_2O result from the used parahydrogen. The experiment in H_2O was performed with 1-day-old parahydrogen, the experiment in D_2O was performed with 2-day-old parahydrogen. The resulting fitting parameters are shown in Table C.1. It can be observed that neither parahydrogen percentage nor solvent have an effect on the resulting reaction rate fit parameter k, which for both experiments lie in the same order of magnitude($(0.158 \pm 0.019) min^{-1}$ in H2O and $(0.140 \pm 0.003) min^{-1}$ in D_2O).

Experiment in H2O		
	Estimate	Standard Error
a	-0.672544	0.00979139
b	-0.0805412	0.0128931
c	0.00482468	0.00087077
d	-0.000149237	0.0000322289
k	0.15835	0.0191012
f	0.70904	0.00960645
R^2	0.9999275	
Experiment in D_2O		
	Estimate	Standard Error
a	-0.775486	0.00513371
b	-0.0773283	0.00238773
c	0.00761155	0.000181722
d	-0.000352648	0.0000108596
k	0.140085	0.00276713
f	0.778732	0.00501268
R^2	0.9999717	

Table C.1.: Results for fit parameters and coefficient of determination R^2 as a measure for goodness of fit for the nonlinear model fit of $U(t) = (a + bx + cx^2 + dx^3) \cdot e^{-kt} + f$ into reaction conversion over time data.

Bibliography

[1] M. Abraham, M. A. H. McCausland, and F. N. H. Robinson. Dynamic nuclear polarization. *Phys. Rev. Lett.*, 2:449–451, Jun 1959.

[2] Johannes Natterer and Joachim Bargon. Parahydrogen induced polarization. *Progress in Nuclear Magnetic Resonance Spectroscopy*, 31(4):293–315, 1997.

[3] F. D. Colegrove, L. D. Schearer, and G. K. Walters. Polarization of he^3 gas by optical pumping. *Phys. Rev.*, 132:2561–2572, Dec 1963.

[4] W. Happer, E. Miron, S. Schaefer, D. Schreiber, W. A. van Wijngaarden, and X. Zeng. Polarization of the nuclear spins of noble-gas atoms by spin exchange with optically pumped alkali-metal atoms. *Phys. Rev. A*, 29:3092–3110, Jun 1984.

[5] M Ebert, T Grossmann, W Heil, E.W Otten, R Surkau, M Thelen, M Leduc, P Bachert, M.V Knopp, and L.R Schad. Nuclear magnetic resonance imaging with hyperpolarised helium-3. *The Lancet*, 347(9011):1297 – 1299, 1996.

[6] M.H. Levitt. *Spin Dynamics: Basics of Nuclear Magnetic Resonance*. Wiley, 2001.

[7] J. Keeler. *Understanding NMR Spectroscopy*. Wiley, 2011.

[8] H. Günther. *NMR spectroscopy: an introduction*. Wiley, 1980.

[9] H. Friebolin. *Basic One- and Two-Dimensional NMR Spectroscopy*. Wiley, 2005.

[10] C.P. Slichter. *Principles of Magnetic Resonance*. Springer Series in Solid-State Sciences. Springer Berlin Heidelberg, 1996.

[11] R.R. Ernst, G. Bodenhausen, and A. Wokaun. *Principles of Nuclear Magnetic Resonance in One and Two Dimensions*. International series of monographs on chemistry. Clarendon Press, 1990.

[12] Theo Mayer-Kuckuk. *Atomphysik: Eine Einführung*. Springer-Verlag, 2013.

[13] Wolfgang Demtröder. *Atoms, Molecules, and Photons*. Springer, 2006.

[14] Hermann Haken and Hans C Wolf. *Atomic and quantum physics: an introduction to the fundamentals of experiment and theory.* Springer Science & Business Media, 2012.

[15] Walther Gerlach and Otto Stern. Der experimentelle nachweis der richtungsquantelung im magnetfeld. *Zeitschrift für Physik*, 9(1):349–352, 1922.

[16] C Russell Bowers and Daniel P Weitekamp. Transformation of symmetrization order to nuclear-spin magnetization by chemical reaction and nuclear magnetic resonance. *Physical Review Letters*, 57(21):2645–2648, 1986.

[17] C Russell Bowers and Daniel P Weitekamp. Parahydrogen and synthesis allow dramatically enhanced nuclear alignment. *Journal of the American Chemical Society*, 109(18):5541–5542, 1987.

[18] Lisandro Buljubasich, María Belén Franzoni, and Kerstin Münnemann. Parahydrogen induced polarization by homogeneous catalysis: theory and applications. In *Hyperpolarization Methods in NMR Spectroscopy*, pages 33–74. Springer, 2013.

[19] Ralph W Adams, Juan A Aguilar, Kevin D Atkinson, Michael J Cowley, Paul IP Elliott, Simon B Duckett, Gary GR Green, Iman G Khazal, Joaquín López-Serrano, and David C Williamson. Reversible interactions with para-hydrogen enhance nmr sensitivity by polarization transfer. *Science*, 323(5922):1708–1711, 2009.

[20] AN Pravdivtsev, KL Ivanov, AV Yurkovskaya, H-M Vieth, and RZ Sagdeev. Spontaneous transfer of para-hydrogen induced polarization to 13 c spins in symmetric molecules. In *Doklady Physical Chemistry*, volume 464, pages 247–250. Springer, 2015.

[21] Clarence Zener. Non-adiabatic crossing of energy levels. *Proc. R. Soc. Lond. A*, 137(833):696–702, 1932.

[22] Max Born and Vladimir Fock. Beweis des adiabatensatzes. *Zeitschrift für Physik*, 51(3-4):165–180, 1928.

[23] Jan-Bernd Hövener, Stephan Knecht, Niels Schwaderlapp, Jürgen Hennig, and Dominik von Elverfeldt. Continuous re-hyperpolarization of nuclear spins using parahydrogen: Theory and experiment. *ChemPhysChem*, 15(12):2451–2457, 2014.

[24] Thomas Theis, Paul Ganssle, Gwendal Kervern, Svenja Knappe, John Kitching, MP Ledbetter, Dmitry Budker, and Alex Pines. Parahydrogen-enhanced zero-field nuclear magnetic resonance. *Nature Physics*, 7(7):571, 2011.

[25] Thomas Theis, Micah P Ledbetter, Gwendal Kervern, John W Blanchard, Paul J Ganssle, Mark C Butler, Hyun D Shin, Dmitry Budker, and Alexander Pines. Zero-field nmr enhanced by parahydrogen in reversible exchange. *Journal of the American Chemical Society*, 134(9):3987–3990, 2012.

[26] John W. Blanchard and Dmitry Budker. Zero- to ultralow-field nmr. *eMagRes*, 5:1395–1410, September 2016.

[27] Micah P. Ledbetter and Dmitry Budker. Zero-field nuclear magnetic resonance. *Physics Today*, 66:44–49, 2013.

[28] John W. Blanchard, Tobias F. Sjolander, Jonathan P. King, Micah P. Ledbetter, Emma H. Levine, Vikram S. Bajaj, Dmitry Budker, and Alexander Pines. Measurement of untruncated nuclear spin interactions via zero- to ultra-low-field nuclear magnetic resonance. *PHYSICAL REVIEW B*, 92, 220202(R), 2015.

[29] Michael CD Tayler, Tobias F Sjolander, Alexander Pines, and Dmitry Budker. Nuclear magnetic resonance at millitesla fields using a zero-field spectrometer. *Journal of Magnetic Resonance*, 270:35–39, 2016.

[30] Sarah J Nelson, John Kurhanewicz, Daniel B Vigneron, Peder EZ Larson, Andrea L Harzstark, Marcus Ferrone, Mark van Criekinge, Jose W Chang, Robert Bok, Ilwoo Park, et al. Metabolic imaging of patients with prostate cancer using hyperpolarized [1-13c] pyruvate. *Science translational medicine*, 5(198):198ra108–198ra108, 2013.

[31] Klaes Golman, Mathilde Lerche, Rikard Pehrson, Jan Henrik Ardenkjaer-Larsen, et al. Metabolic imaging by hyperpolarized 13c magnetic resonance imaging for in vivo tumor diagnosis. *Cancer research*, 66(22):10855–10860, 2006.

[32] Ferdia A Gallagher, Mikko I Kettunen, De-En Hu, Pernille R Jensen, Magnus Karlsson, Anna Gisselsson, Sarah K Nelson, Timothy H Witney, Sarah E Bohndiek, Georg Hansson, et al. Production of hyperpolarized [1, 4-13c2] malate from [1, 4-13c2] fumarate is a marker of cell necrosis and treatment response in tumors. *Proceedings of the National Academy of Sciences*, 106(47):19801–19806, 2009.

[33] Jack J. Miller, Angus Z. Lau, Per Mose Nielsen, Giles McMullen-Klein, Andrew J. Lewis, Nichlas Riise Jespersen, Vicky Ball, Ferdia A. Gallagher, Carolyn A. Carr, Christoffer Laustsen, Hans Erik BÃ¸tker, Damian J. Tyler,

and Marie A. Schroeder. Hyperpolarized [1,4-13c2]fumarate enables magnetic resonance-based imaging of myocardial necrosis. *JACC: Cardiovascular Imaging*, 2017.

[34] Per Mose Nielsen, Abubakr Eldirdiri, Lotte Bonde Bertelsen, Hans Stødkilde Jørgensen, Jan Henrik Ardenkjaer-Larsen, and Christoffer Laustsen. Fumarase activity: an in vivo and in vitro biomarker for acute kidney injury. *Scientific reports*, 7:40812, 2017.

[35] Malcolm H Levitt. Singlet nuclear magnetic resonance. *Annual review of physical chemistry*, 63:89–105, 2012.

[36] Marina Carravetta, Ole G. Johannessen, and Malcolm H. Levitt. Beyond the T_1 limit: Singlet nuclear spin states in low magnetic fields. *Phys. Rev. Lett.*, 92:153003, Apr 2004.

[37] Giuseppe Pileio, Marina Carravetta, and Malcolm H Levitt. Storage of nuclear magnetization as long-lived singlet order in low magnetic field. *Proceedings of the National Academy of Sciences*, 107(40):17135–17139, 2010.

[38] G Pileio. Singlet state relaxation via intermolecular dipolar coupling. *The Journal of chemical physics*, 134(21):214505, 2011.

[39] Yuning Zhang, Pei Che Soon, Alexej Jerschow, and James W Canary. Long-lived 1h nuclear spin singlet in dimethyl maleate revealed by addition of thiols. *Angewandte Chemie*, 126(13):3464–3467, 2014.

[40] Yuning Zhang, Xueyou Duan, Pei Che Soon, Vladimír Sychrovskỳ, James W Canary, and Alexej Jerschow. Limits in proton nuclear singlet-state lifetimes measured with para-hydrogen-induced polarization. *ChemPhysChem*, 17(19):2967–2971, 2016.

[41] Karin Radkowski, Basker Sundararaju, and Alois Fürstner. A functional-group-tolerant catalytic trans hydrogenation of alkynes. *Angewandte Chemie International Edition*, 52(1):355–360, 2013.

[42] Dana Schleyer, Heiko G Niessen, and Joachim Bargon. In situ 1 h-phip-nmr studies of the stereoselective hydrogenation of alkynes to (e)-alkenes catalyzed by a homogeneous [cp* ru]+ catalyst. *New Journal of Chemistry*, 25(3):423–426, 2001.

[43] Dragoş-Adrian Roşca, Karin Radkowski, Larry M Wolf, Minal Wagh, Richard Goddard, Walter Thiel, and Alois FuÌˆrstner. Ruthenium-catalyzed alkyne trans-hydrometalation: Mechanistic insights and preparative implications. *Journal of the American Chemical Society*, 139(6):2443–2455, 2017.

[44] Barbara Ripka, James Eills, Hana Kouřilová, Markus Leutzsch, Malcolm H Levitt, and Kerstin Münnemann. Hyperpolarized fumarate via parahydrogen. *Chemical Communications*, 2018.

[45] Andrey N. Pravdivtsev, Alexandra V. Yurkovskaya, Robert Kaptein, Karsten Miesel, Hans-Martin Vieth, and Konstantin L. Ivanov. Exploiting level anti-crossings for efficient and selective transfer of hyperpolarization in coupled nuclear spin systems. *Phys.Chem.Chem.Phys.*, 15:14660, 2013.

[46] Andrey N Pravdivtsev, Alexandra V Yurkovskaya, Hans-Martin Vieth, and Konstantin L Ivanov. Coherent transfer of nuclear spin polarization in field-cycling nmr experiments. *The Journal of chemical physics*, 139(24):244201, 2013.

[47] Giuseppe Pileio and Malcolm H Levitt. Theory of long-lived nuclear spin states in solution nuclear magnetic resonance. ii. singlet spin locking. *The Journal of chemical physics*, 130(21):214501, 2009.

[48] Alexey S Kiryutin, Konstantin L Ivanov, Alexandra V Yurkovskaya, Hans-Martin Vieth, and Nikita N Lukzen. Manipulating spin hyper-polarization by means of adiabatic switching of a spin-locking rf-field. *Physical Chemistry Chemical Physics*, 15(34):14248–14255, 2013.

[49] Gabriele Stevanato, James Eills, Christian Bengs, and Giuseppe Pileio. A pulse sequence for singlet to heteronuclear magnetization transfer: S2hm. *Journal of Magnetic Resonance*, 277:169 – 178, 2017.

[50] James Eills, Gabriele Stevanato, Christian Bengs, Stefan Glöggler, Stuart J Elliott, Javier Alonso-Valdesueiro, Giuseppe Pileio, and Malcolm H Levitt. Singlet order conversion and parahydrogen-induced hyperpolarization of 13c nuclei in near-equivalent spin systems. *Journal of Magnetic Resonance*, 274:163–172, 2017.

[51] E Delia Corte and F Stirpe. The regulation of rat liver xanthine oxidase. involvement of thiol groups in the conversion of the enzyme activity from dehydrogenase (type d) into oxidase (type o) and purification of the enzyme. *Biochemical Journal*, 126(3):739–745, 1972.

[52] Markus Leutzsch, Larry M Wolf, Puneet Gupta, Michael Fuchs, Walter Thiel, Christophe Farès, and Alois Fürstner. Formation of ruthenium carbenes by gem-hydrogen transfer to internal alkynes: Implications for alkyne trans-hydrogenation. *Angewandte Chemie International Edition*, 54(42):12431–12436, 2015.

[53] Alexandre Guthertz, Markus Leutzsch, Lawrence M Wolf, Puneet Gupta, Stephan M Rummelt, Richard Goddard, Christophe Farès, Walter Thiel, and Alois FuÌˆrstner. Half-sandwich ruthenium carbene complexes link trans-hydrogenation and gem-hydrogenation of internal alkynes. *Journal of the American Chemical Society*, 140(8):3156–3169, 2018.

[54] Aurélien Bornet, Xiao Ji, Daniele Mammoli, Basile Vuichoud, Jonas Milani, Geoffrey Bodenhausen, and Sami Jannin. Long-lived states of magnetically equivalent spins populated by dissolution-dnp and revealed by enzymatic reactions. *Chemistry-A European Journal*, 20(51):17113–17118, 2014.

[55] Michael CD Tayler and Malcolm H Levitt. Paramagnetic relaxation of nuclear singlet states. *Physical Chemistry Chemical Physics*, 13(20):9128–9130, 2011.

[56] Andrey N Pravdivtsev, Alexandra V Yurkovskaya, Hans-Martin Vieth, and Konstantin L Ivanov. Rf-sabre: A way to continuous spin hyperpolarization at high magnetic fields. *The journal of physical chemistry. B*, 119:13619–13629, October 2015.

[57] MP Ledbetter, Thomas Theis, JW Blanchard, Hattie Ring, Paul Ganssle, Stephan Appelt, Bernhard Blümich, Alex Pines, and Dmitry Budker. Near-zero-field nuclear magnetic resonance. *Physical review letters*, 107(10):107601, 2011.

[58] Thomas Theis, Milton L Truong, Aaron M Coffey, Roman V Shchepin, Kevin W Waddell, Fan Shi, Boyd M Goodson, Warren S Warren, and Eduard Y Chekmenev. Microtesla sabre enables 10% nitrogen-15 nuclear spin polarization. *Journal of the American Chemical Society*, 137(4):1404–1407, 2015.

[59] Milton L Truong, Thomas Theis, Aaron M Coffey, Roman V Shchepin, Kevin W Waddell, Fan Shi, Boyd M Goodson, Warren S Warren, and Eduard Y Chekmenev. 15n hyperpolarization by reversible exchange using sabre-sheath. *The journal of physical chemistry C*, 119(16):8786–8797, 2015.

[60] Johannes FP Colell, Angus WJ Logan, Zijian Zhou, Roman V Shchepin, Danila A Barskiy, Gerardo X Ortiz Jr, Qiu Wang, Steven J Malcolmson, Eduard Y Chekmenev, Warren S Warren, et al. Generalizing, extending, and maximizing nitrogen-15 hyperpolarization induced by parahydrogen in reversible exchange. *The Journal of Physical Chemistry C*, 121(12):6626–6634, 2017.

[61] Michael J. Cowley, Ralph W. Adams, Kevin D. Atkinson, Martin C. R. Cockett, Simon B. Duckett, Gary G. R. Green, Joost A. B. Lohman, Rainer Kerssebaum, David Kilgour, and Ryan E. Mewis. Iridium n-heterocyclic carbene complexes as efficient catalysts for magnetization transfer frompara-hydrogen. *JACS*, 133:6134–6137, 2011.

[62] Daniel G Zaccari, James P Snyder, Juan E Peralta, Oscar E Taurian, Rubén H Contreras, and Verónica Barone. Natural j coupling (njc) analysis of the electron lone pair effect on nmr couplings: 2. the anomeric effects on 1 j (c, h) couplings and its dependence on solvent. *Molecular Physics*, 100(6):705–715, 2002.

[63] Daniel Zaccari, Verónica Barone, Juan E. Peralta, Rubén H. Contreras, Oscar E. Taurian, Ernesto DÃez, and Angel Esteban. Solvent effects on nuclear magnetic resonance 2j(c,hf) and 1j(c,h) spin-spin coupling constants in acetaldehyde. *International Journal of Molecular Sciences*, 4:93–106, February 2003.

[64] Oliver Zerbe and Simon Jurt. *Applied NMR spectroscopy for chemists and life scientists*. John Wiley & Sons, 2013.

[65] Andreas Scheithauer, Erik von Harbou, Hans Hasse, Thomas GrÃ$\frac{1}{4}$tzner, Christiaan Rijksen, Daniel Zollinger, and Werner R. Thiel. 1h- and13c-nmr spectroscopic study of chemical equilibria in the system acetaldehyde + water. *AIChE Journal*, 61:177–187, 2015.

[66] A. Brächer, S. Hoch, K. Albert, H. J. Kost, B. Werner, E. von Harbou, and H. Hasse. Thermostatted micro-reactor nmr probe head for monitoring fast reactions. *Journal of Magnetic Resonance*, 242:155–161, 2014.

[67] Éléonore J. Kibrik, Oliver Steinhof, Günter Scherr, Werner R. Thiel, and Hans Hasse. On-line nmr spectroscopic reaction kinetic study of urea-formaldehyde resin synthesis. *Industrial and Engineering Chemistry Research*, 53:12602–12613, 2014.

[68] M. Maiwald. *HochauflÃ¶sende online NMR-Spektroskopie fÃ$\frac{1}{4}$r das Reaktions- und Prozessmonitoring*. Cuvillier Verlag, 2012.

[69] Michael A. Bernstein, Marijan Å tefinoviÄ‡, and Chris J. Sleigh. Optimising reaction performance in the pharmaceutical industry by monitoring with nmr. *Magnetic Resonance in Chemistry*, 45:564–571, 2007.

[70] Michael Maiwald, Holger H. Fischer, Michael Ott, Roger Peschla, Christian Kuhnert, Cornelius G. Kreiter, Gerd Maurer, and Hans Hasse. Quantitative nmr spectroscopy of complex liquid mixtures:Â methods and results for chemical equilibria in formaldehydeâ^'waterâ^'methanol at temperatures up to 383 k. *Industrial and Engineering Chemistry Research*, 42:259–266, 2003.

[71] Ernesto Danieli, Juan Perlo, Bernhard BlÃ$\frac{1}{4}$mich, and Federico Casanova. Small magnets for portable nmr spectrometers. *Angewandte Chemie*, 49:4133–4135, 2010.

[72] James F. Haw, T. E. Glass, D. W. Hausler, Edwin. Motell, and H. C. Dorn. Direct coupling of a liquid chromatograph to a continuous flow hydrogen nuclear magnetic resonance detector for analysis of petroleum and synthetic fuels. *Analytische Chemie*, 52:1135–1140, 1980.

[73] Aleksandr Ivanovich Zhernovoi and Georgii Dmitrievich Latyshev. Nuclear magnetic resonance in a flowing liquid, 1965.

[74] M. C. McIvor. A flow probe for nuclear magnetic resonance spectroscopy. *J. Phys. E*, 2:292–293, 1969.

[75] Keunhong Jeong, Sein Min, Heelim Chae, and Sung Keon Namgoong. Detecting low concentrations of unsaturated c-c bonds by parahydrogen-induced polarization using an efficient home-built parahydrogen generator. *Magnetic Resonance in Chemistry*, 2018.

[76] Sui Seng Tee, Valentina DiGialleonardo, Roozbeh Eskandari, Sangmoo Jeong, Kristin L Granlund, Vesselin Miloushev, Alex J Poot, Steven Truong, Julio A Alvarez, Hannah N Aldeborgh, et al. Sampling hyperpolarized molecules utilizing a 1 tesla permanent magnetic field. *Scientific reports*, 6:32846, 2016.

[77] Sören Lehmkuhl, Martin Wiese, Lukas Schubert, Mathias Held, Markus Küppers, Matthias Wessling, and Bernhard Blümich. Continuous hyperpolarization with parahydrogen in a membrane reactor. *Journal of Magnetic Resonance*, 291:8–13, 2018.

[78] Oliver Neudert, Carlos Mattea, and Siegfried Stapf. Molecular dynamics-based selectivity for fast-field-cycling relaxometry by overhauser and solid effect dynamic nuclear polarization. *Journal of Magnetic Resonance*, 276:113–121, 2017.

[79] Meike Roth, Petra Kindervater, Hans-Peter Raich, Joachim Bargon, Hans W Spiess, and Kerstin Münnemann. Continuous 1h and 13c signal enhancement

in nmr spectroscopy and mri using parahydrogen and hollow-fiber membranes. *Angewandte Chemie International Edition*, 49(45):8358–8362, 2010.

[80] L Buljubasich, MB Franzoni, Hans Wolfgang Spiess, and Kerstin Münnemann. Level anti-crossings in parahydrogen induced polarization experiments with cs-symmetric molecules. *Journal of Magnetic Resonance*, 219:33–40, 2012.

[81] Konstantin L Ivanov, Andrey N Pravdivtsev, Alexandra V Yurkovskaya, Hans-Martin Vieth, and Robert Kaptein. The role of level anti-crossings in nuclear spin hyperpolarization. *Progress in nuclear magnetic resonance spectroscopy*, 81:1–36, 2014.

[82] Andrey N Pravdivtsev, Alexandra V Yurkovskaya, Nikita N Lukzen, Hans-Martin Vieth, and Konstantin L Ivanov. Exploiting level anti-crossings (lacs) in the rotating frame for transferring spin hyperpolarization. *Physical Chemistry Chemical Physics*, 16(35):18707–18719, 2014.

[83] MarÃa BelÃ©n Franzoni, Lisandro Buljubasich, Hans W Spiess, and Kerstin MÃ$\frac{1}{4}$nnemann. Long-lived 1h singlet spin states originating from parahydrogen in cs-symmetric molecules stored for minutes in high magnetic fields. *Journal of the American Chemical Society*, 134:10393–10396, June 2012.

[84] Mathias Haake, Johannes Natterer, and Joachim Bargon. Efficient nmr pulse sequences to transfer the parahydrogen-induced polarization to hetero nuclei. *Journal of the American Chemical Society*, 118(36):8688–8691, 1996.

[85] Stephen Kadlecek, Kiarash Emami, Masaru Ishii, and Rahim Rizi. Optimal transfer of spin-order between a singlet nuclear pair and a heteronucleus. *Journal of Magnetic Resonance*, 205(1):9–13, 2010.

[86] Maurice Goldman and Haukur Jóhannesson. Conversion of a proton pair para order into 13c polarization by rf irradiation, for use in mri. *Comptes Rendus Physique*, 6(4-5):575–581, 2005.

[87] Sébastien Bär, Thomas Lange, Dieter Leibfritz, Jürgen Hennig, Dominik von Elverfeldt, and Jan-Bernd Hövener. On the spin order transfer from parahydrogen to another nucleus. *Journal of Magnetic Resonance*, 225:25–35, 2012.

[88] Lisandro Buljubasich, Ignacio Prina, Maria Belen Franzoni, Kerstin Münnemann, Hans Wolfgang Spiess, and Rodolfo Héctor Acosta. High resolution para-hydrogen induced polarization in inhomogeneous magnetic fields. *Journal of Magnetic Resonance*, 230:155–159, 2013.

[89] Ignacio Prina, L Buljubasich, and Rodolfo Héctor Acosta. High-resolution hyperpolarized j-spectra with parahydrogen discrimination. *The Journal of Physical Chemistry Letters*, 4(22):3924–3928, 2013.

[90] Naoya Ogata and Hozumi Tanaka. Synthesis of polyamide by phosphoroxidation. *Polymer Journal*, 2(5):672, 1971.

Acknowledgements

I would like to thank the following people for their help and support that notably increased the value of this thesis:

- Dr. Kerstin Münnemann
- Prof. Dr. Katharina Landfester
- Prof. Dr. Hans Wolfgang Spiess
- Prof. Dr. Dmitry Budker
- Dr. Peter Blümler
- Dr. John Blanchard
- MSc James Eills
- Dr. Teng Wu
- MSc Anne Friebel
- Dr. Robert Graf
- Dr. Manfred Wagner
- Dr. Markus Leutzsch
- Dr. Martin Ripka
- Beate Schiewe
- Petra Kindervater
- Dr. Dirk Graafen
- Dr. Ignacio Prina
- Dr. Jan Falk Dechent
- Dr. Oliver Neudert
- Manfred Hehn
- Dr. Maricel Repetto
- Dipl.-Ing. Jolanta Piechalska
- Dipl.-Ing. Jacek Piechalski
- MA Jino Khademi
- Sabrina Brand
- Dr. Alexander Schoth
- Dr. Thomas Wolf
- MSc Ernesta Heinrich
- Dr. Sandro Ebert
- Hans-Peter Raich
- Christa Kraft
- Angela Hördt
- Michelle Beuchel
- Prof. Dr. Malcolm H. Levitt
- Dr. Gert-Jan Wetzlaer
- Prof. Dr. Paul Blom
- Dipl.-Phys. Manuel Braun
- Dr. Kristin Bauer
- Dr. Elisabeth Rieger
- MSc Claudia Weber

This work was supported by the Bundesministerium für Bildung und Forschung (grant number VIP HYPER-MRI 03V0443), the Max Planck Graduate Center, Mainz, the Deutsche Forschungsgemeinschaft within the Collaborative Research Center SFB/TRR173 Spin+X.